AN ABSTRACT OF THE DISSERTATION OF

Shuhong Liu for the degree of Doctor of Philosophy in Chemical Engineering presented on July 16, 2007.

Title: Synthesis, Characterization and Deposition of Dendrimers Using a Continuous Flow Microreactor

Abstract approved:

_____

Chih-hung Chang

Dendrimers are nanoscale macromolecules that have highly branched, core-shell structures. Higher generation dendrimers have close-packed peripheral functional groups and a hollow interior. The chemistry of the core and the terminal functionalities can be tailored according to the specific application. These structural characteristics provide room for the design of dendrimers to meet a wide set of supra-molecular recognition and hosting tasks. Dendrimers are synthesized in a stepwise manner to higher generations using a number of chemical reactions; as a result, carrying out the synthesis in a conventional reactor is time-consuming, and the dendrimer products are expensive. In this dissertation, the mixing quality of several micromixers was tested experimentally and computationally, which lead

to consistent testing results. A continuous-flow microreactor is not only used to produce dendrimers via convergent and divergent syntheses strategies, but also it is used as an effective tool to study reaction kinetics. In addition, it provides a convenient and effective method to deposit dendrons and dendrimers on solid surfaces. Dendrons and dendrimers could be synthesized using the microreactors within seconds of residence time. Experimental data and fundamental studies were conducted to compare the synthesis of dedrons and dendrimers by utilizing a microreactor and a conventional batch reactor. Furthermore, the synthesized polyamide dendron was deposited onto a functionalized glass surface through the formation of amide bond using a facile coupling procedure via the microreactor. A variety of techniques were applied to characterize the deposition on glass surfaces. Compared with the conventional synthesis method, the microreactor provides a comparable yield, selectivity, and a considerably faster synthesis rate.

Synthesis, Characterization and Deposition of Dendrimers Using a Continuous Flow Microreactor

by

Shuhong Liu

A DISSERTATION

submitted to

Oregon State University

in partial fulfillment of
the requirements for the
degree of

Doctor of Philosophy

Presented July 16, 2007
Commencement June 2008

Doctor of Philosophy dissertation of Shuhong Liu presented on July 16, 2007.

APPROVED:

_____

Major Professor, representing Chemical Engineering

_____

Chair of the Department of Chemical Engineering

_____

Dean of the Graduate School

I understand that my dissertation will become part of the permanent collection of Oregon State University libraries. My signature below authorizes release of my dissertation to any reader upon request.

_____

Shuhong Liu, Author

ACKNOWLEDGEMENTS

The author sincerely expresses appreciation to Dr. Chih-hung Chang for his continuous encouragement and constructive suggestions, which have been the indispensable to the author in order to finish this dissertation. His diligence, perseverance, serious attitude on research, and his sincerity with which he dealt with people set a good example for the author. The author's gratitude goes to Dr. Vincent Remcho and Dr. Brian Paul for their great advice and generosity for offering facilities which accelerated the research's progress. The author also expresses gratitude to Dr. Greg Rorrer for his wonderful ideas that improved some experiments and his permission to use the facilities in his lab.

In addition, the author would like to thank all fellow graduate students working in Dr. Chih-hung Chang's lab for their cooperation, friendship, and help. They together created a warm and productive working environment which will never be forgotten. Finally, sincere appreciation goes to the author's parents and parents-in-law for all of their support and encouragement.

TABLE OF CONTENTS

TABLE OF CONTENTS (Continued)

TABLE OF CONTENTS (Continued)

TABLE OF CONTENTS (Continued)

LIST OF FIGURES

LIST OF FIGURES (Continued)

LIST OF FIGURES (Continued)

LIST OF FIGURES (Continued)

LIST OF FIGURES (Continued)

LIST OF FIGURES (Continued)

LIST OF FIGURES (Continued)

LIST OF FIGURES (Continued)

LIST OF TABLES

LIST OF APPENDIX TABLES

Synthesis, Characterization and Deposition of Dendrimers Using a Continuous Flow Microreactor

Chapter 1 Introduction

Dendrimers are nanoscale macromolecules that have highly branched, core-shell structures. Higher generation dendrimers have close-packed peripheral functional groups and a hollow interior. The chemistry of the core and the terminal functionalities can be tailored according to specific applications. These structural characteristics provide room for the design of dendrimers to meet a wide set of supra-molecular recognition and hosting tasks. Dendrimers are synthesized in a stepwise manner to higher generations using a number of chemical reactions; as a result, carrying out the synthesis in a conventional reactor is time-consuming, and the dendrimer products are expensive. Here the syntheses of two different dendrimers will be carried out in a continuous flow microreactor. Compared with conventional flask synthesis, microreactor synthesis provides desired products with comparable yield and selectivity but much shorter residence time. Meanwhile, the microreactor is utilized as a powerful tool to study reaction kinetics. Subsequently, the microreactor is used to deposit dendrimer thin film on glass surfaces for further applications. The evaluation of the mixing quality and its impact on the synthesis of dendrimers of several different micromixers will be

experimentally conducted. The experimental results will be compared with simulation of the mixing quality of the micromixers by using the program software, COMSOL. The evaluation and simulation will help the rational design of the microreactor.

Objectives

(1) Compare mixing quality of micromixers having different geometries experimentally and computationally (COMSOL simulation).

(2) Demonstrate the syntheses of dendrimers including convergent and divergent synthesis strategies by utilizing a microreactor.

(3) Study the reaction kinetics of dendrimer formation. The reaction kinetics of amidation reaction of plolyamide G1 dendron will be studied in detail.

(4) Explore the deposition of dendrimers or dendrons on the surface of glass slides by a continuous flow micromixer.

Chapter 2 Literature Review

2.1 General Background of Dendrimer

Polymer chemistry and technology have contributed numerous useful linear and occasionally branched polymeric materials to benefit human condition. Although some of linear polymers displaced three-dimensional characteristics, they are covalently assembled in a one-dimensional style. The special property and potential application of highly branched units in macromolecular was originally studied in theory by Flory and co-workers in 1945.[1]

It was not until 1978, however, that the first dendrimer chemistry emerged when Vögtle and co-workers disclosed a fully controlled synthesis of a low molecular weight, branched amine in an iterative cascade way.[2] Tomalia and co-workers disclosed a thoroughly investigated divergent synthesis and characterization of one of the first dendrimeric members, PAMAM dendrimer, by using an iterative Michael addition of a core ethylenediamine molecule to four molecules of methyl acrylate, followed by exhaustive amidation using a large excess of ethylenediamine.[3] At a later date, another demerimeric family, poly(propylene imine) dendrimers were synthesized based on Vögtle's original work by Mülhaupt and de Brabander by using a divergent strategy.[4] A convergent strategy to grow dendrimers, which nowadays is recognized as the second general approach to dendrimeric structure, was practiced by Hawker and

Frechét.[5] After the foundation of all these corner stones, studies toward the synthesis, properties, and applications of dendrimers had gained tremendous popularity. To date, there are more than fifty families of dendrimers, each of them with some unique properties; many of them are commercially available. Applications of dendrimers are widely ranged from catalysis to drug delivery, gene therapy, and in-vitro diagnosis.

2.2 Structural Characteristics of Dendrimer

The hyperbranched dendritic compound firstly synthesized by Tomalia and co-workers was called dendrimer, originated from a Greek word "dendron" meaning a "tree". Interestingly, in another independent work reported by Newkome,[6] a similar highly branched macromolecule was named arborols from the Latin word "arbor", which also means a "tree". Other names for dendrimers, such as cascade, cauliflower, and starburst also describe its unique structural characteristics.

Compared with a linear or a hyperbranched polymer, two critical differences in producing dendrimers render a uniform structure of dendrimer with a narrow molecular weight distribution or even an exactly single molecular weight. The first difference is the use of AB_n monomers instead of the standard AB monomer, which can only lead to a linear polymer. Secondly, a dendrimer is prepared in an iterative manner, which is fundamental to the narrow distribution of molecular weight. Although a hyperbranched polymer is also assembled from an AB_n monomer, it was generally produced by a non-iterative polymerization procedure; therefore, it contains an unpredictable irregular structure. The molecular weight of

a hyperbranched polymer has a wide molecular weight distribution characterized by the Gaussian distribution rule.

Taking PAMAM as an example (see figure 2-1), one molecule ethylenediamine (AB_n) is used as the core, which reacts with four molecules of methylacrylate to generate the G-0.5. After obtaining G-0.5, an amidation reaction with four molecules of ethylenediamine yields G0 dendrimer. In an iterative manner, this stepwise procedure will lead to a higher generation dendrimer with complete control of the mass and structure. Equally impressive is the fact that a structurally complex macromolecule can be assembled in a manner with only a few steps.

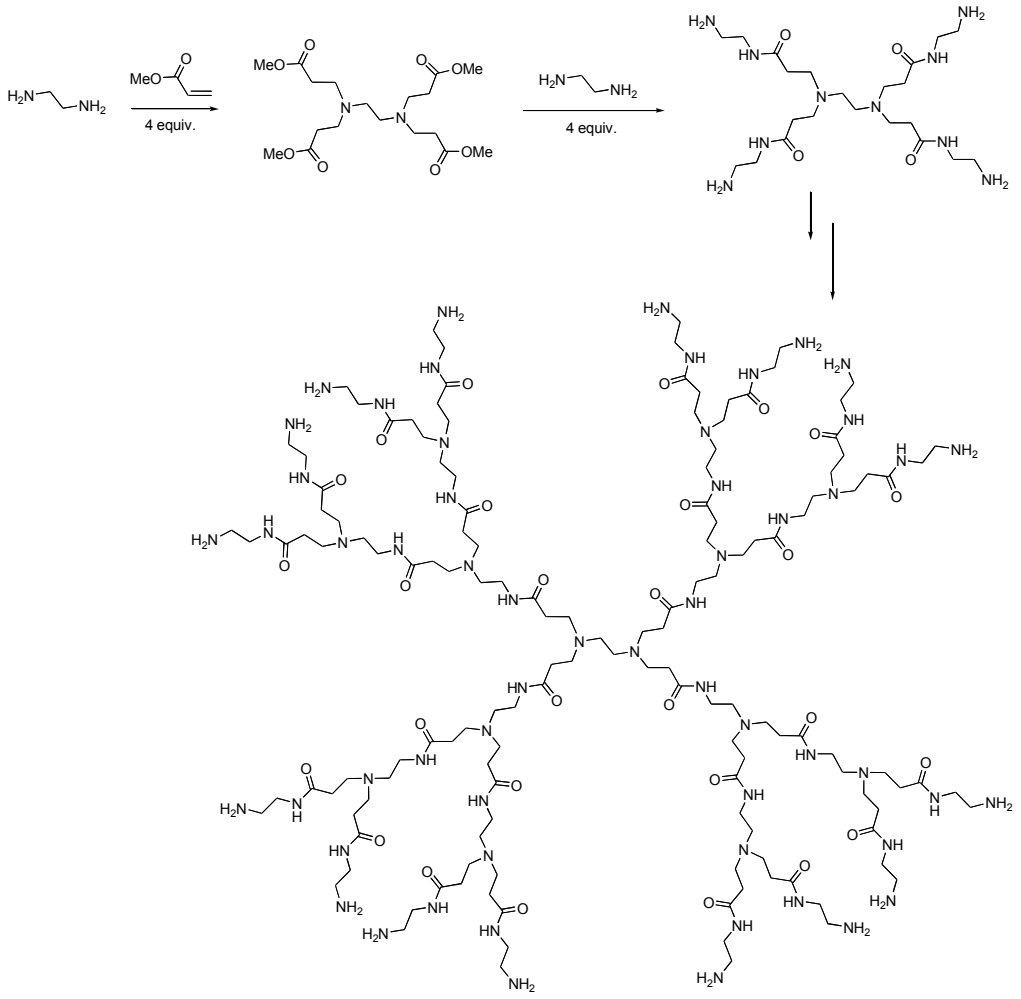

Figure 2-1. Preparation of PAMAM dendrimer.

2.3 Applications Related to the Dendritic Structure

Many applications of dendritic structures were inspired by the extended analogies from nature. For example, neurons (brain cells) take forms of dendritic structures to magnify the mutual conncections; natural polysaccharides take dendritic structures to maximize glucose storage and speed its release, and in a

macro view, a crown of a tree can modify an environment by absorbing CO_2, releasing O_2, and creating shade beneath itself. Likewise, applications related to dendrimers' aesthetically appealing structure involve three levels, the void core, the well-tailored branch, and the crown-like surface.[7]

2.3.1 Applications Related to the Core

A specially designed core of dendrimer can be a ligand for certain transition metals, such as Ru or Pd, which can catalyze certain organic transformation. The branches surrounding the core can serve to modify its catalytic properties to improve either regio or diastereoselectivity.[8] Dendrimers also can be applied to mimic globular proteins. One example would be hemoglobin, which is responsible for transporting and storing O_2 in biological systems. Unlike non-dendritic structures, dendrimers can prevent the formation of porphyrin μ-oxo dimer that leads to the failure of imitation.[9] Also, dendrimers can be used to recognize specific guest molecules such as monosaccharides.[10]

2.3.2 Applications Related to the Dendritic Branches

Protected from the outside world by the dendrimer surface layer, the branches layer is a localized, tailored environment. There are two types of combination of the branches and the surface layers, hydrophilic groups on the surface with hydrophobic moieties in the branches or the opposite order. The former combination resembles surfactants, which form micelles in a polar solvent (i.e. water) with hydrophilic "heads" outside in touch with the polar solvent and hydrophobic "tails" inwardly aggregated toward the central cores. This type of

dendrimer is referred to as a unimolecular micelle,[11] and it shows similar solubility to typical surfactant such as sodium dodecyl sulfate with a wider active concentration range. The other combination was referred to as a reversed micelle, which was applied as a catalyst to some reaction involving a positively charged intermediate in the transition state.[12] In addition, a reversed-micelle-dendrimer could be specially designed as a trap to remove a certain gas such as CO_2.[13]

2.3.3 Applications Related to the Surface

Most of the applications related to dendritic surface are derived from the cauliflower-like, maximized surface area. Dendritic sensors were rooted in the beneficially structural characteristic. As many fluorescent groups can be assembled on the surface, the sensitivity for fluorescent change will be amplified. When a transition metal or an organic compound, such as saccharide molecules, coordinates with aromatic fluorescent functionalities, the change of fluorescence intensity can be sensitively monitored.[14] Also, dendrimers can be applied as recyclable supporters of some organometallic catalyst for some organic transformations.

Among all the application areas of dendrimers, the potential for medical applications is the most exciting one. Ranged from improving Magnetic Resonance Imaging to drug delivery, there is an infinite future of dendrimers in medical use. As one of the powerful diagnostic medical tool, Magnetic Resonance

Imaging (MRI) often requires the use of contrast agents to provide quality image. The unfavorable short-stay time in the blood vessel of the often-used Gd agent makes the Gd agent only partially suitable for imaging the cardiovascular system. Since dendrimers have a large molecular weight and dendritic surface, it can be used as an anchoring platform for multiple Gd ions, the lifetimes of Gd ions in blood vessels can be extended, which renders a lower dosage of Gd and improved image quality.[15]

Lured by the concept of targeted drug delivery, an often-used drug delivery agent, cyclodextrins (CDs), was attached with saccharide-coated dendritic branches by Dafaye and co-workers. The modified cyclodextrin specie has shown promising potential as a targeted drug delivery system.[16] In addition to delivering common drugs, dendrimers are potential alternatives to a viral artificial gene delivery method. Polyamidoamine dendrimers are promising in this area since they contain protonated amine surface groups. This electrostatic interaction with poly-anionic DNA entitles them potential as gene-transfer agents. A broad range of cells has been transported with a minimal cytotoxicity using DNA/dendrimer complexes *in vitro*.[17]

In summary, the unique structural characteristics of dendrimers render them a wide diversity of applications. Ranged from catalysis in organic transformation to medical application, dendrimers arouse lots of attention and interests from chemists in multiple disciplines. The wide spread application, in turn, invokes the syntheses of more structurally diversified dendrimers.

2.4. Preparation of Dendrimers

Generally, there are two different approaches to synthesize dendrimers, the divergent method and the convergent method. Some fundamental differences exist between these two methods.

In a divergent method, a dendrimer grows outwards from a multifunctional core molecule to a hyper-branched surface. In the extremely simplified figure 2-2, a general process is illustrated. The core molecule reacted with 4 molecules of monomer containing two pro-functional groups, which can be activated for further modifications to form the first generation dendrimer. Then, the periphery of the dendrimer will be activated to react with 8 monomers to form the second generation dendrimer. This process will be repeated until a high generation dendrimer is formed. PAMAM is one of the dendrimers synthesized in this way (figure 2-1). The number of the reactive sites of core molecule and monomer molecules determines the multiplicity of the final molecule.

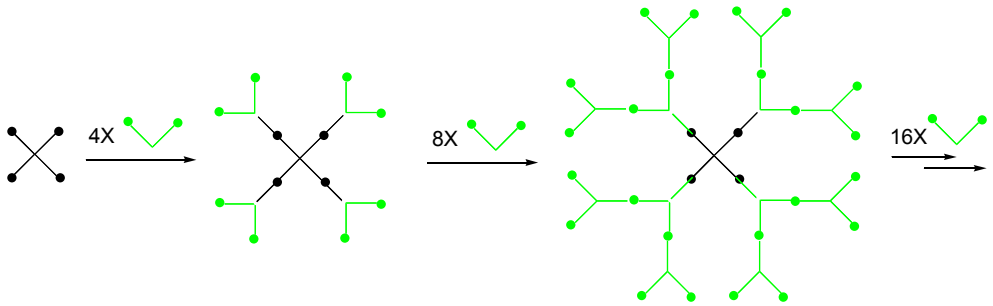

Figure 2-2. Illustration of the divergent method.

Although conceptually straightforward, the divergent approaches might encounter some synthetic difficulties in the syntheses of higher generation. With the increases of generations, the number of the surface functionalities increases accordingly. In this way, an exponentially increasing number of reactions need to be performed to generate the perfect dendrimer. As steric effect becomes more predominant, it will be more difficult to form a high generation dendrimer even with a highly efficient reaction. Separation also proves logistically difficult since flawed by-products are usually structurally similar to the perfect dendrimers.

The convergent methods were invented as a response to the shortcoming of the divergent approaches. In a convergent approach, the dendrimer is constructed from the outer layers and progresses inwards stepwise. In figure 2-3, monomer **A** reacts with two equivalents **B**, outer layer unit, to give the first generation dendron (individual dendritic branch) **C**. Two molecules of **C** react with monomer **A** again to afford the second generation dendron **D**. Repeating this procedure will yield a

higher generation dendron **M**, which reacts with a dendrimer core molecule to generate the dendrimer.[18]

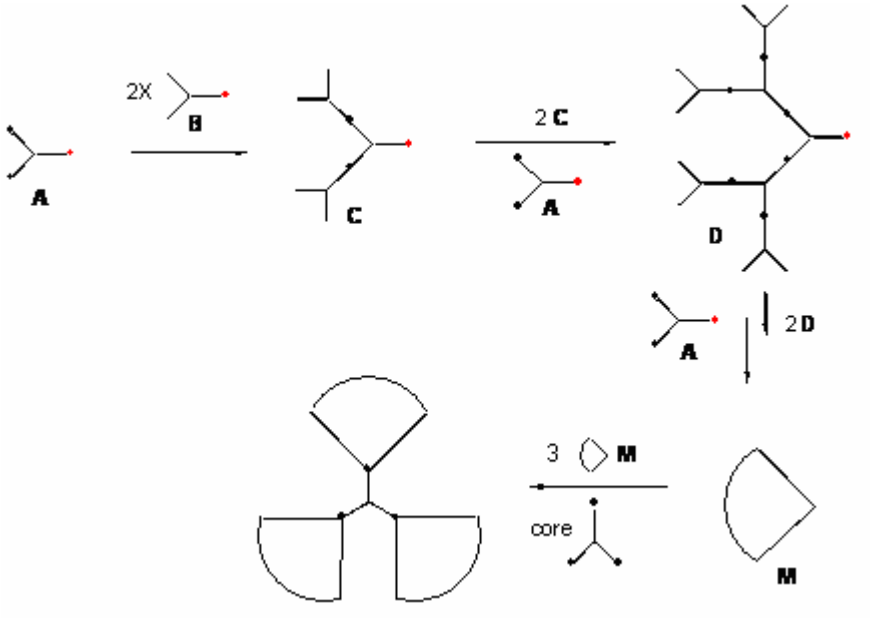

Figure 2-3. Illustration of the convergent approach.

In comparison with the divergent approach, the convergent route has some obvious advantages. There are only a small number of reactions carried out in each step; therefore, it is unlikely to form structurally flawed products. Even when side reactions do happen, the molecular weight difference between by-product and perfect product is comparatively large, which render it an easier separation. Using the convergent method, it becomes possible to subtly engineer the periphery functionalities in the macromolecule. However, the disadvantage is also obvious;

a high generation dendrimer is literally not allowed due to the steric problems predominating in the reactions of the dendrons and the core molecule.

Most applications of dendrimers are based on the characeristic dendritic structures. With continuously increased interests in dendrimers, more and more applications were disclosed. It, in turn, propelled the syntheses of more structurally and functionally diversified dendrimers. Although some of dendrimers have become commercially available, syntheses of most others remain on laboratory scales. Due to the limit of traditional synthetic tools and methods, syntheses of high generation dendrimers are struggling with low yield, difficulties to purify, and elongated time. Therefore, new synthetic tools and methods shall be applied to improve the overall throughput of dendrimer syntheses. We believe dendrimer synthesis can benefit greatly from implementation of a highly-paralleled process-intensified microsystem format.

2.5 Introduction to a Microreactor and Its Advantages over a Conventional Vessel Reactor

2.5.1 Productivity

The idea of using a microfluidic system to perform chemical synthesis was first introduced at a workshop in Mainz in 1995.[19] Since then, microfluidic devices have been widely used in synthetic chemistry. Before the appearance of the microreactor, conventional vessel reactors with volumes ranging from a few milliliters to a thousand liters were widely used in a variety of fields. Productivity is the most significant aspect to be considered in the synthesis of substances.

Space-time yield is the most straightforward parameter to compare the productivity of the batch process taking place in a conventional vessel reactor and the continuous process in a microreactor. It normalizes the obtained mass of the product with respect to reactor volume and reaction time. Obviously, the space-time yield is determined by reaction time and reaction selectivity. Therefore, these two aspects will be focused to address the advantages of a microreactor over a conventional vessel reactor.

Reaction Time

It is common that the reaction taking place in a conventional vessel reactor takes a longer time than its counterpart, the microreactor, due to two major reasons. One reason is the different mixing principles between these two reactors causing different mixing qualities. Mixing quality is the most important prerequisite for the occurrence of reactions. Conventional reaction relies on the impeller to generate turbulent flow to reinforce mass transfer by stirring the reactant mixtures. Turbulent flow produces eddies to stretch or fold the substances therefore to produce thin layers for diffusion. The major limitation of this form of mixing comes with the fact that only a small portion of the fluid in the vicinity of the impeller is involved in the mass transfer; the rest of the fluid has to wait until it reaches the shear field of the turbulence. This will inevitably generate deviations of substances' properties, such as the concentration and temperature in different parts of the reactor. Therefore, the traditional turbulent mixing mechanism takes a long time to produce well-mixing of reactant substances. On the other hand, the

micromixer which can realize a high mixing quality primarily relies on molecular diffusion. The short diffusion pathway in microchannels with dimensions of a few tens to a few hundreds of micrometers can increase the gradient of physical properties (such as concentration), therefore enhancing mass transfer. The accelerated mixing quality will inevitably decrease the reaction time in the microreactor.

Apart from the mixing quality, there is another factor that affects the counting of reaction time, dosing time. For most reactions conducted in the conventional reactor, the long reaction time is not caused by their intrinsic kinetics, but by the requirement of a slow reactant agent dosing. It has been mentioned above that stirring in vessels, especially in big vessels, can generate un-uniform distribution of the properties of substances, such as concentration and temperature, which would result in difficulty of control of reactions and negatively affect product yield by favoring side and consecutive reactions. Therefore the feeding of reactants to the reactor for some reactions has to be controlled at a very slow speed so that the heat which is generated during the reaction can be released effectively without much influence on the rest of the reactants in the reactor. Compared with conventional reactors with a surface to volume ratio of 100 m^2/m^3, the microreactor has interfacial areas per unit volume of 10,000~50,000m^2/m^3, which can enhance heat transfer tremendously.[20] The heat generated during reaction can be released sufficiently in the microreactor, so there is no need for extra dosing time. The improved mass and heat transfer inherited from the microreactor

contribute the less reaction time which is needed by utilizing a microreactor rather than a conventional vessel reactor.

Selectivity

Selectivity is another important factor determining the space-time yield: the higher the selectivity on a desired product, the higher the space-time yield. Selectivity is closely associated with the temperature and the concentration distribution in the reactor. The un-uniform distribution in a conventional vessel reactor (especially in a big reactor) inevitably leads to an undesired side-reaction, causing the decrease of desired product, as well as the difficulty of post-treatment such as separation and purification. The comparison of how the temperature distribution affects selectivity in a conventional reactor and a microreactor is illustrated in figure 2-4 and figure 2-5.[21]

Figure 2-4 shows that the microreactor features with a narrow temperature distribution, but the batch reactor has a much wider temperature distribution. Combining the relationship between the temperature spread and the potential energy profile shown in figure 2-5, it is obvious why the microreactor and batch reactor behave differently with regard to selectivity. The narrower temperature distribution within a microreactor does not provide sufficient energy for side reaction (A→C) which needs a higher activation energy; therefore, the selectivity favored to the desired reaction A→B is increased. In contrast, a conventional batch reactor features a broad temperature distribution, which leads to formation of various products causing the decrease of selectivity of the desired product.

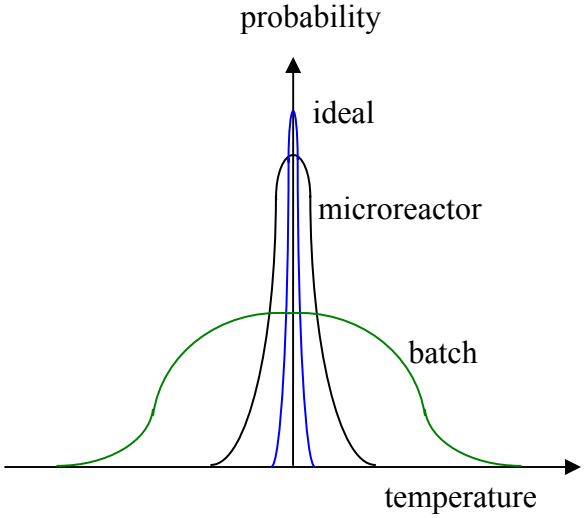

Figure 2-4. Schematic temperature spreads in a batch reactor and a microreactor

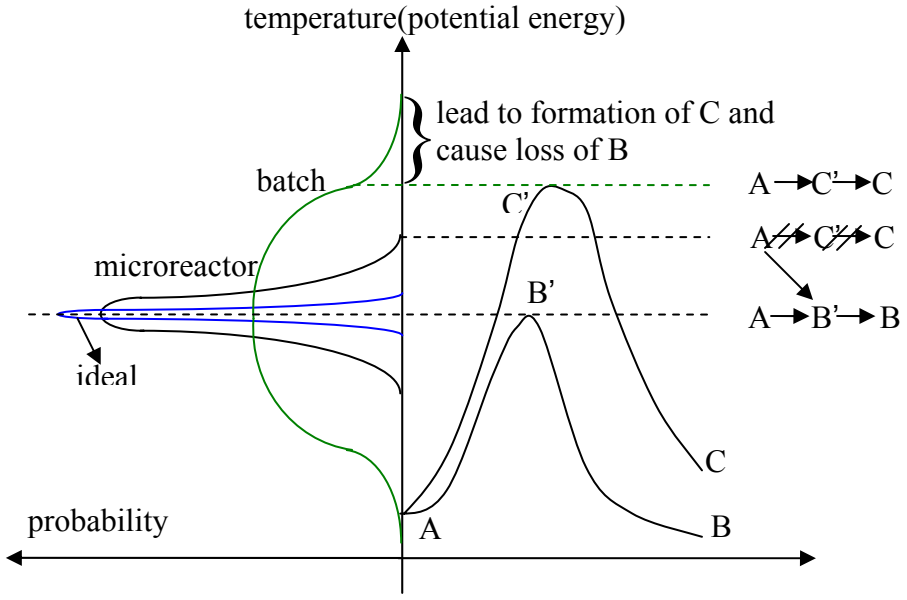

Figure 2-5. Schematic demonstration of the influence of temperature spreads and a potential energy profile on reaction products in a microreactor and a batch reactor.

Compared with a traditional vessel reactor, the microreactor is featured with an efficient mass and heat transfer. Therefore, the reaction time (including reaction kinetic need and dosing time) can be tremendously decreased, and the selectivity of the desired product can be improved dramatically in the microreactor. All of these improvements inevitably reinforce the productivity of reactions taking place in the microreactor.

2.5.2 Other Advantages of a Microreactor

(1) In addition to the benefits mentioned above, another attractive advantage of implementing a microreactor is the ability to "number-up" laboratory-scale reactors by simply arraying the identical microreactors without a need for further process development and parameterization. This numbering-up process has been demonstrated by Clariant, where a pigment was created in the quantity of 80 tons per year within a microchannel format.[22]

(2) The process taking place in the microreactor is easy to simulate because the laminar flow in the microscale has well-established simulating models. The simulation result of the microreactor will predict the real outcome with a much more precise degree than its counterpart, the conventional reactor. As a consequence, the simulation method will provide insights for the microreactor design and guide the operation of the microreator. On the other hand, the turbulent flow in the conventional reactor is hard to be simulated, because the simulation models are usually semi-empirical models which are dependent on specific study cases.

(3) The microreactor is an efficient tool for a reaction kinetics study, not only because it can provide quick well mixing, but also it requires a small amount of reactants with an easy reaction control. Also the microreactor provides a continuous process, and it can be easily integrated with analysis instruments to have an in-situ reaction monitor. In contrast, the turbulent mixing in a conventional reactor takes a long time to produce well mixing of reactant substances, so it is an inconvenient tool to study reaction kinetics, especially for a fast reaction. Reactions are often monitored off-line by withdrawing aliquots from the reaction mixtures. The inherent uncontrollable reaction-to-analysis time delay will inevitably influence the reaction kinetics study.

Numerous micromixers with different geometries have been designed to reinforce reactions, but, basically, they are classified into two categories: passive mixing and active mixing. In passive mixing, only pumping energy is inputted. However, the active mixing not only involves pumping mixing, but also extra energy such as ultrasound, microwave, and electrical field are involved.[23] Based on the information above, implementing a microreactor on synthesis of a dendrimer will be a promising research field.

Chapter 3 Experimental Set-up and Introduction of Characterization Instruments

3.1 Experimental Set-up

A schematic diagram of the microreactor setup is given in figure 3-1A. The micromixer (Institut für Mikrotechnik Mainz) consists of a mixing element, interdigital microchannels, in the center of a substrate made of thermally grown silicon dioxide. The mixing element is embedded in a two-piece housing, the top and bottom stainless steel plates. The top plate is connected with two inlets and one outlet (see figure 3-1B). The mixing element contains 30 sinusoidally shaped fluid channels (see figure 3-1C) fabricated by an advanced silicon etching technique. This technique utilizes alternating processes of SF_6 etching and C_4F_8 passivation. The SF_6 etches silicon to produce a gaseous phase of SiF_2 and SiF_4, and the C_4F_8 passivation process deposits a polymer-like film on microchannel walls to give rise to an anisotropic etching process. This technique can result in a 90^o sharp side wall feature. Each microchannel has a dimension of 30 μm in width and 100 μm in height. Figure 3-2 illustrates the principle of mixing via an interdigital micromixer. Two streams of reactants were simultaneously delivered to the interdigital micromixer at the same flow rate through two programmable syringe pumps (Kloehn syringe pumps). Each stream is divided into a number of lamellas by the microchannels. Furthermore the lamellas are hydrodynamically focused when they pass through a slit in the direction perpendicular to the

oncoming streams. Once the lamellas of the two reactants pass through the slit, a reaction occurs due to the fast diffusion between the thin layers of the two reactants. The mixture of the product and the un-reacted reactants from the microreactor passed through a PEEK tubing (ID of 750 μm), and was collected at a tubing outlet by pouring directly into a solvent to quench the reactions. Aliquots of samples will be taken for analysis. A double-jacked beaker that was connected with a constant temperature circulator was used for temperature control. For the purpose of forming a dendron thin film on the surface of a glass slide, a heated rotating disc substrate holder was used to heat and rotate the glass substrate.

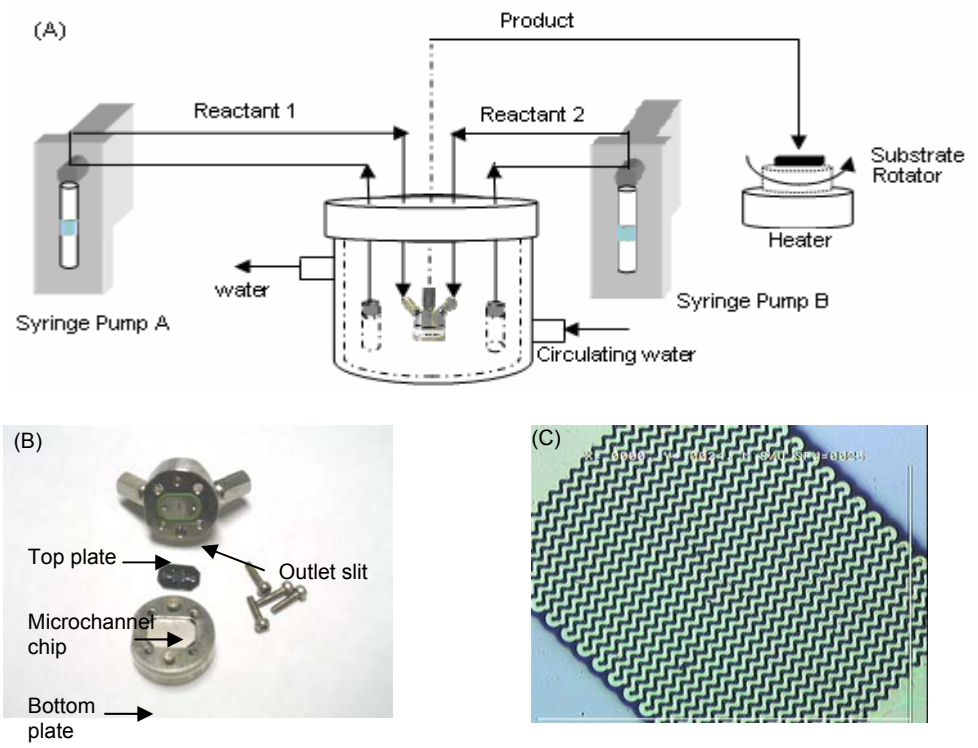

Figure 3-1. (A) A schematic diagram of the continuous flow microreactor; (B) photograph of the interdigital mixer; (C) the microscope image of the sinusoidally shaped microchannels.

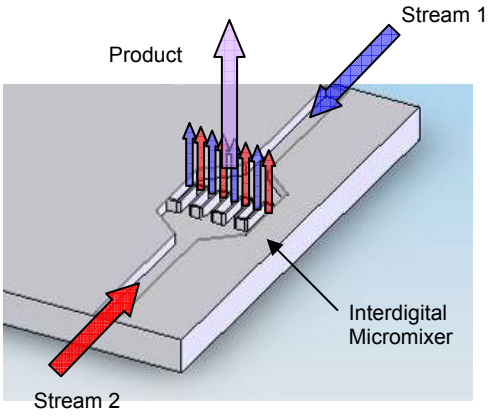

Figure 3-2. Illustration of mixing via an interdigital micromixer.

3.2 ^{1}H-NMR Introduction

Nuclear magnetic resonance spectrometry (NMR) is an invaluable technique to study the structure information of chemicals. Hydrogen NMR was frequently used in this research to identify the chemical structure of synthesized samples, to explore reaction mechanisms, and to study reaction kinetics. The principle of ^{1}H-NMR is based on the magnetic properties of a hydrogen nucleus. When a compound containing hydrogen is placed in a very strong magnetic field, the nuclei of the hydrogen will align with the direction of the external magnetic field. If the compound is irradiated with a specific value of electromeganetic energy, the nuclei will absorb energy to flip over to align against the direction of the external magnetic field. This energy absorption will result in a tiny electrical current to flow in an antenna coil surrounding the sample. The instrument then amplifies the current and displays it as a signal. The hydrogen nuclei under a different chemistry

environment will absorb energy at a different level, showing different chemical shifts on the spectrum. Therefore, the structure information of the sample can be obtained by studying the spectrum.

^{1}H-NMR spectra were recorded in solvents of deuterochloroform (for PAMAM) and deuterated dimethylsulfoxide (for polyamide dendrons and dendrimers) with a Bruker nuclear magnetic resonance spectrometer (300MHz).

3.3 Mass Spectrometry Introduction

Mass spectrometry is a powerful analytical technique that is used to identify unknown compounds, to quantify known compounds, and to elucidate the structure and chemical properties of molecules. In order to measure the characteristics of individual molecules, a mass spectrometer converts them to ions so that they can be moved about and manipulated by external electric and magnetic fields. A mass spectrometer includes three essential components: an ion source, a mass analyzer and a detector. The ion source is used to convert molecules into ions. The common ionization techniques include electron impact, chemical ionization, electrospray ionization (ESI), matrix-assisted laser desorption ionization (MALDI), and fast atom bombardment (FAB). The first two methods are suitable for volatile, thermally stable molecules with a small molecular mass. The other methods are advantageous for compounds that are thermally labile and have molecular mass up to 10,000 amu or even bigger.

The ionization methods of FAB and SIMS were utilized in this research, so the principles of these two methods will be described bellow. Essentially, the

principles of these two methods are the same. The analyte distributed in a matrix is bombarded by a high energy beam, then sample molecules are generated and desorbed into the gas phase, where they undergo ion/molecule reactions to form secondary ions. The ions can be accelerated by applying a high voltage between the sample surface and the mass analyzer. The ions will be sorted based on their mass-to-charge ratio in the mass analyzer, and be detected in a detector to give an intensity versus mass/charge spectrum. The only difference between SIMS and FAB is that SIMS uses primary ions (usually Cs^+ at 35 keV) to bombard the sample, but FAB ionization method uses neutral atoms (e. g. Ar) as a bombarding beam.

The combination of the Time of Flight (TOF) mass analyzer with the SIMS ionization method was used in this research to characterize the surface of glass slides on which the polyamide dendron was deposited. The mechanism of the TOF mass analyzer is based on the flight time of ions from the sample to the detector. Once the secondary ions are generated, they are electrostatically accelerated into a field-free drift region with a kinetic energy of

$$E_k = eV = mv^2 / 2 \tag{3-1}$$

Where V is the accelerating voltage, m the mass of ion, v the flight velocity of ion, e its charge. Obviously the ion with the lower mass has a higher flight velocity than one with the higher mass. Thus, they will reach the detector earlier. As a

result, the mass separation is obtained in the flight time t from the sample to the detector. The flight time t is expressed by:

$$t = L/(2eV/m)^{1/2} \tag{3-2}$$

where L is the effective length of the mass spectrometer. A full mass spectrum is obtained by measuring the arrival times of the secondary ions at the detector and performing a simple time to the mass conversion. There are three different modes of analysis in TOF-SIMS: 1) mass spectra are acquired to determine the chemical compositions of species on a surface; 2) images are acquired to visualize the distribution of individual species on the surface; and 3) depth profiles are used to determine the distribution of different chemical species as a function of depth from the surface. All of these three modes were used in this research to characterize the polyamide dendron-deposited surface.

Mass spectra of products were collected using a JEOL MSRoute mass spectrometer with a positive FAB ionization method. The polyamide dendron-deposited glass surface was characterized by an ION-TOF GmbH IV TOF-SIMS spectrometer with a bismuth LMIG primary ion source. The ion beam was composed of 25 keV Bi_3^+ ions. The primary ion dose during the acquisitions was less than 10^{12} ions/cm^2.

3.4 Contact Angle Measurement

Contact angle measurement (CA) is a convenient method for surface analysis related to surface energy and tension. The contact angle describes the shape of a

liquid droplet resting on a solid surface. For a droplet resting on solid surface, the contact angle is defined as the angle between the tangent line of the droplet and the solid surface. If a liquid with well-known properties is used, the resulting interfacial tension can be used to identify the nature of the solid. This technique is extremely surface sensitive with the ability to detect properties on monolayers. When a droplet of liquid rests on the surface of a solid, the shape of the droplet is determined by the balance of the interfacial liquid/vapor/solid forces (figure 3-3). The contact angle is expressed in the form of an equation (3-3).

$$\cos(\theta) = \frac{\gamma_{SV} - \gamma_{SL}}{\gamma} \tag{3-3}$$

Where: θ is the contact angle;

γ_{SV} is interfacial energy between solid and vapor;

γ_{SL} is interfacial energy between solid and liquid;

γ is surface tension;

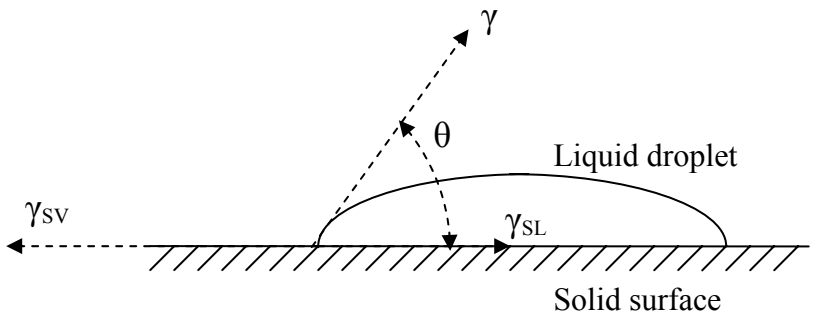

Figure 3-3. Balance of interfacial forces exerted on a liquid droplet.

The glass surface treated with different methods will appear with different water contact angles, so it can be affirmed whether the dendron is deposited on the glass surface or not based on the contact angle measurement. The water contact angle measurements were conducted at room temperature using an FTA 135 Dynamic Contact Angle Analyzer equipped with a B/W (Monochrome) CCD camera.

3.5 Fluorescence Microscopy

Fluorescence measurement in this research is used to determine the uniformity of the solid surfaces that are modified by substances. Fluorescence is a luminescence that is an optical phenomenon in cold bodies. Essentially, it consists of three major processes: the molecular absorption of high energy photons; the excitation of the electronic state of the fluorophore; the energy loss of the electronic state of the fluorophore and emission of low energy photons from the fluorophore. These processes are illustrated in figure 3-4. The molecular absorption of high energy photon triggers the emission of another photon with a longer wavelength (low energy). The energy difference between the absorbed and emitted photons ends up as molecular vibrations or heat (energy loss). In this research, a Leica DMIL fluo-optical microscope equipped with DAPI filter was utilized to investigate the fluorescence generated from modified glass surfaces. The excitation light is 340-380 nm.

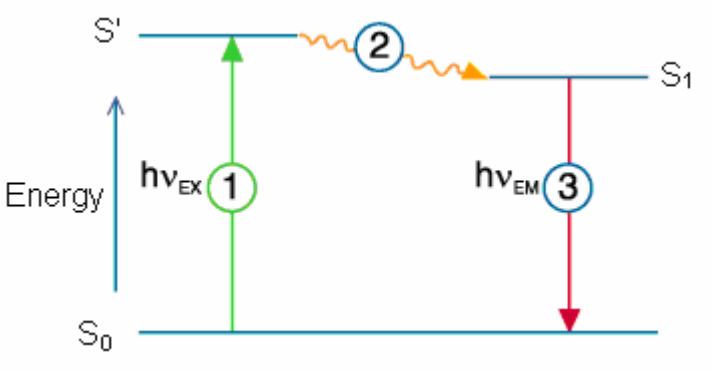

Figure 3-4. Schematic diagram of the fluorescence process; S_0, S' and S_1 represent ground state, excited state and emission state of electronic state respectively; process 1, 2 and 3 are the excitation process, energy loss, and emission process respectively.

3.6 X-ray Photoelectron Spectroscopy (XPS)

XPS is a widely used method of determining the chemical composition of a surface. Once radiation photons (usually Mg Kα radiation $h\nu$ = 1253.6 eV and Al Kα radiation $h\nu$ = 1486.6 eV are used as radiation sources) are absorbed by the atoms in materials on the solid surface, the atoms are ionized and core-level photoelectrons are released. The photoelectrons are collected and their energy is analyzed by an electron analyzer. Usually, XPS analysis results include two different formats: kinetic energy distribution and binding energy distribution of the emitted electrophotons. The relationship between these two energy forms is described as follows. The overall process of photoionization can be considered as follows:

$$A + h\nu = A^{+} + e- \quad (3\text{-}4)$$

where A represents atom; $h\nu$ is the energy of radiation photon; A^{+} is the ionized atom; and e^{-} is the escaping electrophoton from atom.

During the photoionization process, the conservation of energy requires that:

$$E(A) + h\nu = E(A^{+}) + E(e-) \quad (3\text{-}5)$$

Since the electron's energy is present solely as kinetic energy (KE), this can be rearranged to give the following expression for the KE of the photoelectron:

$$KE = h\nu - (E(A^{+}) - E(A)) \quad (3\text{-}6)$$

The final term in brackets, representing the difference in energy between the ionized and neutral atoms, is generally called the *binding energy* (BE) of the electron. This then leads to the following commonly quoted equation:

$$KE = h\nu - BE \quad (3\text{-}7)$$

Since each element has a unique set of binding energies, the presence of peaks at particular energies, therefore, indicates the presence of a specific element in the sample under study. Furthermore, the intensity of the peaks is related to the concentration of the element within the sampled region. Thus, the technique provides a quantitative analysis of the surface composition. Small shifts in these binding energies (chemical shifts) provide powerful information about sample chemical states and short-range chemistry.

In this research, ESCALAB 250 from Thermo VG Scientific with radiation source of Al Kα radiation $h\nu$ = 1486.6 eV is utilized to conduct the XPS investigation.

Chapter 4 The Mixing Quality of the Micromixer

The mixing quality is the most significant aspect for evaluating a micromixer. Two methods, COMSOL computational simulation and an experimental test of utilizing a pair of competitive reactions, are conducted in this chapter to compare the mixing quality of several mixers: IMM interdigital mixer, Tee mixer, and an OSU mixer. The former two mixers are commercially available and will be studied by both methods. The OSU mixer was only utilized for the experimental test.

4.1 COMSOL Simulation to Compare the Mixing Quality of Different Micromixers and to Assist the Design of the Micromixer

4.1.1 Simulation Rationale

Nowadays, computational fluid software such as COMSOL can model many flow phenomena with a high degree of accuracy. It provides a platform to investigate the feasibility of processes in microreaction, to optimize the reaction conditions to minimize the expense of time and money, or to help design an efficient microreactor. In this research, simulation software, COMSOL, is facilitated to compare the mixing quality of two kinds of micromixers, interdigital micromixer, and Tee mixer. Meanwhile parameterization is studied to help gain a comprehensive understanding of the hydrodynamic aspects involved in the mixing process that is crucial for optimization of the mixer designs. The numerical results presented in this work are based on the following assumptions:

(1) The fluid is incompressible, Newton and laminar flow.

(2) It is steady state.

(3) The reaction is a second order reaction.

Therefore, the following equations: incompressible Navier-Stokes equation (4-1), continuity equation (4-4) can be used to solve the velocity profile in the numerical solution method.

$$\frac{\partial u_i}{\partial t} + (\mathrm{v}\cdot\nabla)u_i = -\frac{1}{\rho}\nabla_i p + \frac{\eta}{\rho}\nabla^2 u_i \tag{4-1}$$

where $$(\mathrm{v}\cdot\nabla)u_i = u_x\frac{\partial u_i}{\partial x} + u_y\frac{\partial u_i}{\partial y} + u_z\frac{\partial u_i}{\partial z} \tag{4-2}$$

$$\nabla^2 u_i = \frac{\partial^2 u_i}{\partial x^2} + \frac{\partial^2 u_i}{\partial y^2} + \frac{\partial^2 u_i}{\partial z^2} \tag{4-3}$$

The continuity equation for incompressible fluids:

$$\nabla\cdot\mathrm{v} = 0 \tag{4-4}$$

And a convection-diffusion equation (4-5) is used to solve for the concentration field:

$$-D\nabla^2 c + u_i\cdot\nabla c = R \tag{4-5}$$

where $$R = -kc_1c_2 \tag{4-6}$$

Where: v- velocity vector;

u_i- fluid velocity in i direction (anyone among u_x, u_y or u_z)(m/s);

ρ-density (kg/m^3);

p-pressure (Pa);

η-dynamic viscosity (Pa/s);

D-diffusion constant (m^2/s);

c-concentration (mol/m^3);

R-reaction rate ($mol.m^{-3}.s^{-1}$);

k-reaction rate constant ($m^3.s^{-1}.mol^{-1}$).

The following reaction (4-7) is assumed to take place in the micromixers with different geometry designs. The concentrations of A, B and C are represented by c1, c2 and c3 respectively. The simulation will compare the outlet conversion of the product for all micromixers under the same parameters to figure out how the different micromixer design affects the result. From the perspective of synthesis throughput, the higher outlet conversion, the better the result is. From equation (4-5), it can be seen that diffusion, convection, and reaction are important parts affecting the concentration distribution. Therefore, diffusion constant D, inlet flowrate of each stream V, and reaction rate constant k are the key parameters to be studied to investigate their influences on outlet conversion of the product.

$$A+B \rightarrow C \tag{4-7}$$

4.1.2 Geometries of IMM and Tee Mixer and the Data Analysis Method

The geometries of IMM and Tee mixer are illustrated in figure 4-1 and 4-2 respectively. The dimensions are based on the real mixers.

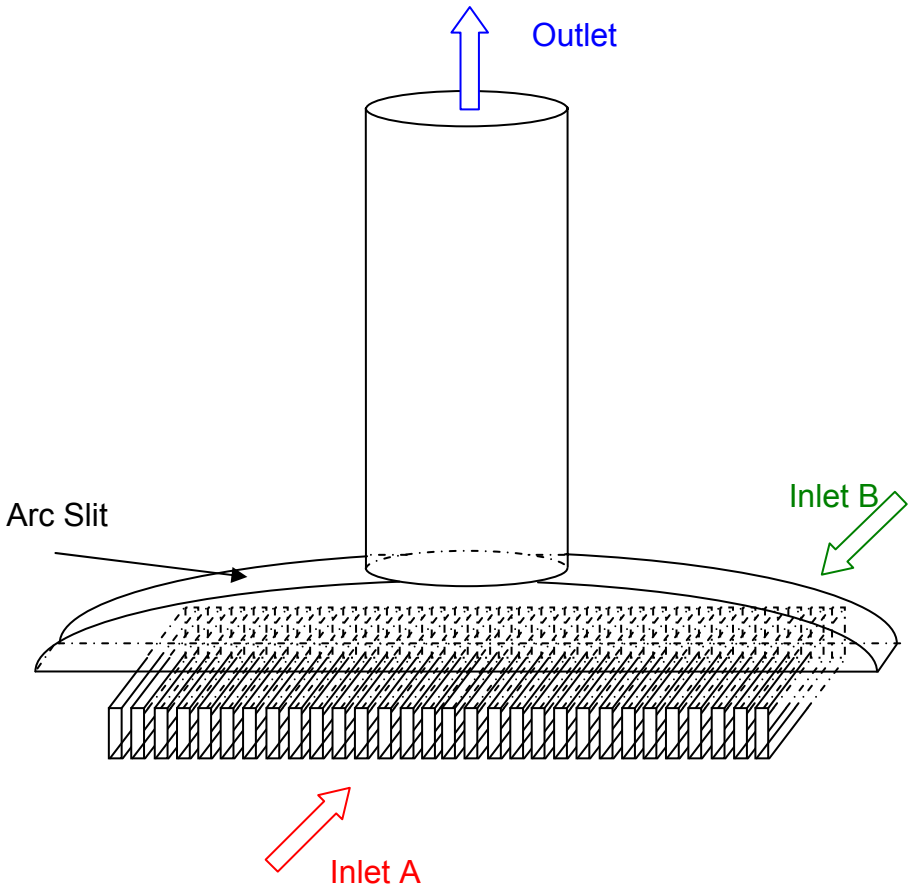

Figure 4-1 (A). 3D Illustration of IMM mixer.

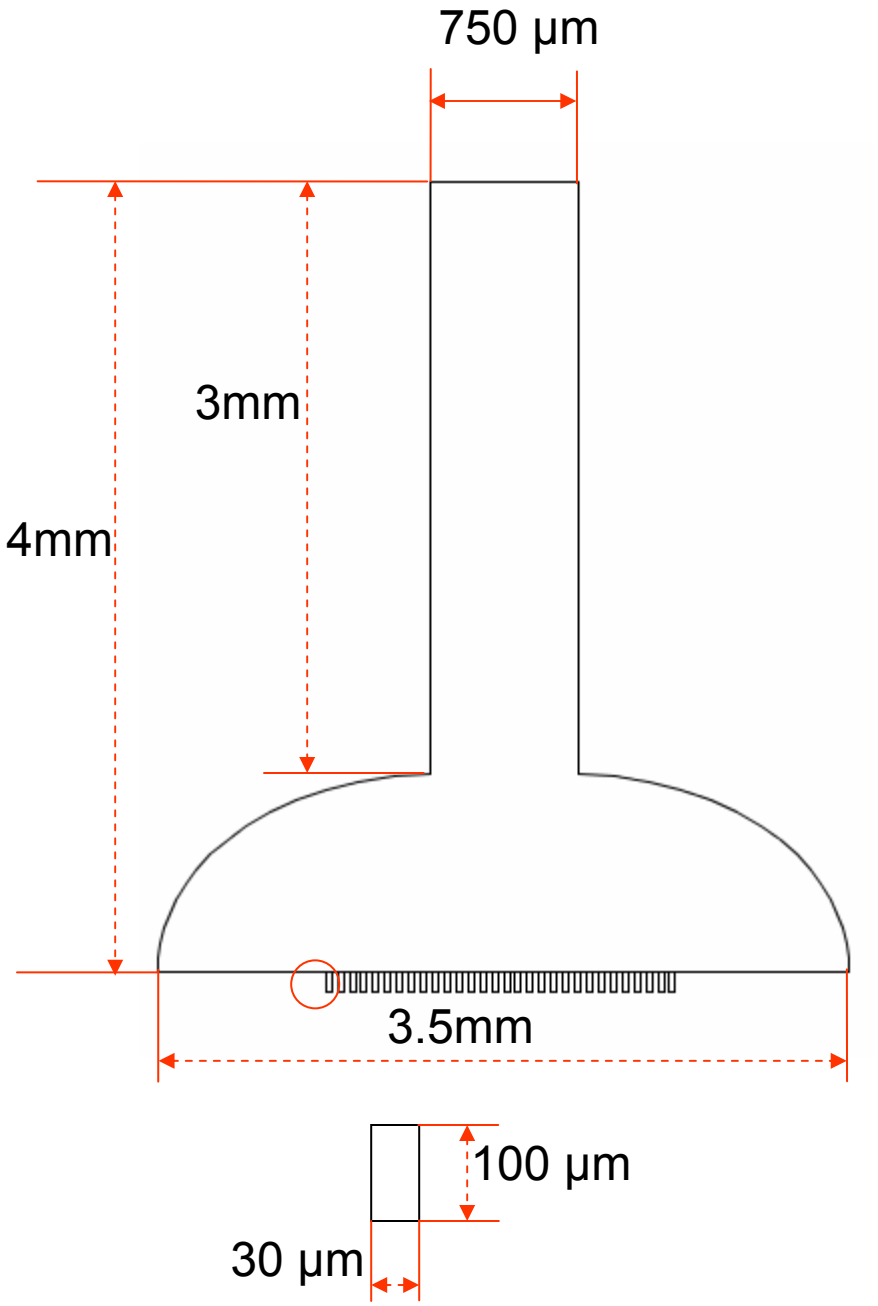

Figure 4-1 (B). Illustration of cross-section of IMM mixer used for COMSOL simulation.

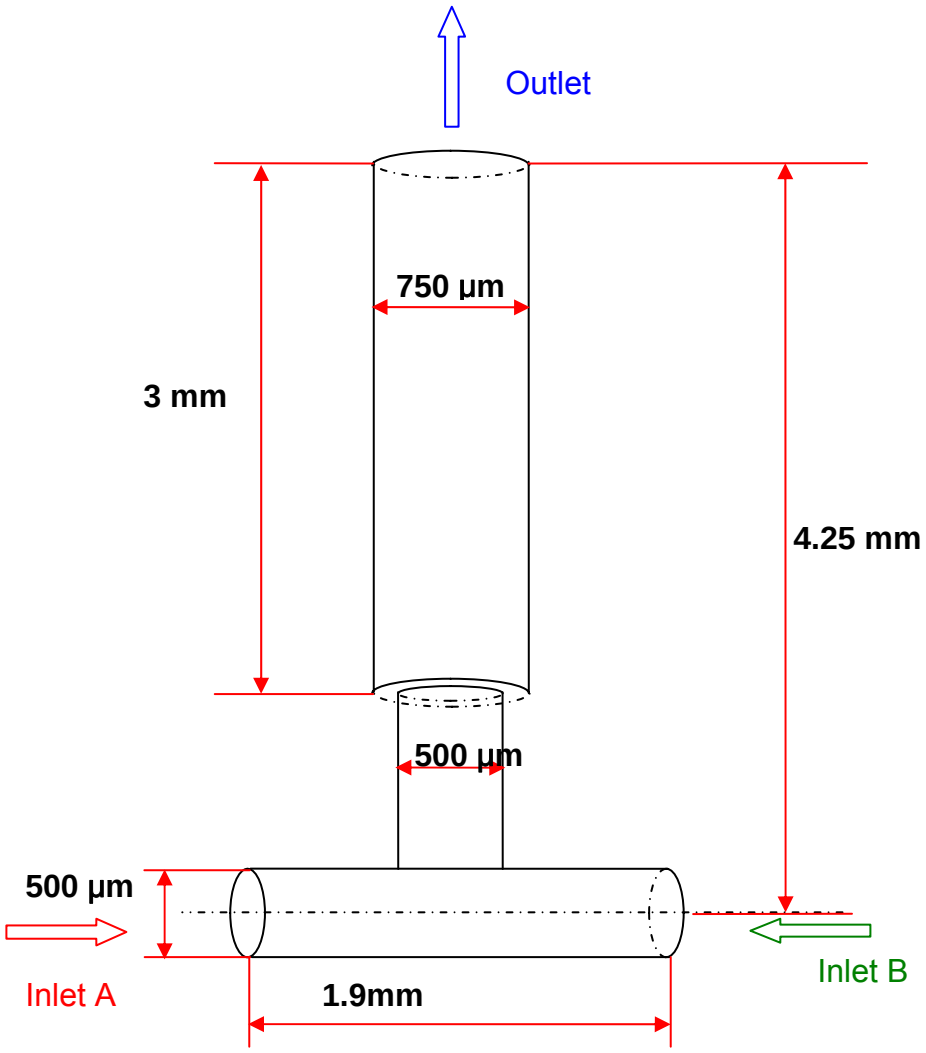

Figure 4-2. Illustration of Tee mixer geometry used for COMSOL simulation.

Figure 4-3 shows the concentration distribution of product C on the cross section of the IMM mixer and tubing simulated by COMSOL under a certain condition. Figure 4-4 is the concentration distribution of product C along the outlet of the tubing which is connected to the IMM mixer. In order to obtain the average concentration of product C at the outlet, the graph in figure 4-4 was exported as an Excel file. Averaging the numerical data of the concentration at each point of the outlet gives rise to the average outlet concentration. The conversion of product C is obtained as the quotient of the average outlet concentration to the ideal concentration of C. The ideal concentration of product C is defined as the concentration of C when the starting materials are completed converted, which is determined by the inlet concentration of the limiting reactant. For example, the inlet concentrations of reactants A and B were set to be 400 mol/m^3 and 1200 mol/m^3 for all simulations in this chapter, so the limiting reactant is A based on the stoichiometry of reaction 4-7. Therefore the ideal concentration of product C is one half (200 mol/m^3) of the inlet concentration of A due to the equal volume flowrate input of two streams of reactants. The above is the general method of obtaining the outlet conversion of product C for simulations under all conditions including both the IMM mixer and the Tee mixer.

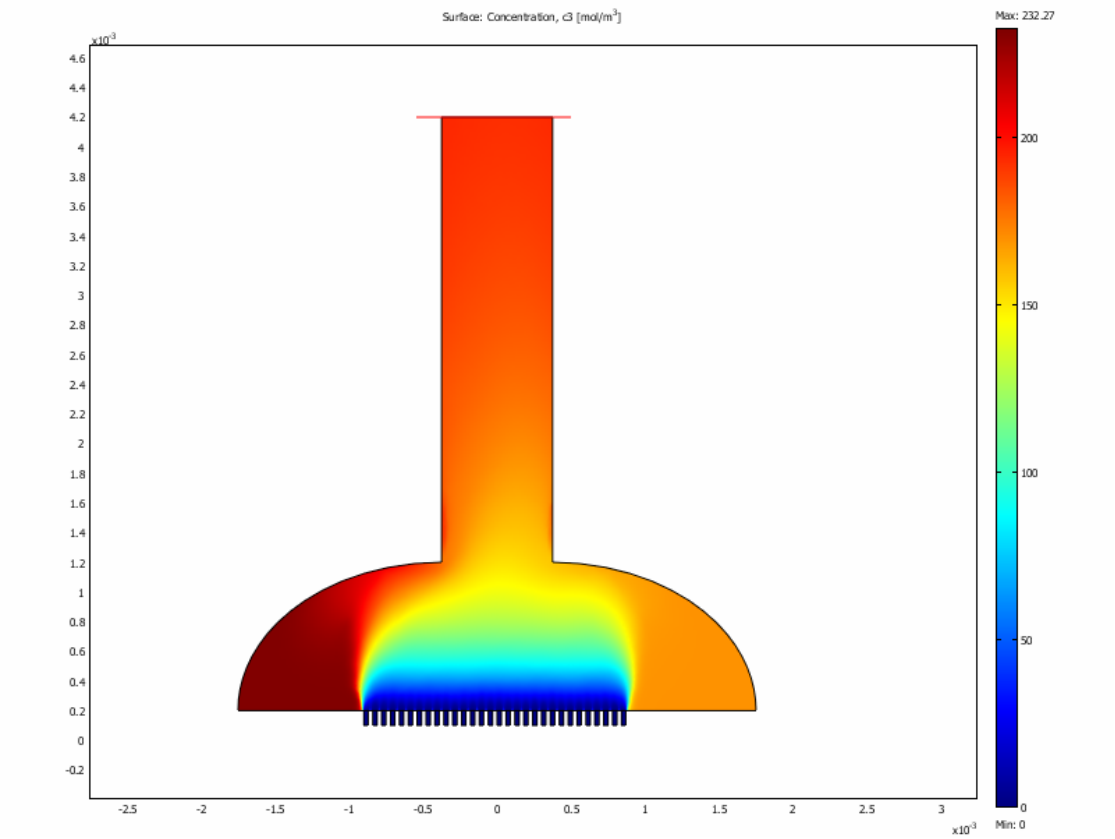

Figure 4-3. The concentration distribution of product C on the cross section of IMM mixer and tubing simulated by COMSOL under a certain condition: k=1 $m^3/(mol.s)$, V=1.56 ml/min and D=1e-9 m^2/s.

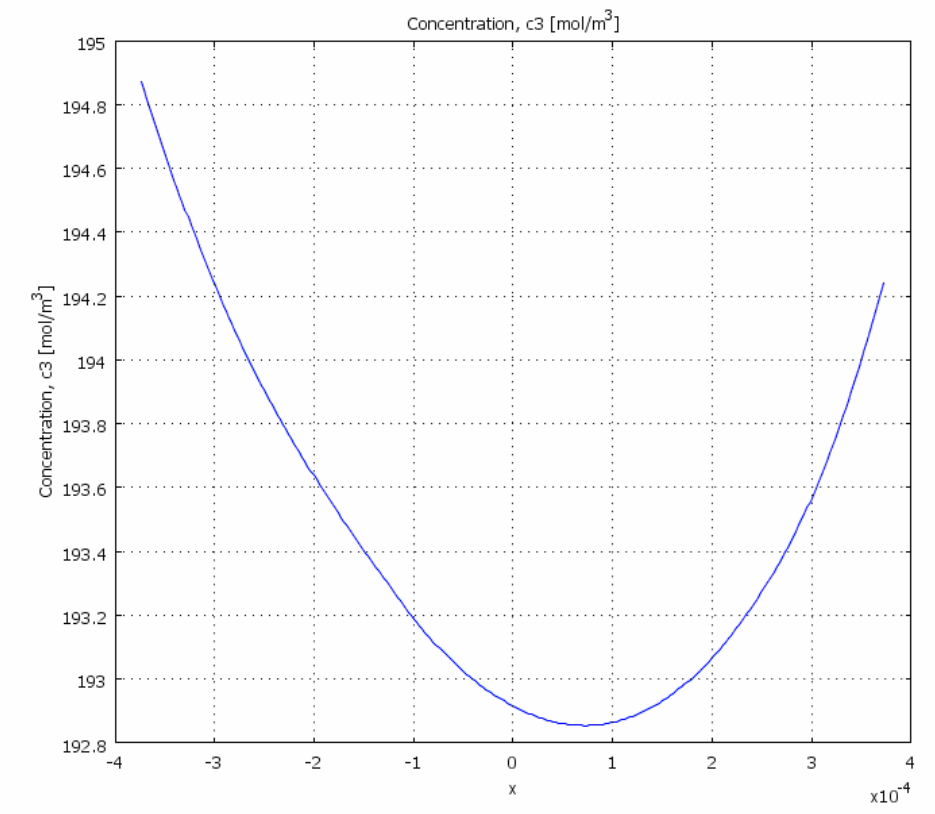

Figure 4-4. The concentration distribution of product C along the outlet of the tubing which is connected to the IMM mixer shown in figure 4-3; the average concentration of product C at the outlet is calculated in Excel to be193 mol/m^3.

Figure 4-5 and 4-6 show the concentration distribution of product C on the cross section and outlet of the Tee mixer. The simulation results were obtained under the same parameter conditions as the IMM mixer. Apparently, the concentration of product C produced via the Tee mixer is much less than the IMM mixer. The method to acquire the average concentration of product C and its conversion at the outlet of the Tee mixer is similar to what was described above for the IMM mixer.

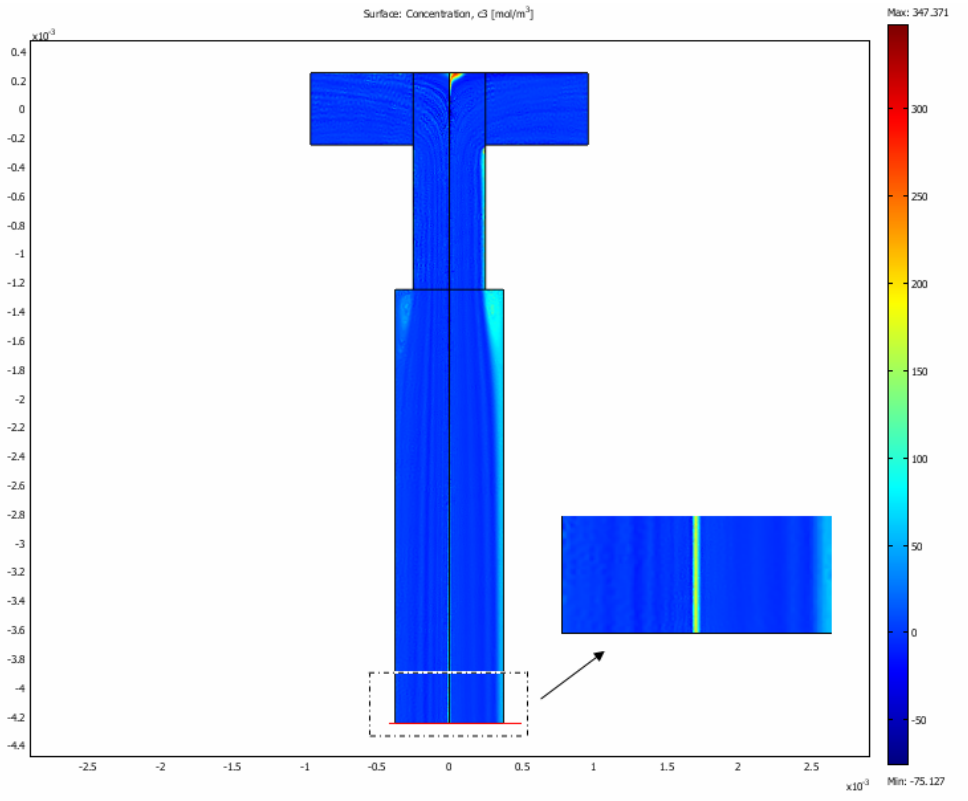

Figure 4-5. The concentration distribution of product C on the cross section of the Tee mixer simulated by COMSOL under the same condition as the IMM mixer: k=1 m^3/(mol.s), V=1.56 ml/min and D=1e-9 m^2/s.

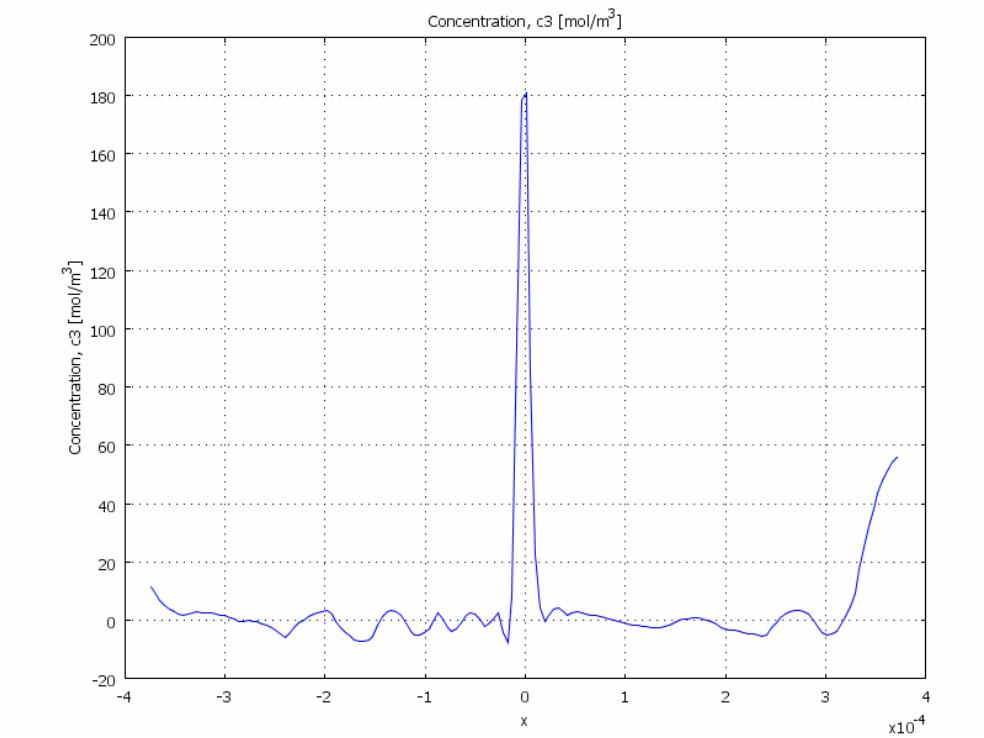

Figure 4-6. The concentration distribution of product C along the outlet of the tubing which is connected to the Tee mixer shown in figure 4-5. The average concentration at outlet is 1.43 mol/m^3. Only the center area of the Tee mixer produce product C, but the reaction does not occur on the rest areas of the outlet due to no interfacial area for reactants to collide.

4.1.3 The Influence of the Diffusivity on the Synthesis Throughput

Figures from 4-7 to 4-12 show the simulation results of the interdigital mixer and the Tee mixer when the diffusion coefficient D is the variant while other parameters are kept constant. The mass diffusion coefficient of most liquid species is in the order of 10^{-9} m^2/s. In order to investigate the influence of the diffusivity on the synthesis throughput, four values of diffusivity: 10^{-9} , 10^{-8} , 10^{-7} and10^{-6} m^2/s were chosen for study. The simulations were conducted at two different

reaction rate constants: k=0.001 and k=1 m^3/(mol.s) to investigate how the diffusivity influences the throughput under different reaction kinetics. Figures 4-7 and 4-8 show the concentration distribution of product C along the outlet of the tubing of the IMM mixer and the Tee mixer respectively under different diffusivities when the reaction constant k=0.001 m^3/(mol.s). Figures 4-10 and 4-11 show the concentration distribution of product C along the outlet of the tubing of the IMM mixer and the Tee mixer respectively under different diffusivities when the reaction constant k=1 m^3/(mol.s). Figures 4-9 and 4-12 summarized the influence of diffusivity on the conversion of product C at outlets of the IMM mixer and the Tee mixer when k= 0.001 and k=1 respectively.

From the figures showing the concentration distribution (figures 4-7, 4-8, 4-10 and 4-11), it is seen that the IMM mixer shows relatively even spreads of concentration along the outlet under all diffusivities, but the Tee mixer shows an uneven concentration distribution with high concentration in center and low or zero concentration on other zones. This is because the IMM mixer is featured with large interfacial areas for reactant molecules to contact, but the Tee mixer only provides the center areas for molecules to collide and react.

Focusing on figures 4-9 and 4-12, the influence of diffusivity on throughput under different reaction kinetics can be concluded. A same trend of the influence of diffusivity on throughput is found for the IMM mixer when the reaction rate constant k changes from 0.001 and 1. The interdigital micromixer has almost a constant performance in the diffusion coefficient range of D=1e-9 to D=1e-6 m^2/s

under both ks. The outlet conversion of the product reaches 96.7% at all diffusion constants from D=1e-9 to D=1e-6 m^2/s when k=1 (see figure 4-12). On the other hand, the Tee mixer shows an abrupt increase of outlet conversion when D increases from 1e-7 to 1e-6 m^2/s under both reaction rate constants. Under both circumstances, the outlet conversion of C synthesized from the interdigital mixer is much higher than the Tee mixer. For example, when k=0.001, it is 81, 28, 8.8 and 1.4 times higher than that from the Tee mixer when D=1e-9, 1e-8, 1e-7 and 1e-6 m^2/s respectively.

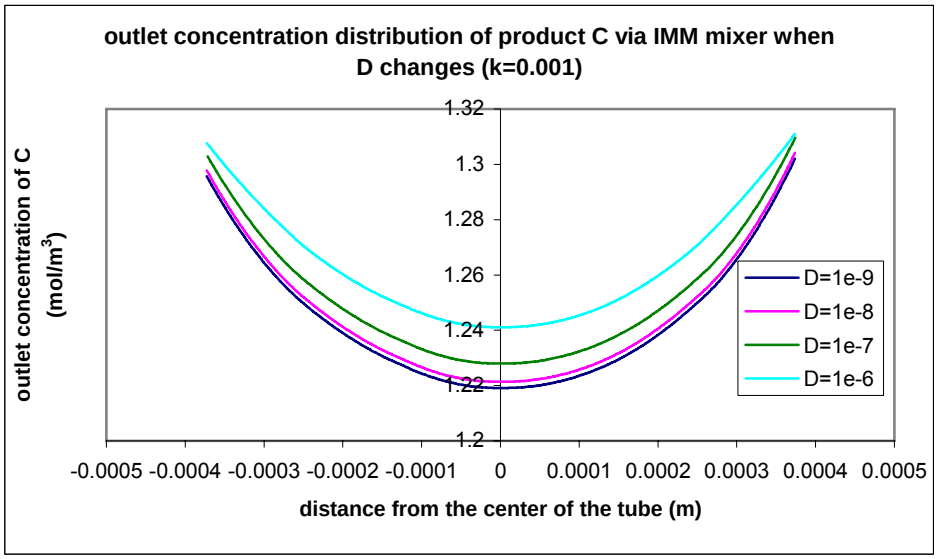

Figure 4-7. The concentration distribution of product C produced via the IMM mixer along the outlet of the tubing connected with the mixer under different diffusivities; k=0.001 $m^3/(mol.s)$, V=1.56 ml/min.

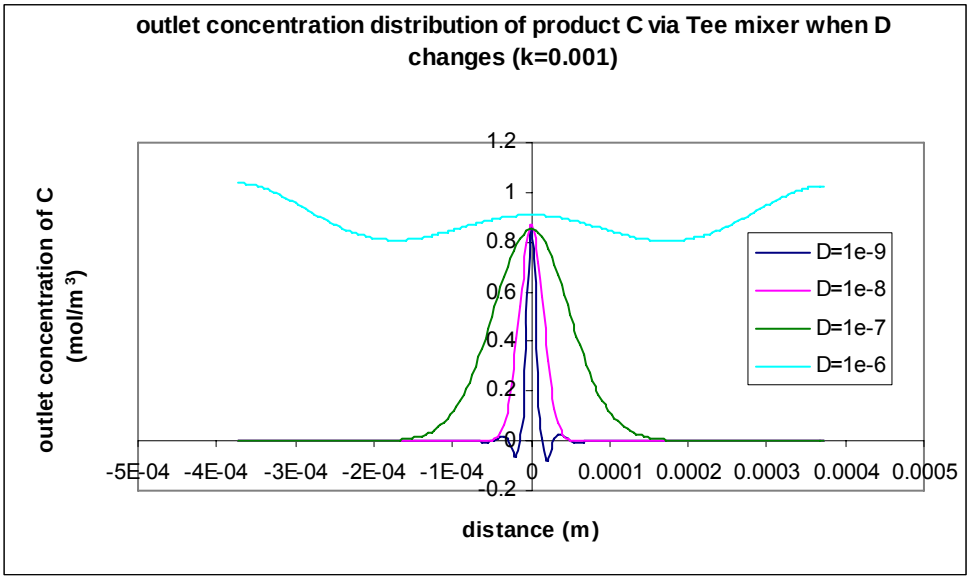

Figure 4-8. The concentration distribution of product C produced via the Tee mixer along the outlet of the tubing connected with the mixer under different diffusivities; k=0.001 m^3/(mol.s), V=1.56 ml/min.

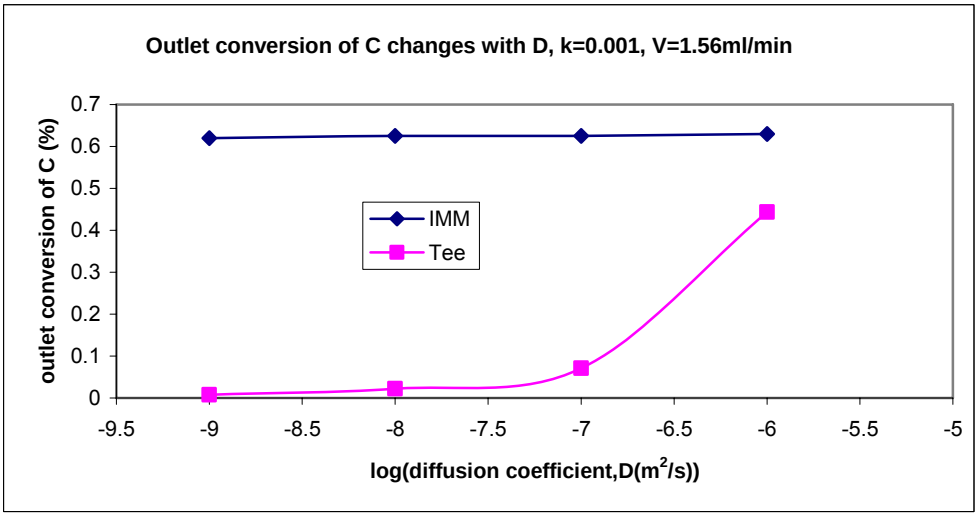

Figure 4-9. Comparison of the Tee mixer and the IMM interdigital mixer when the diffusion coefficient D is changed from 1e-9 to 1e-6 m^2/s and other parameters are kept constant: k=0.001 $m^3.mol^{-1}.s^{-1}$; flowrate V=1.56 ml/min.

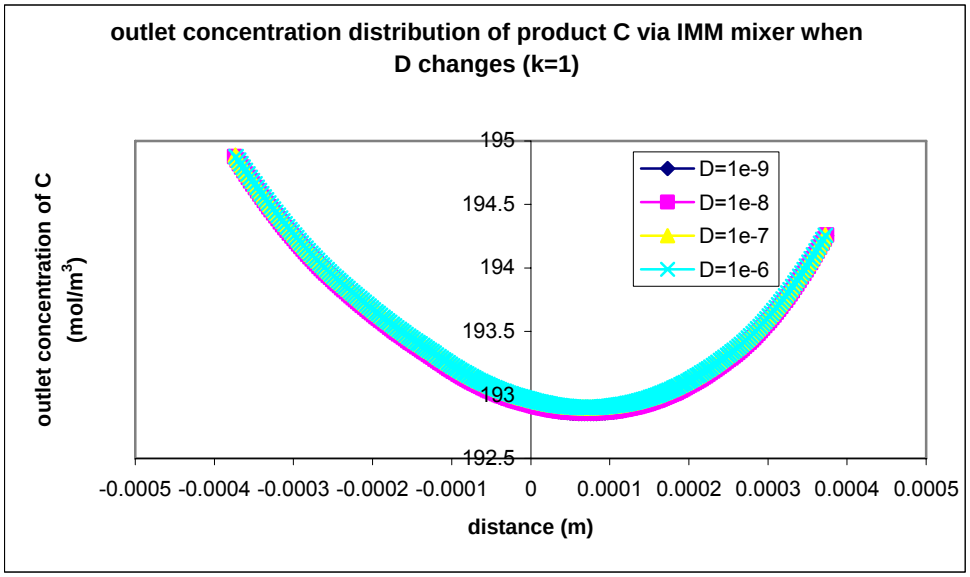

Figure 4-10. The concentration distribution of product C produced via the IMM mixer along the outlet of the tubing connected with the mixer under different diffusivities; k=1 m^3/(mol.s), V=1.56 ml/min.

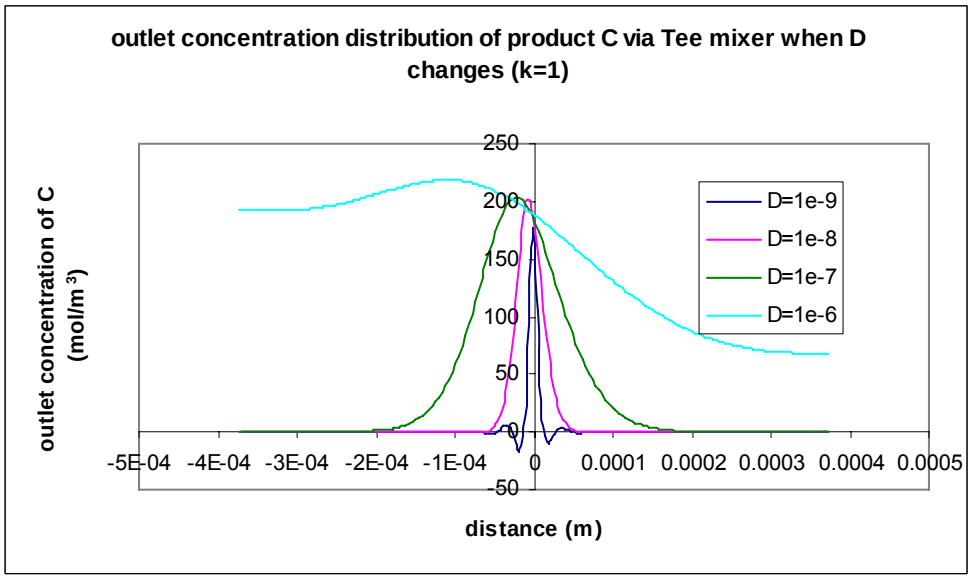

Figure 4-11. The concentration distribution of product C produced via the Tee mixer along the outlet of the tubing connected with the mixer under different diffusivities; k=1 m^3/(mol.s), V=1.56 ml/min.

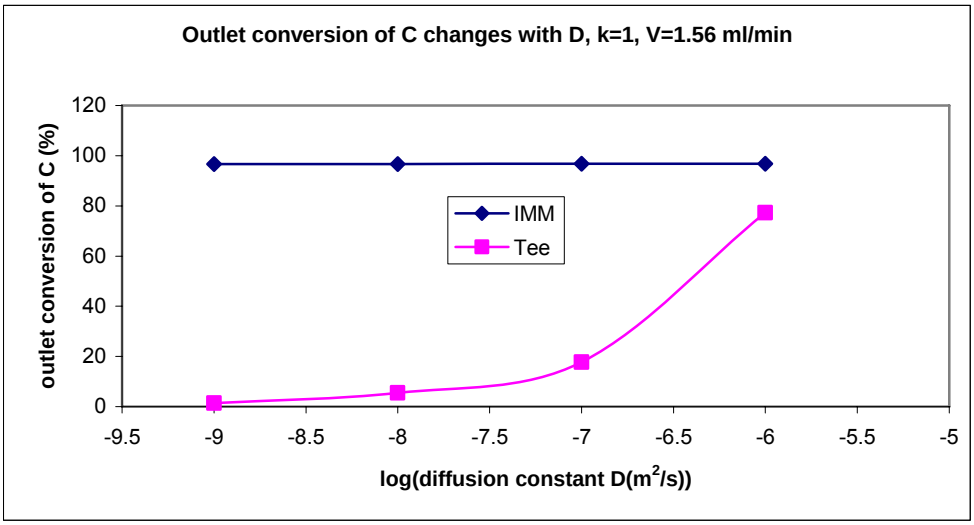

Figure 4-12. Comparison of the Tee mixer and the IMM interdigital mixer when the diffusion coefficient D is changed from 1e-9 to 1e-6 m^2/s and other parameters are kept constant: k=1 $m^3.mol^{-1}.s^{-1}$; flowrate V=1.56 ml/min.

The constant performance of the IMM interdigital mixer under all different diffusion coefficients is due to the quick mixing taking place in the mixer. The reactants can mix with each other effectively even with a small diffusion coefficient, such as D=1e-9 m^2/s. In contrast, the Tee mixer cannot perform an effective mixing; therefore diffusivity plays a very important role to improve mixing in the Tee mixer. However, the diffusion coefficient of most liquids is around 1e-9 m^2/s, so the interdigital micromixer will perform a significantly better result than the Tee mixer for most liquid reaction regarding to synthesis throughput.

4.1.4 The Influence of the Reaction Constant on the Synthesis Throughput

The reaction constants of second order organic reactions are reported in a wide range from 10^{-6} [24] to 10^{4} m^3/(mol.s) [25]. Here four values of k, 0.001, 0.01, 0.1 and 1 m^3/(mol.s) are used to simulate. The concentration distributions of product C along the outlet of the tubing under different reaction constants while D and V kept constants are shown in figures 4-13 and 4-14 for the IMM mixer and the Tee mixer respectively. Again, the concentration of product C produced via the interdigital mixer is spread evenly along the outlet of the tubing. In contrast, it shows only the center area of the tubing has the product C via the Tee mixer. Figure 4-15 summarized the comparison of the Tee mixer and the IMM interdigital mixer about how the reaction constant influences throughput when k is changed from 0.001 to 1 $m^3/mol.s^{-1}$ and other parameters are kept constant: D=1e-9 m^2/s, flowrate V=1.56 ml/min.

Obviously, the reaction constant, k, affects the outlet conversion of C significantly for both mixers. The outlet conversion of C increased 156 and 188 times for the IMM mixer and the Tee mixer respectively when k increased from k=0.001 to k=1 m^3/(mol.s). Although the Tee mixer has a tremendous increase of 188 times, the absolute outlet conversion of C is only 1.4% when k=1 m^3/(mol.s), which is much lower than its counterpart, the IMM mixer of 97%. This is because the poor mixing quality of the Tee mixer cannot effectively bring reactant molecules to contact each other; therefore, little reaction occurs even though the reaction rate constant is big. However, the IMM mixer can provide sufficient

mixing; therefore, the diffusion is not the limiting factor, and the throughput is high as long as the reaction kinetic is fast enough.

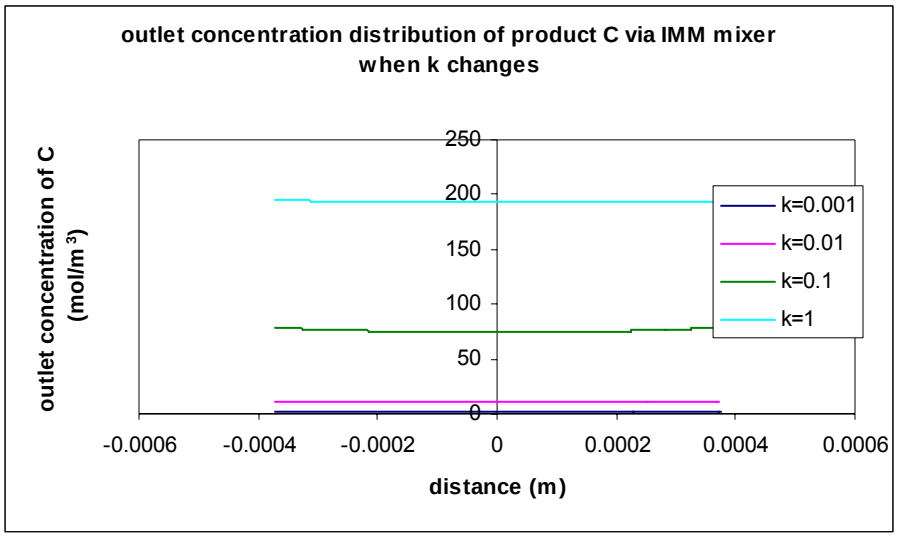

Figure 4-13. The concentration distribution of product C produced via the IMM mixer along the outlet of the tubing connected with the mixer under different reaction constants; D=1e-9 m^3/(mol.s), V=1.56 ml/min.

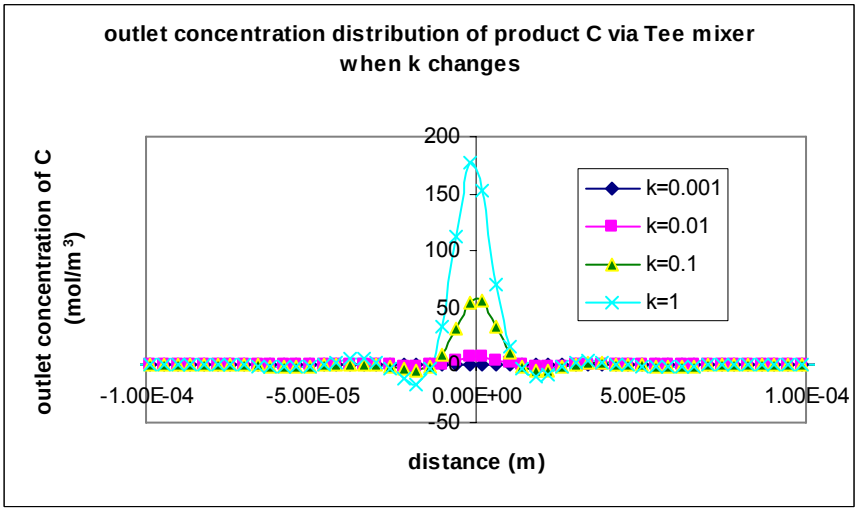

Figure 4-14. The concentration distribution of product C produced via the Tee mixer along the outlet of the tubing connected with the mixer under different reaction constants; D=1e-9 m^3/(mol.s), V=1.56 ml/min.

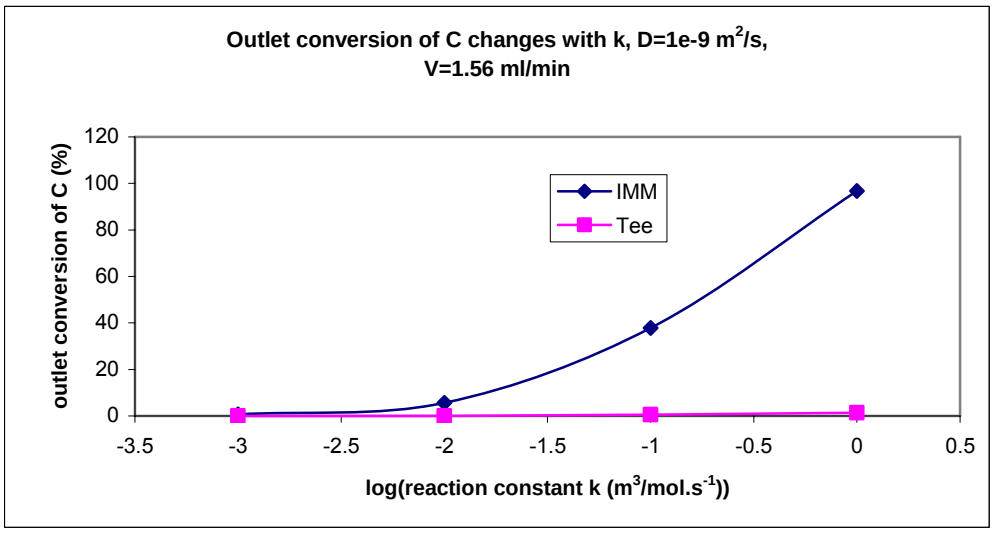

Figure 4-15. Comparison of the Tee mixer and the IMM interdigital mixer when the reaction constant k is changed from 0.001 to 1 $m^3/mol.s^{-1}$ and other parameters are kept constant: D=1e-9 m^2/s, flowrate V=1.56 ml/min

4.1.5 The Influence of the Flowrate on the Synthesis Throughput

Figures from 4-16 to 4-21 show the simulation results of the interdigital mixer and the Tee mixer when the flowrate V of each stream is the variant while other parameters are kept constant. The simulations were conducted at two different reaction rate constants: k=0.001 and k=1 $m^3/(mol.s)$ to investigate how the flowrate influences the throughput under different reaction kinetics. Figures 4-16 and 4-17 show the concentration distribution of product C along the outlet of the tubing of the IMM mixer and the Tee mixer respectively under different flowrates when the reaction constant k=0.001 $m^3/(mol.s)$. Figures 4-19 and 4-20 show the concentration distribution of product C along the outlet of the tubing of the IMM

mixer and the Tee mixer respectively under different flowrates when the reaction constant k=1 m^3/(mol.s). Figures 4-18 and 4-21 summarized the influence of the flowrate on the conversion of product C at outlets of the IMM mixer and the Tee mixer when k= 0.001 and k=1 respectively.

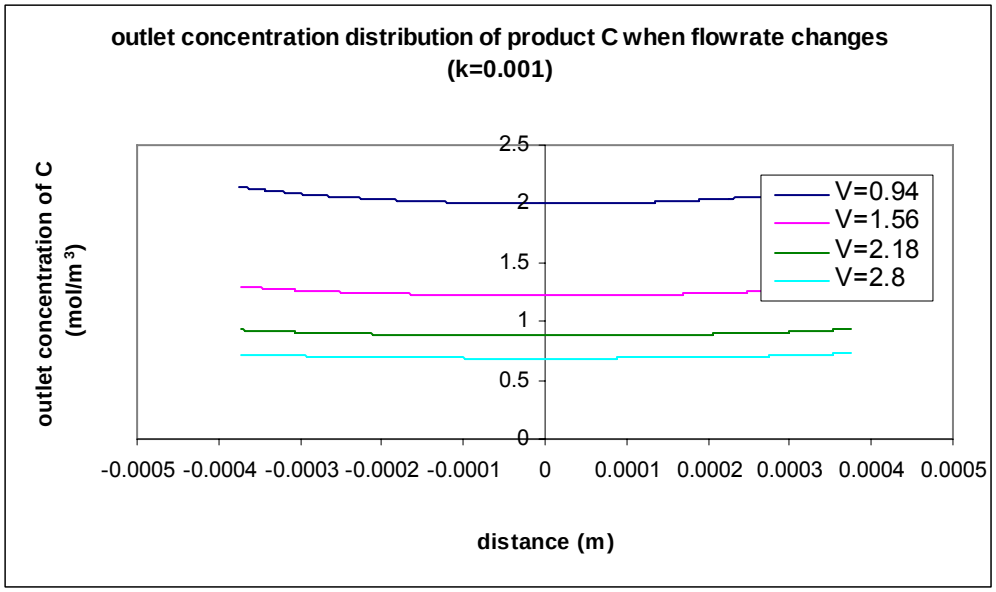

Figure 4-16. The concentration distribution of product C produced via the IMM mixer along the outlet of the tubing connected with the mixer under different flowrates; D=1e-9 m^2/s, k=0.001 m^3/(mol.s).

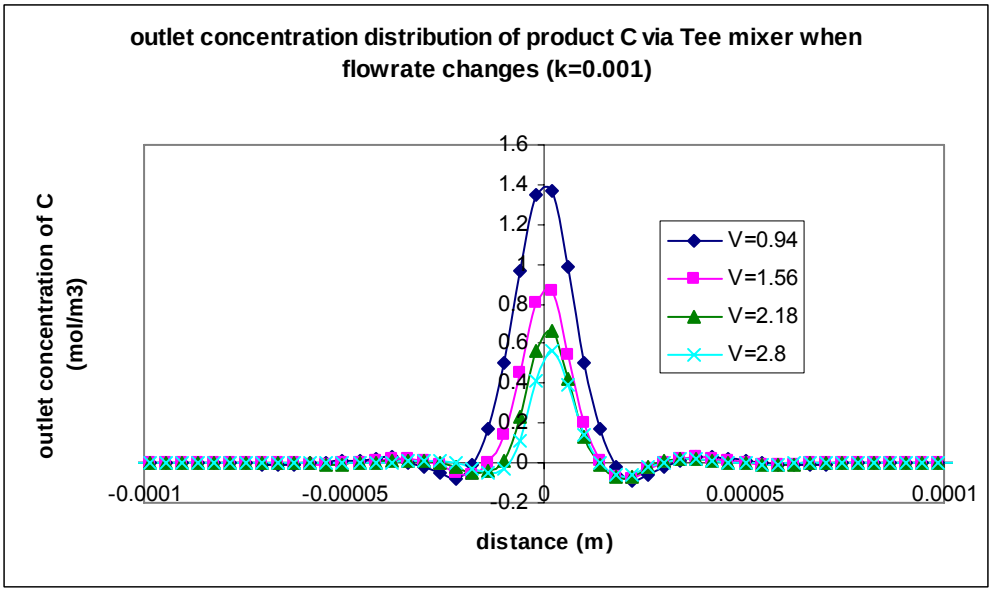

Figure 4-17. The concentration distribution of product C produced via the Tee mixer along the outlet of the tubing connected with the mixer under different flowrates; D=1e-9 m^2/s, k=0.001 $m^3/(mol.s)$.

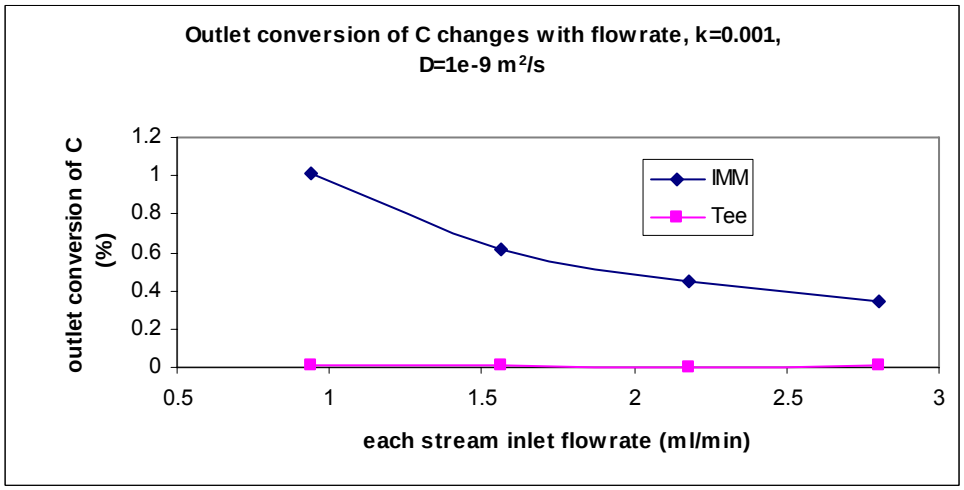

Figure 4-18. Comparison of the Tee mixer and the interdigital mixer when the inlet flowrate is changed from 0.94 to 2.8 ml/min and other parameters are kept constant: k=0.001 $m^3.mol^{-1}.s^{-1}$; D=1e^{-9} m2/s.

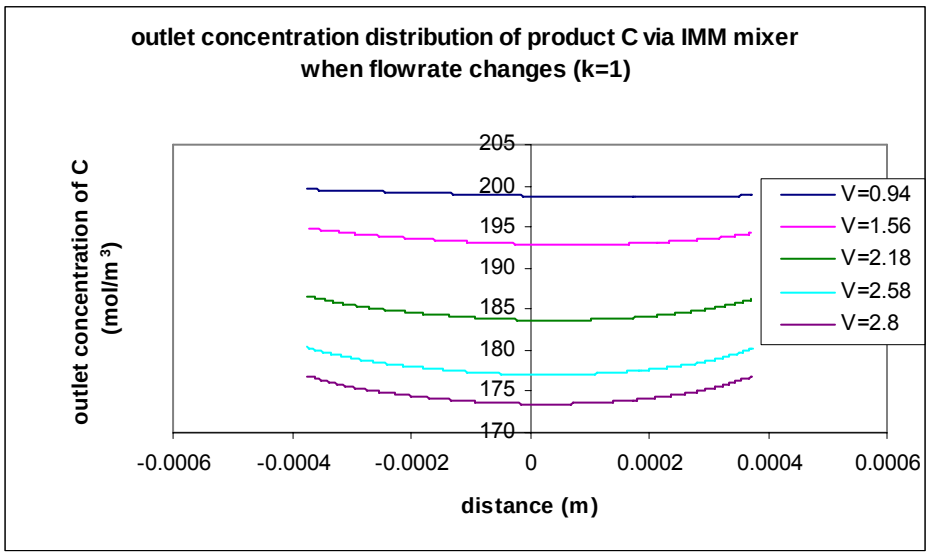

Figure 4-19. The concentration distribution of product C produced via the IMM mixer along the outlet of the tubing connected with the mixer under different flowrates; D=1e-9 m^2/s, k=1 $m^3/(mol.s)$.

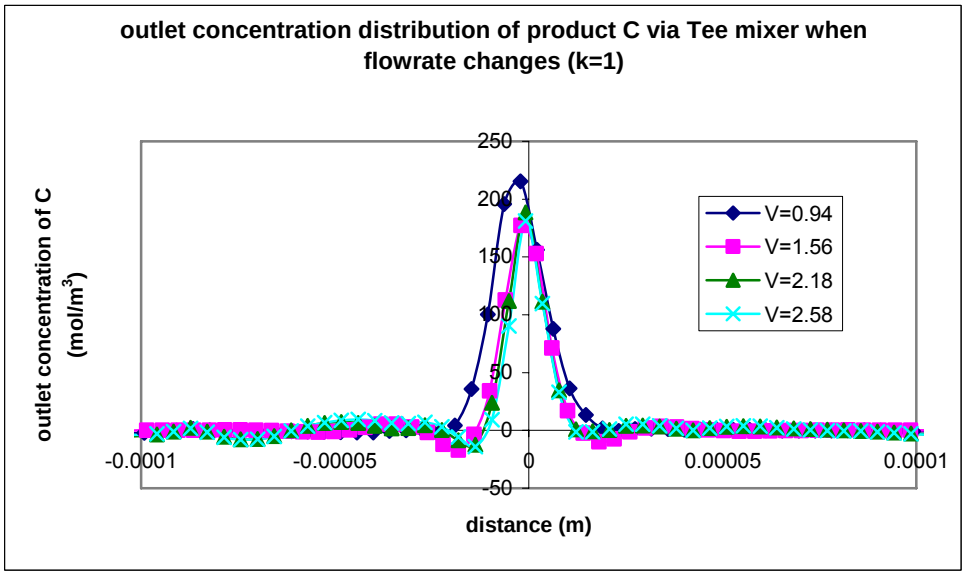

Figure 4-20. The concentration distribution of product C produced via the Tee mixer along the outlet of the tubing connected with the mixer under different flowrates; D=1e-9 m^2/s, k=1 $m^3/(mol.s)$.

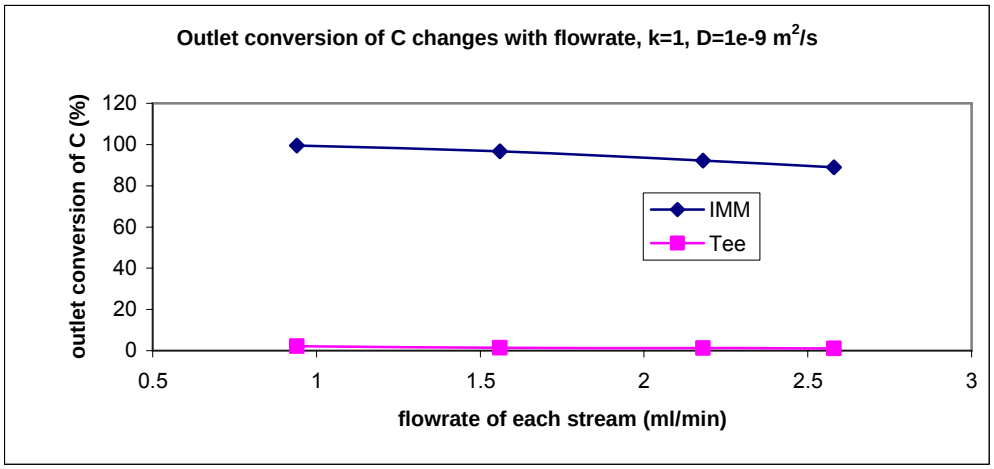

Figure 4-21. Comparison of the Tee mixer and the IMM interdigital mixer when the inlet flowrate is changed from 0.94 to 2.6 ml/min and other parameters are kept constant: k=1 $m^3.mol^{-1}.s^{-1}$; D=1e^{-9} m^2/s.

Apparently, the conversion of product C synthesized from interdigital micromier is much higher than that from the Tee mixer at all flowrates from 0.94 to 2.8 ml/min under both low and high reaction constants. The conversion of C declines with the increase of the flowrate at low reaction constant (figure 4-18), and it decreased 66% and 75% for the IMM and the Tee mixer respectively. This is because that faster flowrate decreases the residence time, which cannot provide a sufficient residence time for the reaction to be completed at low reaction constant. On the other hand, the flowrate has less effect on the conversion for IMM mixer at high reaction constant and the conversions decreased 10% from 0.94 to 2.6 ml/min (figure 4-21), but the conversion of C decreased 51% for the Tee mixer when the flowrate is in the same range at k=1 m^3/(mol. s). The reaction with the high

reaction constant is efficient and does not need a long residence time to be completed as long as the reactants are well mixed. This explains the simulation result from the IMM interdigital mixer shown in figure 4-21. The tee mixer cannot provide sufficient mixing, so even at the high reaction constant, the reduced residence time due to the increased flowrate still decreases the conversion dramatically.

4.2 The Principle of the Measurement of Mixing Quality of the Micromixer

The mixing quality is the most important aspect of the micromixer. The measurement of the mixing quality of a micromixer is based on a pair of known competing reactions (Dushman reaction) shown in figure 4-22. The neutralization reaction (reaction 4-8) between acid and sodium acetate is an ultrafast process and will always mask the slower process, namely the formation of iodine (reaction 4-9). The generated iodine (I_2) can combine with iodide ions (I^-) to form complex of I_3^- which has two pronounced UV absorption peaks at 352 nm and 290 nm. If the mixing quality is good, there is no local excess of acid and therefore the formation of iodine will be masked. By measuring the concentration of I_3^- by means of UV-vis absorption using a 1cm cuvette, the extent of mixing can be characterized. The more UV absorption due to iodine formation, the worse is the mixing quality. The UV absorption at 352 nm was chosen to compare the mixing quality of different mixers.

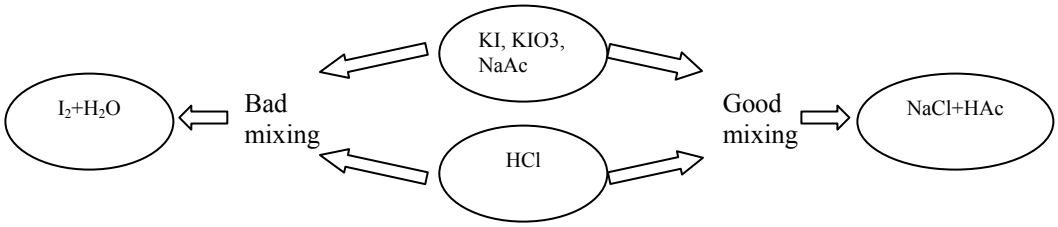

$$H^+ + Ac^- \rightarrow HAc \qquad \text{(ultrafast)} \qquad (4\text{-}8)$$

$$5\,I^- + IO_3^- + 6H^+ \rightarrow 3I_2 + 3H_2O \qquad \text{(fast)} \qquad (4\text{-}9)$$

$$I^- + I_2 \rightarrow I_3^- \ \text{(yellow)} \qquad (4\text{-}10)$$

Figure 4-22. Reactions for the characterization of the mixing quality of the continuous flow micromixer

4.2.1 Experimental Measurements of Different Micromixers

Three stock solutions were prepared: 100ml of 0.1374 mol/l HCl solution, 50 ml of 0.0319mol/L KI/1.33mol/L NaAc solution, and 50 ml of 0.00635 mol/L KIO3/1.33 mol/L NaAc solution. Equal amounts of the last two solutions were combined immediately before the measurement, and then 1.7 ml of the combined solution was pumped into the syringe of a Kloehn pump. 1.7 ml of HCl solution was pumped into the syringe of another Kloehn pump. These two solutions were introduced into the micomixer at the same flowrate. Three different micromixers: the Tee mixer (purchased from UPCHURCH), the OSU mixer (fabricated by Dr. Brian Paul's research group in the Mechanical and Industrial Department at OSU), and the IMM interdigital mixer were tested for mixing quality. The measurements were conducted at the same conditions including the same temperature at 25 ^{o}C.

All of the mixers were connected with outlet tubings which have the same volume, 0.185 ml. Therefore, mixed solutions from all of the mixers have same residence time at a certain flowrate. UV-vis characterization was conducted off-line with quick operation by two operators in order to minimize the time delay between the mixing and the measurement. One operator took charge of the collection of the mixed solution into a cuvette, and another operator was in charge of the UV-vis software for data acquisition. The data acquisition was conducted as quickly as possible because the time delay between the mixing and the measurement will cause the increase of the iodine amount due to the slow HAc-catalyzed reaction.

The UV-vis instrument used for the measurement is an Ocean Optics USB2000 with a plastic 1 cm cuvette.

4.2.2 Mixing Measurement Results and Comparison

The UV-vis absorption spectra of iodine obtained from the three mixers at different flowrates (inlet flowrate of each stream) are shown in figure 4-23, 4-24 and 4-25 respectively.

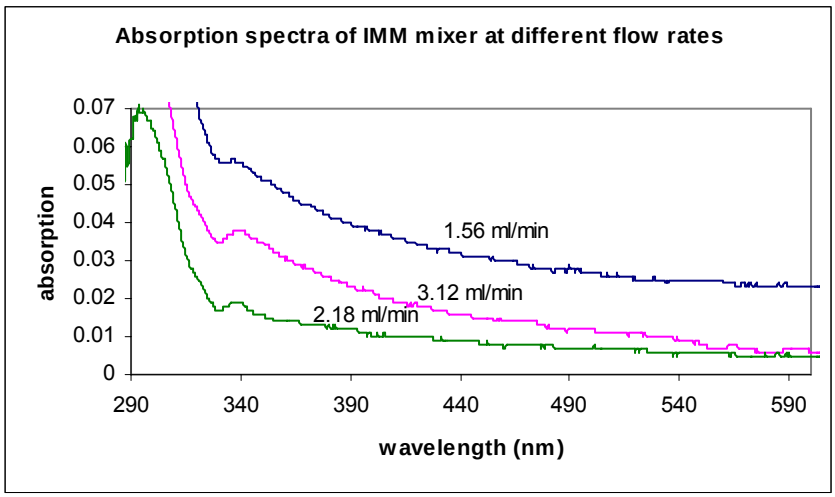

Figure 4-23. UV-vis absorption spectra of iodine obtained from the interdigital micromixer at different flowrates.

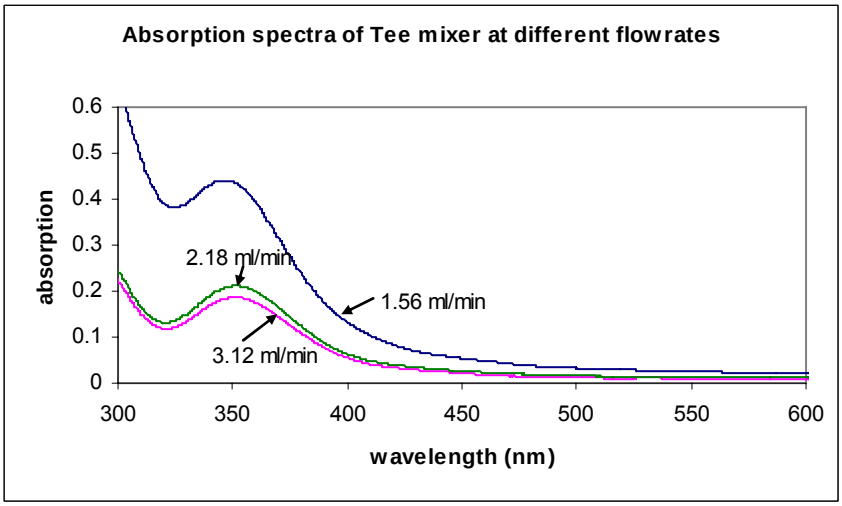

Figure 4-24. UV-vis absorption spectra of iodine obtained from the Tee mixer at different flowrates.

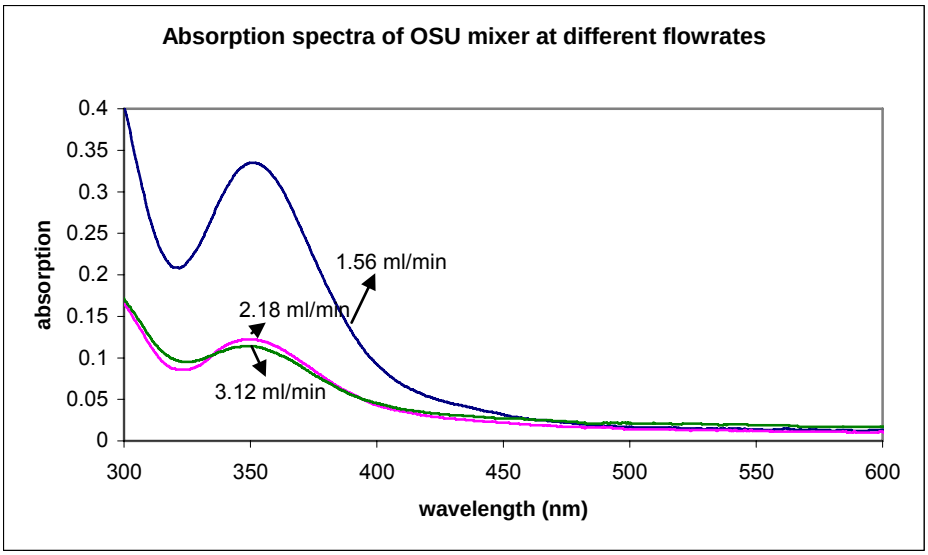

Figure 4-25. UV-vis absorption spectra of iodine obtained from the OSU mixer at different flowrates.

The absorptions at 352 nm versus flowrate for these three micromixers are illustrated in figure 4-26. It shows that the mixing quality of the interdigital micromixer is obviously better than the other two mixers over all flowrates, and the OSU mixer is ranked the second among these three. This is attributed to the multilamination principle of the interdigital micromixer, which accelerates the mass transfer between the reactant lamella. Moreover, the figure 4-26 also shows that the absorption decreases with the increasing flowrate for all of these three mixers. Especially, the absorption declines substantially at the low flowrate range, such as in the flowrate range of 1.56-2.18 ml/min. The extent of the decrease becomes less at the high flowrate range from 2.18 ml/min to 3.12 ml/min.

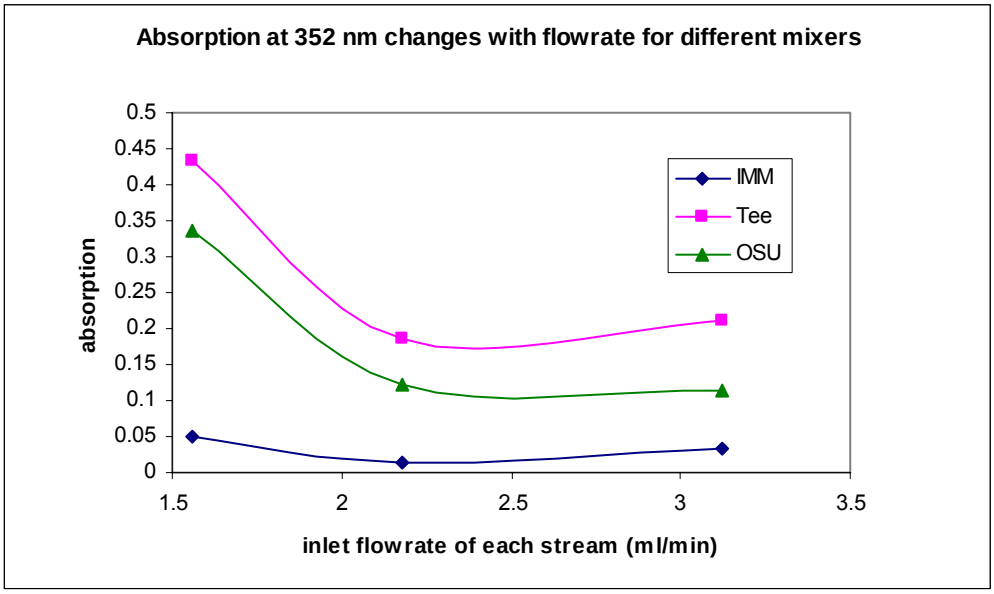

Figure 4-26. Comparison of UV-vis absorption (at 352 nm) of iodine collected from the interdigital micromixer, the OSU mixer, and the Tee mixer at different flowrates.

Originally, two possibilities were believed to be causing the bad mixing quality at low flow rates. The first possibility is the longer time delays between the mixing and the measurement at low flow rates. Once solutions are mixed through micromixers, HAc is formed and as an acid it will slowly catalyze the iodine formation reaction, though the reaction rate is much slower compared with the involvement of strong acid, HCl. The lower flowrate, the longer time delay between mixing and measurement, is causing more formation of iodine. This effect is experimentally verified by measuring the time dependence of the absorption of a well-mixed sample: a sample was mixed via the IMM mixer at a flowrate of 2.18 ml/min, and the absorption at 352 nm changing with time was monitored. A linear

relationship between the absorption and the time resulted and is shown in figure 4-27. The absorption A is correlated with the time t (minute) in a relation shown in equation 4-11.

$$A = 0.0014t + 0.0088 \qquad (4\text{-}11)$$

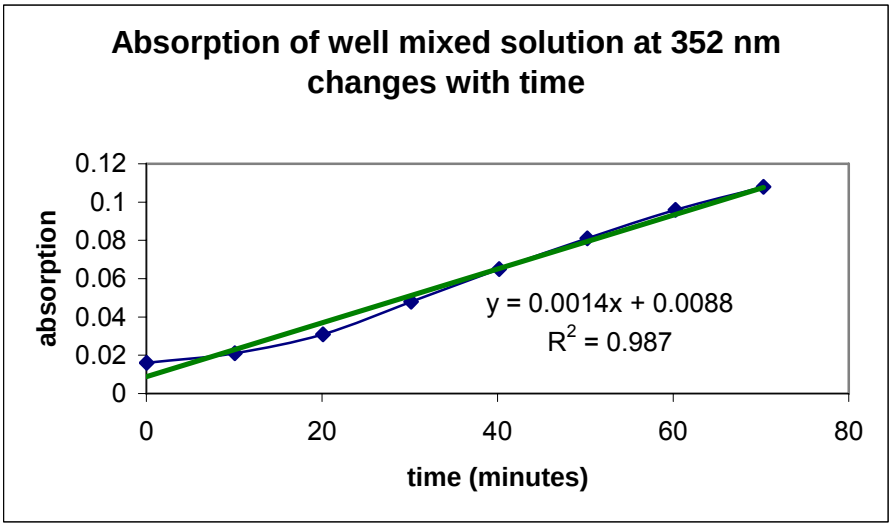

Figure 4-27. The UV absorption at 352 nm of a well-mixed solution through the IMM interdigial micromixer changes with time.

If a time delay between the mixing and the measurement is the predominant factor causing the more iodine formation at low flowrates, the increased amount of the absorption due to the lower flowrate can be calculated based on equation 4-11. Take the absorption differences between the flowrates of 1.56 and 2.18 ml/min as examples. 1.7 ml solution of each stream takes 1.09 min and 0.78 min to be pumped through the mixer at flowrates of 1.56 ml/min and 2.18 ml/min respectively. The time delay between these two operations is 0.31 min. Substitute

0.31 min into equation 4-11, an absorption difference of 0.009 is obtained. This means that if a time delay between the mixing and the measurement is the predominant factor of introducing more formation of iodine, only a trace of absorption difference about 0.009 can be observed between flowrates of 1.56 and 2.18 ml/min. However, the absorption differences observed experimentally (see figure 4-26) are 0.036, 0.213 and 0.247 for the IMM, the OSU and the Tee mixer respectively, which are 4, 23, and 27 times bigger than the expected difference of 0.009. Therefore, it is clear that the time delay between the mixing and the measurement is not the predominant factor influencing the formation of iodine, and it can be neglected for explaining the bad mixing quality at the low flow rate.

With elucidating the role of the time delay between the mixing and the measurement on the evaluation of the mixing quality, the second possibility that the high flow rate tends to improve the mixing quality was believed as the predominant reason causing the different mixing quality at different flow rates. It was thought that the high flow rate tends to disturb the flow pattern and may cause partial turbulence in some parts of the mixer such as the connection between the tubing and the mixer, therefore accelerating the mixing. It has to been noted that the major flow pattern in a micromixers is laminar flow.

However, based on the simulation studied in section 4.1, the flowrate has a little effect on the outcome for the IMM mixer and has a negative influence on the outcome for the Tee mixer (increased flowrate reduces the throughput) at high reaction kinetics. Apparently the experimental result conflicts with the simulation

result. Besides, if the flowrate plays an important role for the mixing quality, the UV-absorption should remain decreased with the increasing flowrate. However, the experimental data shown in figure 4-26 indicates that the flowrate does not affect the mixing quality at a high flowrate range. Therefore, more care has to be taken for interpreting the experimental phenomena: the low flowrate leads to a bad mixing quality.

It is speculated that the major reason causing the above experimental phenomena is neither the time delay between the mixing and the measurement, or that the high flowrate caused a partial turbulent flow, but rather the pulsation of fluids at low flowrates . The unavoidable pulsation inherited from the syringe pump could cause the contact delay of the two reactant streams. The delay is more pronounced at low flowrate, resulting in the inefficient mixing at the low flowrate. In contrast, fluid will be more continuous at higher flowrate. The two streams can reach the same point simultaneously in a mixer and have a better chance to contact each other; therefore, a better mixing quality can be observed at a high flowrate.

4.3 Summary of the Mixing Quality and COMSOL Simulation.

COMSOL software is a convenient tool to simulate processes taking place in micromixers to understand the hydrodynamic, reaction kinetic, and other influences on the outcome. In micromixers, diffusion is the most important mechanism for mass transfer. Therefore, the size of the mass transfer pathway substantially affects the throughput of the products. The IMM Interdigital micromixer has channels with a width of 30 μm; the size of the diffusion pathway

of the Tee mixer, on the other hand, is 500 μm. The short mixing pathway in the IMM mixer provides it with a much better mixing quality. In COMSOL simulation, diffusivity, reaction constant and flowrate were studied to investigate their influences on the outcome from the IMM and the Tee mixer. For the Tee mixer, the diffusivity plays a more significant role than the other two factors to improve the throughput; however, the diffusivities of most liquid species are around 1e-9 m^2/s and are not controllable. In addition, fast reaction kinetics and low flowrate can improve the outcome from the Tee mixer. On the other hand, the value of the diffusivity ranging from 1e-9 to 1e-6 m^2/s does not influence the throughput from the IMM mixer due to its effective mixing. The outcome is determined by reaction kinetics. The influence of the flowrate on the throughput from the IMM mixer depends on reaction kinetics. The flowrate has little effect on the outcome at a high reaction constant; whereas, it decreases throughput at a low reaction constant.

The method described in section 4.2 to measure the relative mixing quality of micromixers is an easily accessible method. The more pronounced pulsation of fluid is believed as the major reason causing the bad mixing at the low flowrates. From both the simulation and the mixing quality measurement, it is obviously seen that the interdigital micromixer has much better performance than the Tee mixer under all conditions. Therefore, interdigital micromixer was chosen as the major tool to synthesize dendrimers in later chapers. The combination of these two methods is an effective tool for testing the mixing quality of micromixers and for designing efficient micromixers.

Chapter 5 The Convergent Synthesis of Polyamide Dendrimer

5.1 Reactions of Polyamide Dendrimer Synthesis

The reactions for the convergent synthesis of polyamide dendrons and dendrimers are illustrated in figure 5-1. The synthesis used 3, 5-bis (4-aminophenoxy)-benzoic acid (compound 1) as building blocks and N-methyl-2-pyrrolidinone (NMP) as the solvent. The synthesis of each generation dendron, except generation 1 (G1) dendron, includes two steps: an activation step with thionyl chloride and a coupling step with the building block 1. The synthesis of the dendrimer consists of two similar steps: an activation step with thionyl chloride and a coupling step with a core molecule 2. This synthetic strategy has been fulfilled in a conventional flask by Washio *et al.* [26], with the exception of the G1 dendrimer. The reported synthetic reactions for each generation of dendron and dendrimer required cooling and inert gas protection, and they typically took 4 to 6 hours to complete in a flask.

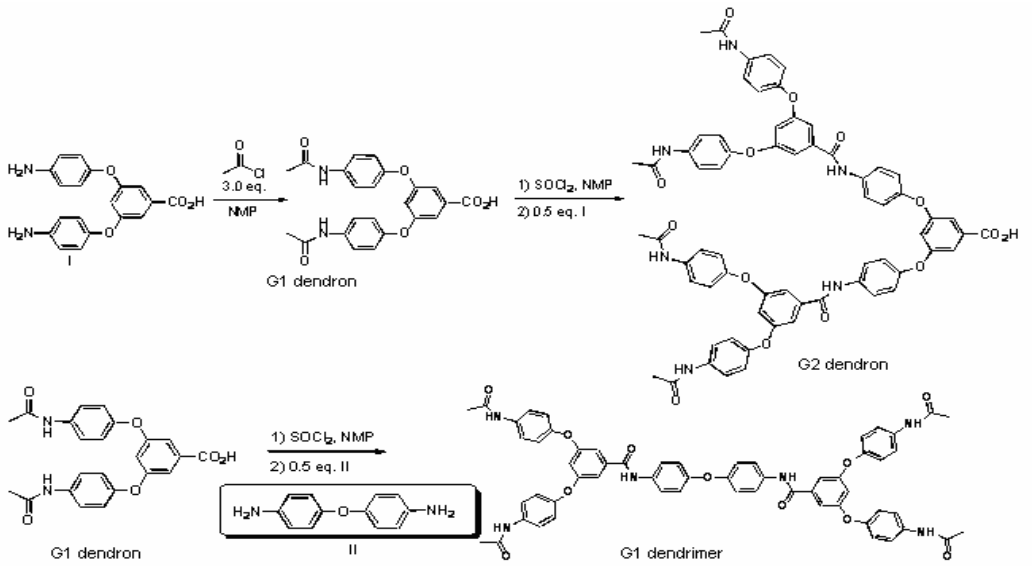

Figure 5-1. Reactions of the convergent synthesis of polyamide dendrons and dendrimers.

The reaction mechanism of the first step: activation of carboxylic acid by thionyl chloride is illustrated in figure 5-2. The lone pair electrons of the acid oxygen attack the electrophilic sulfur, and chloride is expelled from the tetrahedral intermediate. Deprotonation yields a chlorosulfite anhydride, and the liberated chloride ion now attacks the electrophilic carbon of the anhydride. This tetrahedral intermediate then expels leaving group which fragments into SO_2 and chloride ion, and produces acid chloride. One advantage of using thionyl chloride as the reagent is that only gaseous byproducts such as SO_2 and HCl are generated, which makes the following purification process much easier.

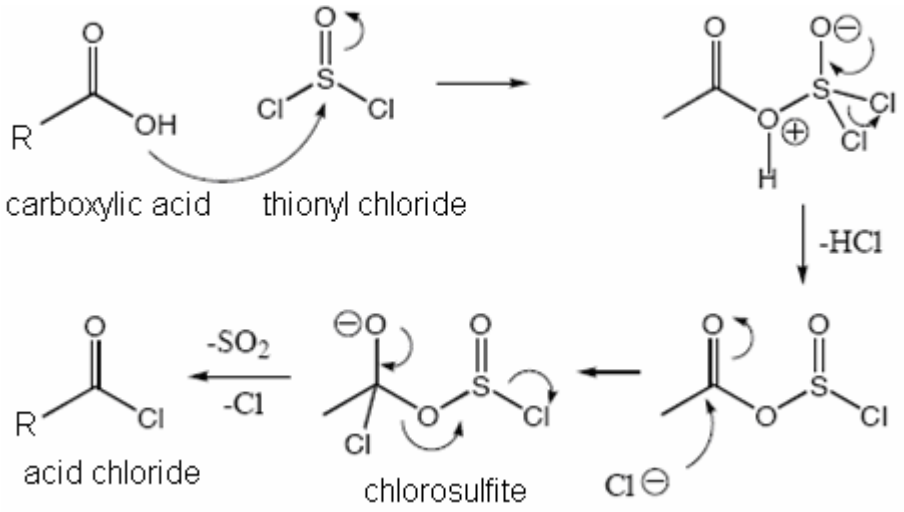

Figure 5-2. The reaction mechanism of the first step of the synthesis of polyamide dendrons and dendrimers.

The reaction mechanism of the second step is an acrylation (or amidation) reaction. The mechanism is illustrated in figure 5-3. The lone pair electrons of the amine nitrogen attack the electrophilic carbon in the acid chloride, and chloride is expelled from the tetrahedral intermediate. Deprotonation yields the final product, an amide (dendrons or dendrimers)

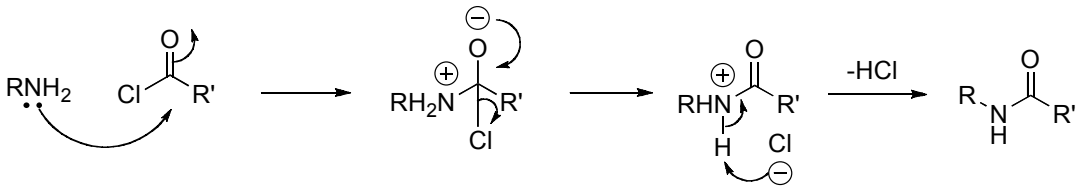

Figure 5-3. The reaction mechanism of the second step of the synthesis of polyamide dendrons and dendrimers.

5.2 The Synthesis of Polyamide Dendrons and Dendrimer via the Interdigital Micromixer for Production Purpose

5.2.1 Experimental Method of Utilizing the Interdigital Micromixer

Synthesis of Dendron G1.

Solutions of 3, 5-bis(4-aminophenoxy)-benzoic acid (monomer) dissolved in NMP (concentration of 0.4 mol/L) and 3 equivalent of acetyl chloride dissolved in NMP (concentration of 1.2 mol/L) were introduced into microchannels of the IMM mixer by syringe pumps at a flow rate of 0.026 ml/s. The mixture was poured into water directly to quench the reaction. The mixture poured into water and formed precipitation which was collected and dried at 120 ^{o}C. The dried powder product (G1 dendron) was used as a precursor for the synthesis of the next generation.

Synthesis of Dendron G2.

Solutions of dendron G1 dissolved in NMP (concentration of 0.323 mol/L) and 1.04 equivalent of thionyl chloride dissolved in NMP (concentration of 0.336 mol/L) were introduced into microchannels. The intermediate was collected at the outlet of the tubing. Then, solutions of the intermediate and 0.5 equivalent of monomer that has been dissolved in NMP (concentration of 0.08 mol/L) were fed into the micromixer by syringe pumps at a flow rate of 0.026 ml/s. The mixture was poured into water directly to form precipitate (G2 dendron). The precipitate was collected and dried at 120 ^{o}C.

Synthesis of Dendrimer G1.

Solutions of dendron G1 dissolved in NMP (concentration of 0.2 mol/L) and 1.5 equivalent of thionyl chloride dissolved in NMP (concentration of 0.3 mol/L) were introduced into microchannels by syringe pumps at a flow rate of 0.026 ml/s. The intermediate was collected at the outlet. Then, solutions of the intermediate and 0.5 equivalent of the core molecule that has been dissolved in NMP (concentration of 0.05 mol/L) were fed into the micromixer by syringe pumps at a flow rate of 0.026 ml/s. The mixture was poured into water directly to form precipitate (dendrimer G1). The precipitate was collected and dried at 120 ^{o}C.

5.2.2 The Synthesis Results via the Interdigital Micromixer

The dried powder of each product was analyzed by proton NMR and mass spectrometry. The ^{1}H-NMR spectra of dendrons G1, G2 and dendrimer G1 synthesized via the interdigital micromixer, the spectrum of the monomer and their corresponding chemical structures are shown in figure 5-4. The disappearance of the characteristic peaks of the monomer and the appearance of new peaks indicated the conversion of the monomer into G1 dendron. Comparing the spectrum of G2 dendron with that of G1 dendron, the appearance of new peaks at 10.32 (f), 7.76 (g), and 6.91 (i) indicated that the dendron G2 was obtained through the microreactor. Comparing the spectrum of the G1 dendrimer with that of the G1 dendron, the signals assigned to the protons of position d shifted from 6.84 to 6.71 ppm, position e from 7.04 to 7.25 ppm and the signals in 0.26 (f), 7.71 (g) and 6.98 (h) appeared after the coupling reaction, indicating the formation of the G1 dendrimer.

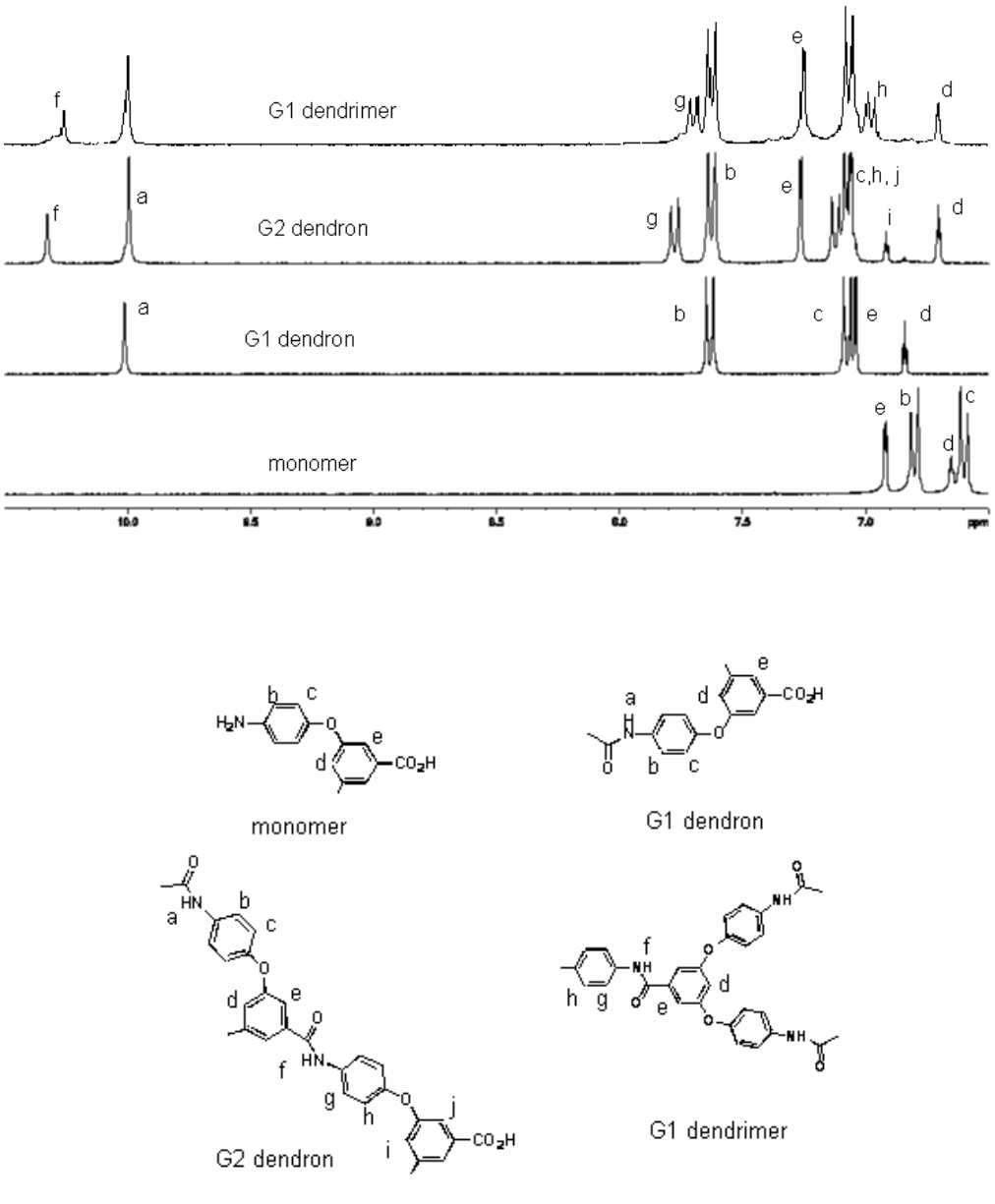

Figure 5-4. ^{1}H-NMR spectra and corresponding chemical structures of monomer, dendrons G1, G2 and dendrimer G1 synthesized via the IMM micromixer.

The mass spectra in figure 5-5 show the signals at m/z=1005 and 1141, indicating the successful synthesis of dendrimer G1 (calculated molecular weight of 1004) and dendron G2 (calculated molecular weight of 1140), respectively.

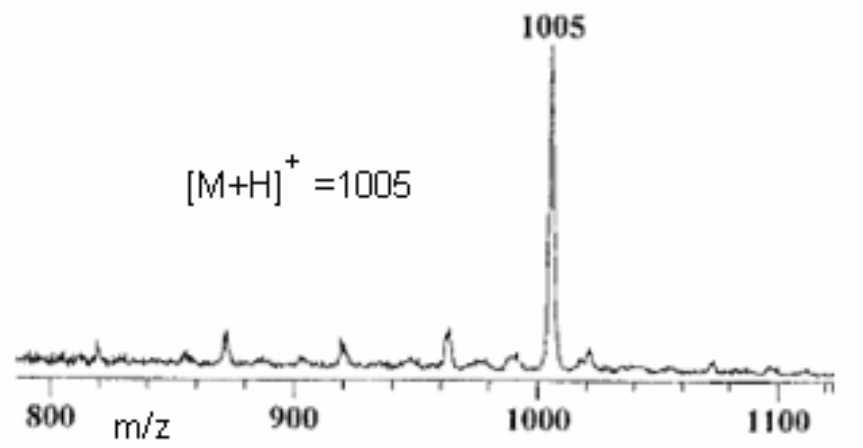

(a)

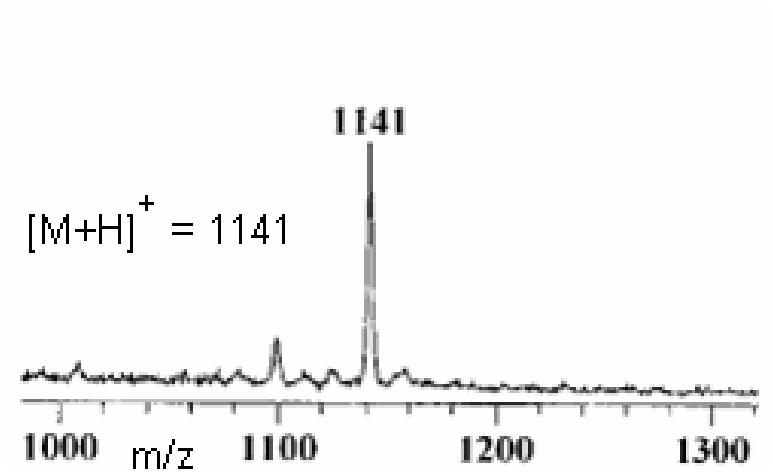

(b)

Figure 5-5. Mass spectra of dendrimer G1 (a) and dendron G2 (b).

5.3 The Reaction Kinetics Study of Dendron G1

For a reaction kinetics study, the mixing time has to be less than the reaction time, so the mixing quality is very important in studying the reaction kinetics. In ordinary size systems, the mixing time usually is long and hard to determine whether the sufficient mixing is achieved or not. Meanwhile, a big amount of reactant is required, and the reaction conditions are hard to control. On the other hand, microsystems offer the possibility of improving kinetic measurement by considerably reducing the sample size, providing a fine temperature control and allowing the analysis of fast kinetics. As a result, we studied the reaction kinetics of the formation of generation G1 dendron via a continuous flow interdigital micromixer.

5.3.1 The Experimental Method of Studying the Reaction Kinetics of Dendron G1

1 ml solution of 3, 5-bis(4-aminophenoxy)-benzoic acid (monomer) dissolved in NMP (concentration of 0.4 mol/L) and 1 ml solution of acetyl chloride dissolved in NMP (concentration of 1.2 mol/L) were introduced into microchannels by syringe pumps at a flowrate of 0.026 ml/s, respectively. The mixture was poured into 35 ml of stirring methanol directly to quench the reaction. Aliquots of the mixture in methanol solution were taken for vacuum drying and then run for ^{1}H-NMR. The residence time was controlled by changing the length of the tubing which was connected to the outlet of the micromixer; meanwhile, the flowrate of each stream was kept constant. The temperature was controlled by the

circulator. Usually, the method used to change the residence time is to change the flowrate, meanwhile keeping the tubing length at a constant. This method is easy to fulfill in practice. The reason for not choosing this method here is that the Kloehn pumps used in this study can provide a limited range of flowrate and a flowrate slower than 0.026 ml/s cannot be reached. Therefore, a long residence time cannot be obtained with a reasonable length of tubing by using this method.

It was mentioned in section 5.2.1 that water was used to terminate the reaction for the production of the G1 dendron. However, instead of water, methanol was used to quench the reaction for the purpose of studying the reaction kinetics. This change of solvent is based on the observation shown in figure 5-6 in which water can accelerate the reaction. In other words, the reaction of producing dendron G1 still takes place even after the reaction mixture is introduced into a large amount of water. It is speculated that the un-reacted reactant does not disperse in water. Therefore, the drops flowing out from the mixer are isolated from the surrounding water solution, and the components inside of each drop are compressed by the pressure from the water. The collision frequency between reactants inside of each drop is increased, causing the accelerated reaction rate. On the other hand, the polarity of methanol is weaker than water, so the reactant species can be promptly spread in methanol causing the abrupt dilution of the un-reacted species and the quench of the reaction. Based on the above observation, methanol was chosen as the quench solvent for the study of the reaction kinetics of the formation of G1 dendron.

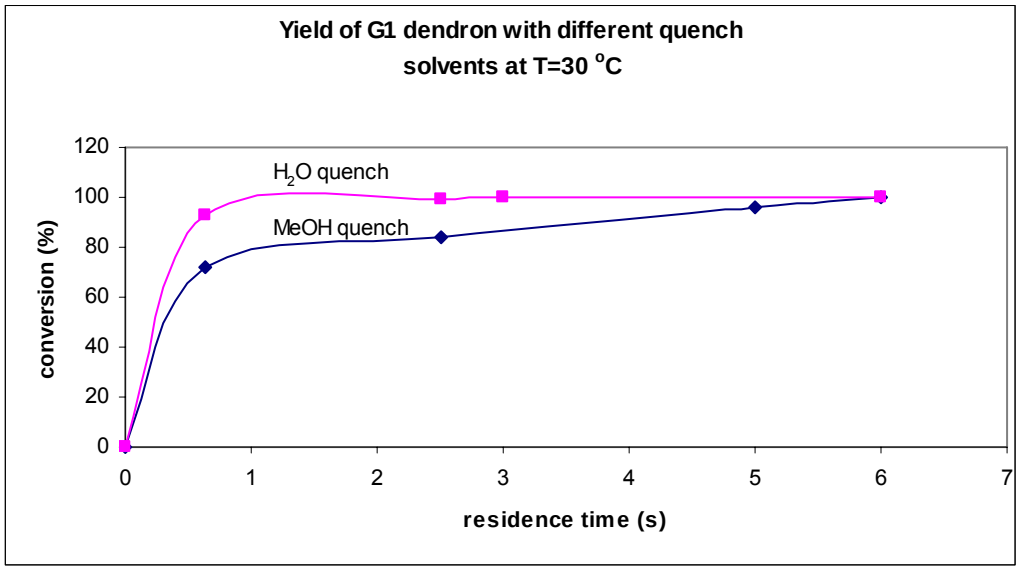

Figure 5-6. Yield of G1 dendron changes with residence time when different solvents were used to quench the reaction at temperature of T=30 °C.

5.3.2 The Reaction Kinetics Study Results

The syntheses of the G1 dendron via the interdigital micromixer at different residence times under different temperatures were conducted, and the corresponding ^{1}H-NMR spectra are shown in figures 5-8, 5-9 and 5-10, respectively. It is obviously seen that the starting material, the monomer, consumed rapidly within only 0.63 second under all reaction conditions. However, the starting material did not immediately convert to the desired product, the G1 dendron, completely. An intermediate, only one branch of the starting material having the reaction (chemical structure shown in figure 5-7), occurred and it took a longer time to convert to the desired product.

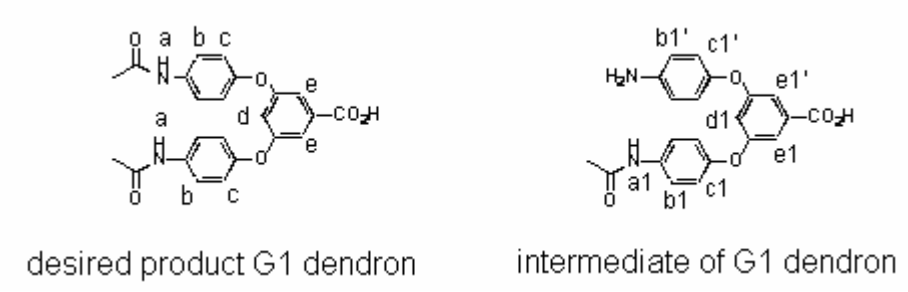

Figure 5-7. Comparison of the chemical structures of the desired product and the intermediate of the G1 dendron

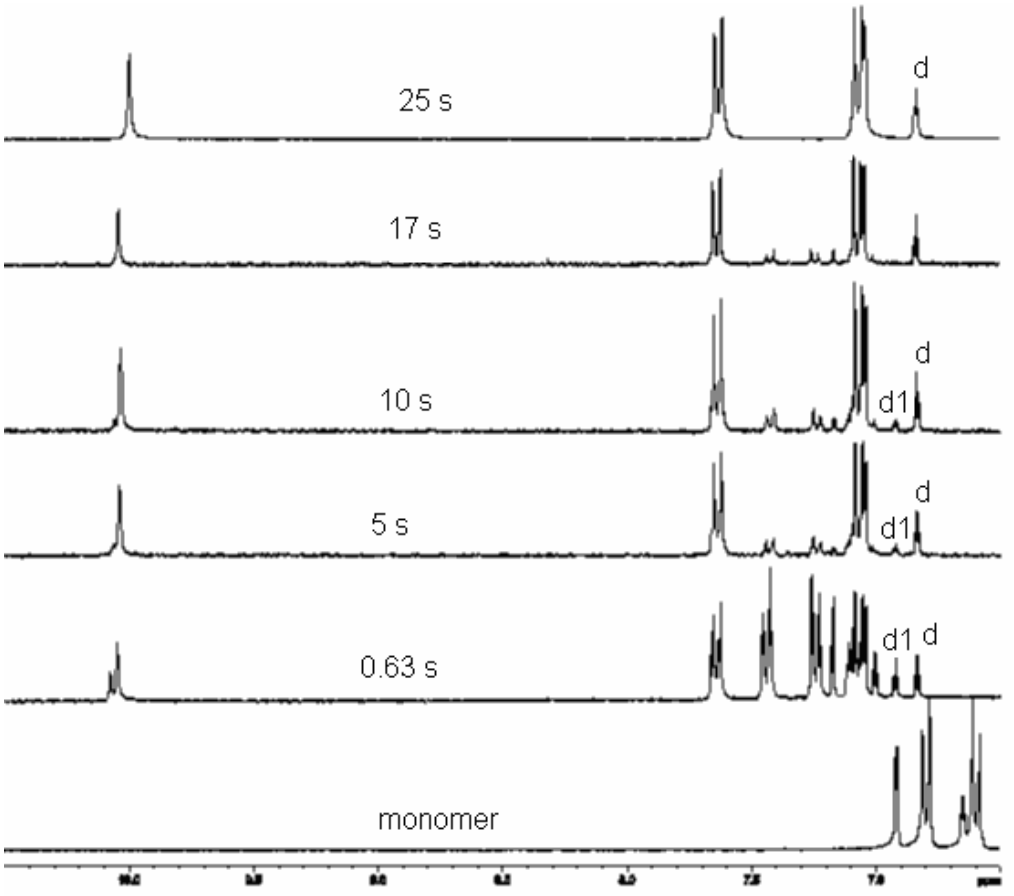

Figure 5-8. ^{1}H-NMR spectra of the dendron G1 synthesized via the interdigital micromixer at different residence times under a temperature of 6 ^{o}C.

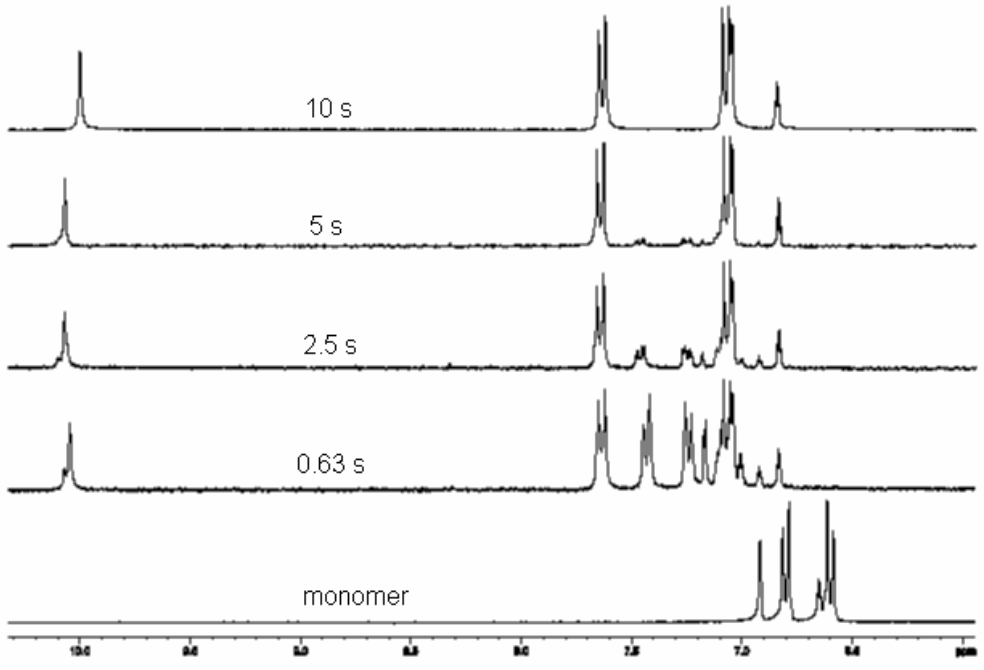

Figure 5-9. ^{1}H-NMR spectra of the dendron G1 synthesized via the interdigital micromixer at different residence times under a temperature of18 ^{o}C.

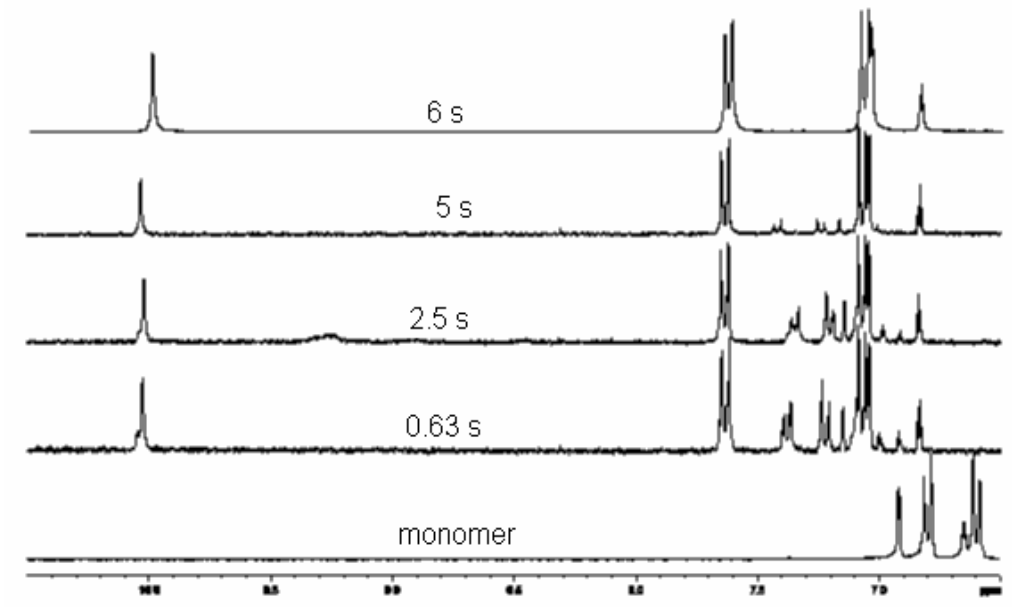

Figure 5-10. ^{1}H-NMR spectra of the dendron G1 synthesized via the interdigital micromixer at different residence times under a temperature of 30 ^{o}C.

Two peaks will be focused on to analyze the reaction kinetics: the peak of the desired product at 6.82 ppm (labeled as d in figure 5-8) and the peak of the intermediate (with only one branch reacted) at 6.91 ppm (labeled as d1 in figure 5-8). The reason for choosing these two peaks is that each of these two peaks is clear without overlapping with peaks of other materials. In other words, these two peaks represent the production of the pure desired G1 dendron and the intermediate, respectively. The peak areas of these two peaks were calculated (automatically by H-NMR software) to follow the course of the reaction. The yield of the desired G1 dendron product is defined as the ratio of the peak area of the desired product to the sum of both peak areas. The yield of the desired G1 dendron as a function of the residence time under different temperatures is illustrated in figure 5 -11.

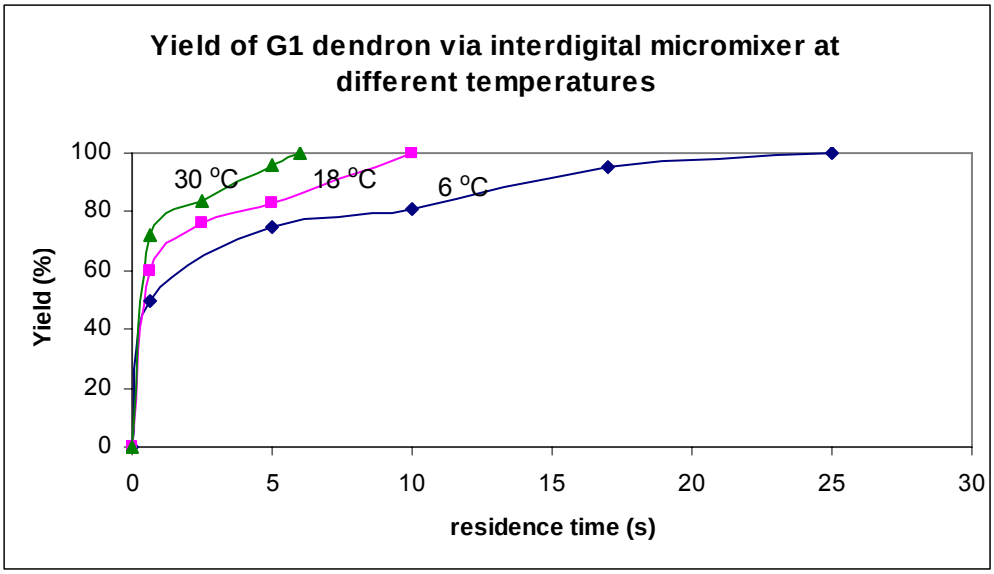

Figure 5-11. Yield of the G1 dendron versus residence time via the interdigital mixer at temperatures of 6 °C, 18 °C and 30 °C.

Apparently, the reaction takes place rather fast within the first 0.63 s. Over 50% of the desired product is generated at 0.63 s even at a temperature of 6 ^{o}C. The reaction rate is slower after 0.63 s for this reaction under all temperatures. Besides, the conversion to the desired product increases with increasing the temperature at the same residence time. The complete conversion to the desired product requires 25 seconds under a temperature of 6 ^{o}C. However, it takes 10 seconds and 6 seconds to complete the conversion to the desired product under temperatures of 18 ^{o}C and 30 ^{o}C, respectively.

According to the ^{1}H-NMR spectra following the reaction course under different temperatures shown above, it is reasonable to assume that the formation of the dendron G1 includes two steps: (1) an acrylation reaction on one branch of the monomer molecule to produce intermediate; (2) an acrylation reaction on another branch of the intermediate to generate the desired product. The first step is a much faster reaction than the second step. This assumption is based on the evidence that all spectra show the rapid complete disappearance of the starting material, the monomer, even at the possible shortest measurable residence time, 0.1 second, by using this set-up. Therefore, the second step is the limit reaction for the formation of the G1 dendron. The reaction kinetics study here is essentially for the second step reaction.

The details of finding out the reaction constants under different temperatures are described bellow. The two-step reaction is simplified as following:

$$A+B \rightarrow C \quad \text{(first step)} \qquad (5\text{-}1)$$

$$C+B \rightarrow D \text{ (second step)} \tag{5-2}$$

Where A represents the monomer; B, acetyl chloride; C intermediate (the reaction only takes place on one branch of the molecule); and D, the final desired product. The initial concentrations of A and B right after mixing in the micromixer are 200 and 600 mol/m^3 (each value is reduced to half of the inlet value due to the equal flowrate was used to feed the two streams into the microchannels). Therefore, the initial concentrations of C and B for the second step reaction are approximated as C_{C0} =200, C_{B0} =400 mol/m^3.

The conversion shown in figure 5-11 is the ratio of the amount of product D over the sum of the amount of D and the amount of C and is expressed in equation (5-3).

$$X = \frac{C_D}{C_C + C_D} \tag{5-3}$$

Where X-conversion of product D; C_D- concentration of product D; C_C- concentration of C.

Noting that the amounts of C and B which have reacted at any time t are equal and given by equation (5-4),

$$C_{C0} - C_C = C_{B0} - C_B = C_D \tag{5-4}$$

Therefore,

$$C_C + C_D = C_{C0} \tag{5-5}$$

Combine equations (5-3) and (5-5), it can be obtained that:

$$C_D = C_{C0} X \tag{5-6}$$

Substitute equation (5-6) into (5-5), the concentration of C can be expressed in equation (5-7).

$$C_C = C_{C0}(1 - X) \tag{5-7}$$

From equation (5-4), it can be obtained that:

$$C_B = C_{B0} - C_{C0} + C_C \tag{5-8}$$

Based on the conversion of product D at different times shown in figure 5-11, and equations (5-7) and (5-8), the concentrations of C and B at any time can be calculated and the concentrations of C and B versus time under different temperatures are plotted in figure 5-12.

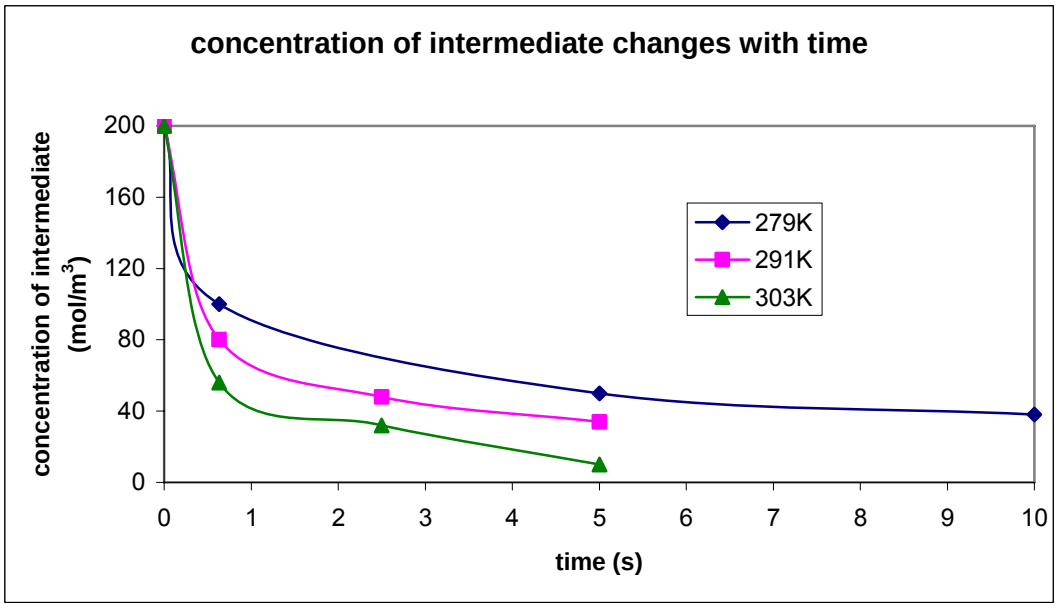

Figure 5-12. The concentration of intermediate changes with time under different temperatures.

The reaction rate law of the second step reaction can be expressed as equation (5-9).

$$R = -\frac{dC_C}{dt} = kC_c^{\ a}C_B^{\ b} \tag{5-9}$$

Taking a logarithm on both sides of equation (5-9) gives to equation (5-10).

$$\log R = \log(-\frac{dC_C}{dt}) = \log k + a * \log C_C + b * \log C_B \tag{5-10}$$

Where: R- reaction rate; t-time; k- reaction constant; a and b are reaction orders.

The technique, the *method of least squares*, will be used to solve the equation (5-10) to obtain constants, k, a and b. The detailed procedure is described as follows. [27]

Now let: $y = \log(-\frac{dC_C}{dt}), x1 = \log C_C, x2 = \log C_B, b0 = \log k, b1 = a, b2 = b$.

Then equation (5-10) becomes:

$$y = b0 + b1 \cdot x1 + b2 \cdot x2 \tag{5-11}$$

These constants, b0, b1 and b2 can be found by solving the following three equations:

$$\begin{aligned} &N \cdot b0 + b1 \cdot \sum x1 + b2 \cdot \sum x2 = \sum y \\ &b0 \cdot \sum x1 + b1 \cdot \sum x1^2 + b2 \cdot \sum (x2 \cdot x1) = \sum (y \cdot x1) \\ &b0 \cdot \sum x2 + b1 \cdot \sum (x1 \cdot x2) + b2 \cdot \sum (x2^2) = \sum (y \cdot x2) \end{aligned} \tag{5-12}$$

Where, N- the number of runs.

Take the solving procedure for a temperature of 6 ^oC (279 K) as an example, a series of data of gradient ($-dC_C/dt$) and corresponding concentrations of C_C and C_B

at different times can be obtained based on figure 5-12 and equation (5-8). Find the logarithm of each data, and these logarithms become the variables, y, x1 and x2, as shown in table 5-1.

Table 5-1. The data required for the calculation of the reaction constant and the reaction order when the temperature is 6 ^{o}C (279 K).

run			y		x1		x2
	Time,t(s)	-dc/dt	log(-dc/dt)	Cc	logC_C	C_B	logC_B
1	0.63	28	1.447158	100	2	300	2.477121
2	1	22	1.342423	90.9	1.958564	290.9	2.463744
3	2	11	1.041393	75.9	1.880242	275.9	2.440752
4	3	10	1	65.1	1.813581	265.1	2.42341
5	5	7	0.845098	50	1.69897	250	2.39794
6	7	5	0.69897	43.3	1.636488	243.3	2.386142
7	10	4	0.60206	38	1.579784	238	2.376577
8	12	3.6	0.556303	30.6	1.485721	230.6	2.362859
9	14	1.25	0.09691	22.4	1.350248	222.4	2.347135
		Sum	7.630314		15.4036		21.67568
		Notation	Σy		Σx1		Σx2

Then find the sum of the squares of the variables x1 and x2, the sums of the products of all of the combinations of variables, and tabulate them as in table 5-2.

Table 5-2. Details of computation based on table 5-1.

run	$x1 \cdot y$	$x2 \cdot y$	$x1^2$	$x2^2$	$x1 \cdot x2$
1	2.894316	3.584786	4	6.13613	4.954243
2	2.629221	3.307385	3.835972	6.070033	4.825399
3	1.95807	2.541781	3.535309	5.957269	4.589203
4	1.813581	2.42341	3.289076	5.872915	4.39505
5	1.435796	2.026494	2.886499	5.750116	4.074028
6	1.143856	1.667842	2.678093	5.693674	3.904893
7	0.951124	1.430842	2.495716	5.648118	3.754477
8	0.826511	1.314465	2.207368	5.583104	3.510551
9	0.130853	0.227461	1.82317	5.509042	3.169214
Sum	13.78333	18.52447	26.7512	52.2204	37.17706
Notation	$\Sigma(x1 \cdot y)$	$\Sigma(x2 \cdot y)$	$\Sigma\ x1^2$	$\Sigma\ x2^2$	$\Sigma(x1 \cdot x2)$

Substitute the values in tables 5-1 and 5-2 into equations (5-12), one has:

$$9 \cdot b0 + 15.4 \cdot b1 + 21.68 \cdot b2 = 7.63 \quad (5\text{-}13)$$

$$15.4 \cdot b0 + 26.75 \cdot b1 + 37.18 \cdot b2 = 13.78 \quad (5\text{-}14)$$

$$21.68 \cdot b0 + 37.18 \cdot b1 + 52.22 \cdot b2 = 18.52 \quad (5\text{-}15)$$

Solving the above equations simultaneously, the values of b can be obtained as follows: b0 = -3.26, b1= 1.71, b2= 0.49.

Therefore, at temperature T=279 K, the reaction constant, $k=10^{b0}$=5.5E-4, reaction order, a=1.71, b=0.49.

Following the same procedures, the reaction constant k, the reaction order a and b under temperatures of 18 ^{o}C (291 K) and 30 ^{o}C (303 K) can be obtained respectively. (The detailed computations are listed in tables 12 -15 in Appendices). These values of k, a and b under different temperatures are listed in table 5-3.

Table 5-3. The calculated reaction constants and the reaction order under different temperatures.

T (K)	k	a	b
279	0.00055	1.71	0.48
291	0.000955	1.89	0.41
303	0.00132	1.91	0.5
	Average reaction order	1.84	0.46

It can be seen from table 5-3, the values of a and b under different temperatures are close to each other and the average value of a is 1.84, and of b is 0.46.

The activation energy of the second step reaction can be obtained according to Arrhenius' law:

$$k = k_0 e^{(-E_a / RT)} \tag{5-16}$$

Where: k_0- frequency factor, a constant for a specific reaction; E_a- an activation energy with a unit of J/mol; R- the gas constant, 8.314 J/(mol.K); T- the temperature with a unit of K.

Taking the natural logarithm of both sides of equation (5-16) gives to equation (5-17):

$$\ln k = \ln k_0 - \frac{E_a}{R} \cdot \frac{1}{T} \tag{5-17}$$

According to the data shown in table 5-3, plot ln(k) versus 1/T in figure 5-13, the slope is related to the activation energy, and

$$-\frac{E_a}{R} = -3096.2 \Rightarrow E_a = 2.57 \times 10^4 \text{ (J/mol)} \tag{5-18}$$

Meanwhile, it is found that k_0=37.23. Therefore, the reaction constant of the second step reaction of producing the dendron G1, k, can be expressed in equation (5-19):

$$k = 37.23 e^{(-2.57 \times 10^4 / RT)} \tag{5-19}$$

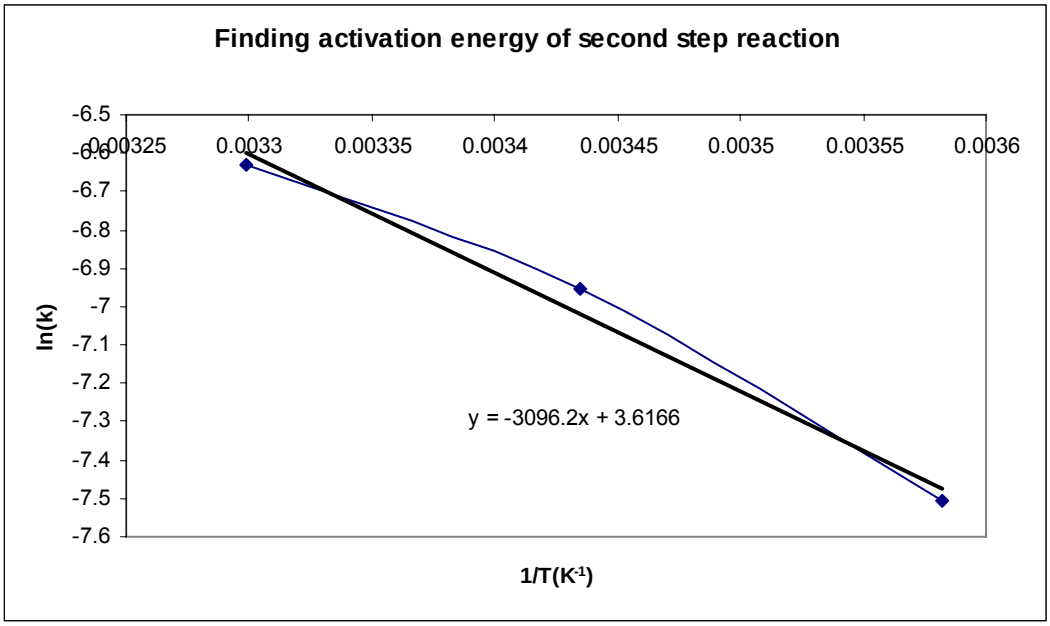

Figure 5-13. The plot of ln(k) versus 1/T with the intention of finding the activation energy of the second step reaction.

5.4 The comparison of the Synthesis via the Interdigital Micromixer with the Tee Mixer and the Conventional Reactor

5.4.1 The Comparison of the G1 Dendron Yield via the Interdigital Micromixer and the Tee Mixer

In order to explore the efficiency and mixing quality of the interdigital micromixer in practice, the syntheses of the G1 dendron via the interdigital micromixer, the Tee mixer and a conventional flask reactor under a temperature of 30 ^{o}C were conducted for comparison. Figure 5-14 shows the ^{1}H-NMR spectra of the G1 dendron synthesized via the Tee mixer at different residence times. Figure 5-15 illustrates the comparison of the yield of the G1 changing with the residence

time via the Tee mixer and the interdigital micromixer. Obviously, the yield of the G1 synthesized via the interdigital micromixer is about double that via the Tee mixer at the same reaction condition. This result demonstrates that the mixing quality of the interdigital micromixer is much better than the Tee mixer, which is consistent with the COMSOL simulation. The diffusion path way in the interdigital mixer is 30 μm which is the width of each sheet of the multilamination, so it takes about 0.9 second to diffuse for most liquid components. However, the internal diameter of the Tee mixer is 500 μm, so it will take about 2.5 seconds to diffuse for liquid components having a diffusion coefficient of 10^{-9} m^2/s. Therefore, the interdigital mixer shows a faster conversion.

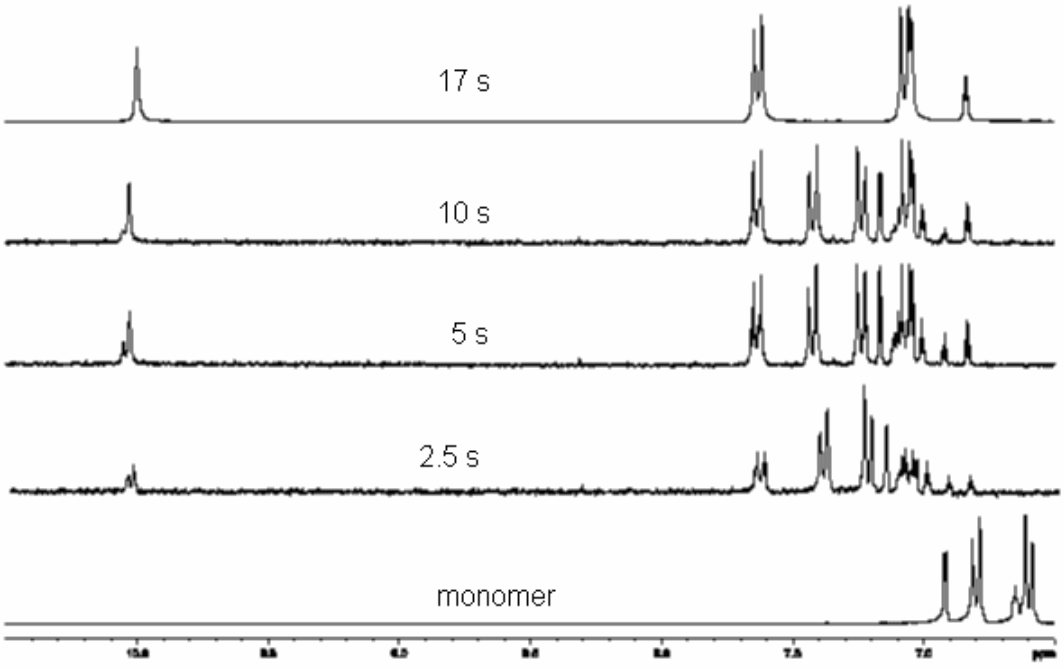

Figure 5-14. ^{1}H-NMR spectra of the dendron G1 synthesized via the Tee micromixer at different residence times at 30 ^{o}C.

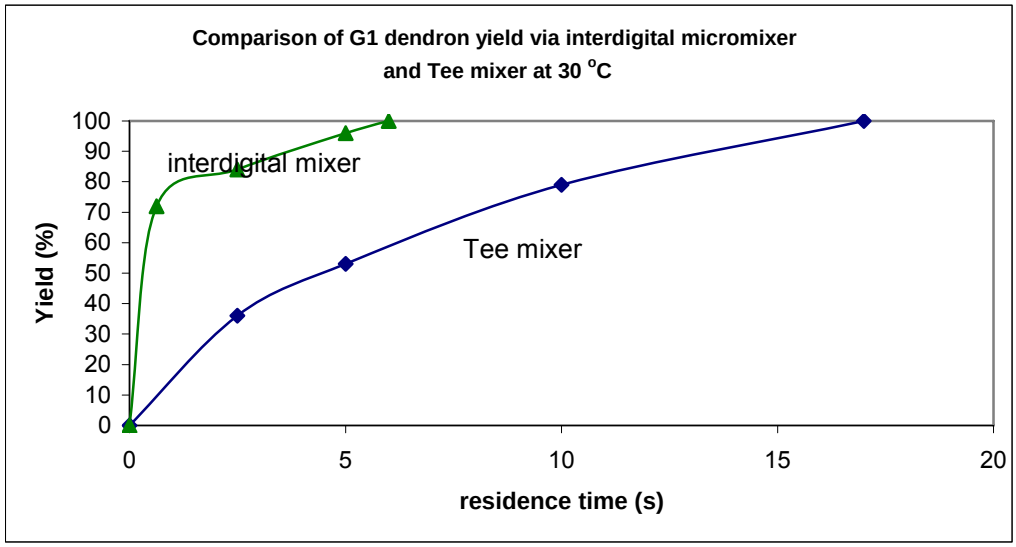

Figure 5-15. Yields of the G1 denron synthesized via the interdigital micromixer and the Tee mixer at 30 °C

5.4.2 The Comparison of the G1 Dendron Yield via the Interdigital Micromixer and the Conventional Flask Reactor

In order to demonstrate the advantages of utilizing a microreactor to synthesize a dendrimer over a conventional flask reactor, a controlled reaction of the G1 dendron synthesis was carried out in a flask. 3 equivalents of acetyl chloride were added drop-wise to a 2ml stirred solution of 3, 5-bis(4-aminophenoxy)-benzoic acid (monomer) dissolved in NMP (concentration of 0.2 mol/L). The reaction temperature was kept at 30 °C by a water circulator. 2 hours later, aliquots of the sample (about 0.1 ml) were taken out from the reactor and were poured into 2 ml of stirring methanol directly to quench the reaction. Aliquots of the mixture in the methanol solution were taken for vacuum drying, and then run for ^{1}H-NMR. It has

to be noted that although the reactant concentration (0.2 mol/l of the monomer and 0.6 mol/l of acetyl chloride) in the control reaction seems different from that in the reaction conducted in the microreactor (prepared reactant concentration of 0.4 mol/l of the monomer and a 1.2 mol/l of acetyl chloride, respectively); the reaction conditions are essentially the same for the reactions conducted in these two reactors. This is because the two streams with the same flow-rate will merge together finally in the microreactor, causing the concentration of each stream to be reduced to half of the original concentration.

H-NMR spectrum of the dendron G1 produced by the conventional flask reactor (in figure 5-16) showed that the intermediate and other impurities still existed after 2 hours of stirring. On the other hand, the synthesis via the interdigital micromixer only took 6 seconds to complete the reaction and a pure G1 dendron was obtained at the same reaction conditions.

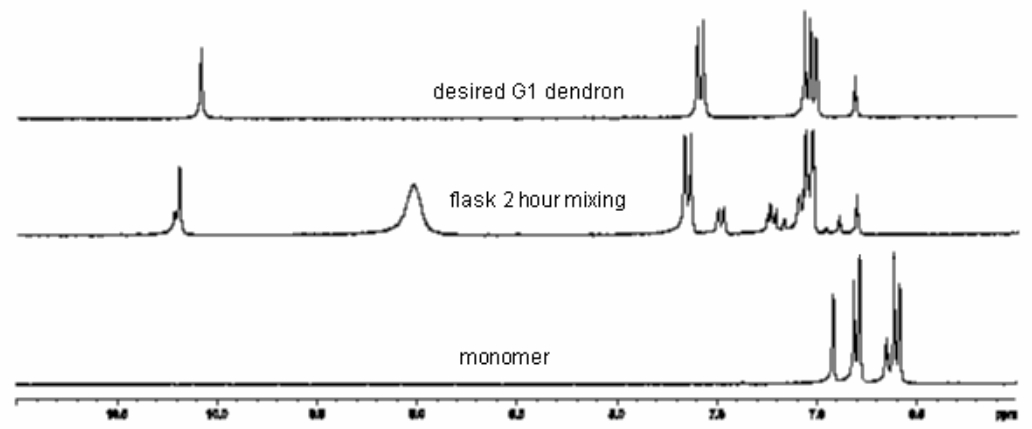

Figure 5-16. ^{1}H-NMR spectrum of the G1 dendron synthesized via a conventional flask stirring for 2 hours, under a constant temperature of 30 ^{o}C.

In order to improve the reaction, the reaction was conducted differently. The same amount (2 ml) and the concentration of the reactants as previous set were applied, but the reactor was kept at 0 ^{o}C cooling for 5 minutes by using a mixture of water and ice, during which period of time another reactant was dropwise added into the reactor. Then, the reactor was brought to 30 ^{o}C, and aliquots of the sample were taken out for NMR analysis. Figure 5-17 shows NMR spectra of samples taken out at different times. The reaction was completed 3 minutes later after the temperature was increased to 30 ^{o}C. When the volume of the reactants is increased to 25 ml, the literature reported that it took 3 hours to complete the reaction. [26]

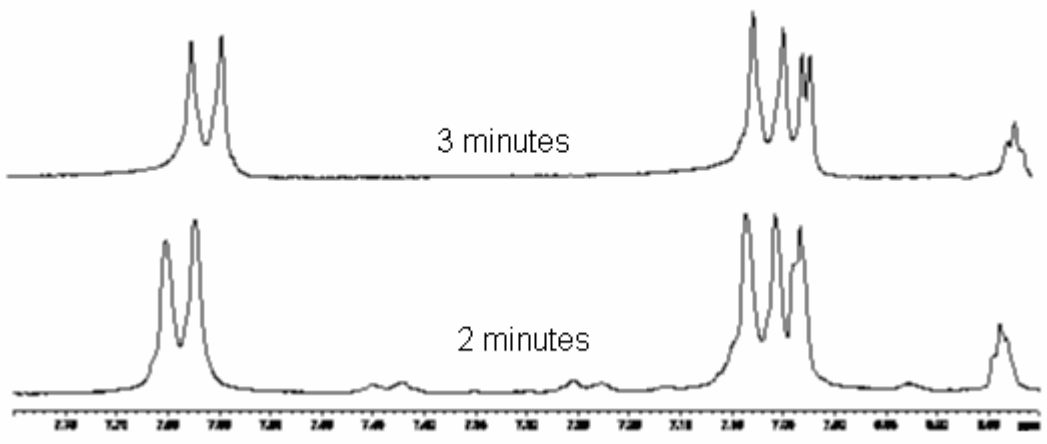

Figure 5-17. ^{1}H-NMR spectra of the G1 dendron synthesized via a flask reactor, mixed at 0 ^{o}C for 5 minutes then brought to 30 ^{o}C. 2 minutes and 3 minutes marked in the spectra are the times accounted from the moment when the temperature was started to be raised to 30 ^{o}C.

5.5 The Analysis of Reasons Leading to the Advantages of a Microreactor over a Conventional Flask Reactor for the Specific Reaction of G1 Dendron Synthesis

The experiment results show that the interdigital micromixer realized complete conversion within 6 seconds. However, in the batch reactor, the reaction was not completed even after hours of mixing when the temperature was kept constant at 30 ^{o}C (see figure 5-16). When the solutions were mixed at 0 ^{o}C for 5 minutes in the batch reactor, then brought to 30 ^{o}C, it still took minutes to complete the reaction (see figure 5-17).

The comparison of the yield of the G1 dendron synthesized via the interdigital micromixer and the conventional flask reactor described above indicates that it is suitable to implement a microreactor for the synthesis of G1 dendron. The reasons leading to these advantages of a microreactor over its counterpart, a conventional flask reactor, are explained as follows:

(1) The effective heat transfer in a microreactor can benefit fast and exothermic reactions like the reaction to produce polyamide dendron G1 described above. It is believed that the dominating reason leading to the existence of impurities and the intermediate after 2 hours mixing in the flask reactor (see figure 5-16) is not due to the un-effective mixing quality of the conventional flask, but the insufficient heat transfer. This speculation is based on the fact that the reaction volume is only 2 ml, which is supposed to be mixed well within a short period of time, and the fact that the product NMR spectrum stayed the same even after 3 hours mixing. The latter fact indicates that at least one of the starting reactants has

been consumed before the desired reaction was completed, so the intermediate could not proceed for a further reaction to produce the desired product. The major reason causing the un-completion of the desired reaction, insufficient heat transfer, resulted in hot spots; therefore, parts of the starting material were consumed for irreversible side reactions. For this kind of fast and exothermic reaction, the traditional method to avoid side reactions is to lower the temperature, such as to 0 ^{o}C, which can be reached by using an ice-water mixture; or to -78 ^{o}C which can be reached by using a mixture of acetone and dry ice and so on. Meanwhile, the dosing time of the reactants into the reactor needs to be prolonged by drop-wise adding. The mixture solutions are usually mixed at a low temperature for a certain period of time to ensure it is well mixed. Then the temperature is brought to a higher temperature to accelerate the reaction. In other words, traditionally, the mixing and heat transfer steps of fast and exothermic reactions in a batch reactor have to be dealt sequentially. This inevitably will increase the operation time of the whole process, even though the intrinsic kinetics of the reaction is fast.

(2) In order to avoid the hot spots caused by insufficient heat transfer, the mixtures in the batch rector were mixed at 0 ^{o}C for 5 minutes then brought to 30 ^{o}C. The result showed that it still took minutes to complete the reaction. This is because it takes time to bring the temperature from 0 ^{o}C to 30 ^{o}C in a batch reactor. During the period of time to raise the temperature, the reaction rate is lower than the one taking place in the micromixer where the temperature is kept

constant as 30 ^{o}C. Therefore, the conversion to the desired product is slower in a batch reactor compared with that in a micromixer.

The effective mass and heat transfer provide a microreactor with easy operation, because the mixing and heat transfer steps can be combined in one apparatus and taken simultaneously. Therefore it takes a shorter time to complete reactions in miroreactor.

5.6 Summary of Chapter 5

Polyamide dendrons and dendrimers were successfully synthesized by using a continuous flow microreactor. The microreactor demonstrated several advantages over a conventional batch reactor. One of the most attractive advantages is that pure dendrons and dendrimers could be synthesized within few seconds of residence time in contrast to a long time of stirring in a flask. In addition, the required reaction conditions are easier to implement. For example, for the synthesis performed in a flask, the mixture needs to be stirred at a low temperature (i.e. 0^{o}C) at the beginning of the mixing to avoid side reactions. In contrast, the pure dendrons and dendrimers can be synthesized at a constant temperature without the need of pre-mixing at a low temperature by utilizing a micromixer system,

The rather slow conversion from the flask synthesis is attributed to the poor mass and heat transfer: the insufficient heat transfer accumulates heat to form hot spots favoring un-wanted side reactions; it takes a long time for mixtures to reach a high temperature; therefore, reactions occur at a low reaction rate, prolonging the

completion time. The effective heat and mass transfer taking place simultaneously in a micromixer system lead to a reaction with a high reaction rate because the temperature can be kept at a high temperature all of the time.

The microreactor is an effective tool for reaction kinetics study for fast reactions. The mechanism of the formation of the desired dendron G1 includes two steps: the first step with only a one-branch occurring reaction is a much faster reaction than the second step with another branch having a reaction. The reaction rate of the second step can be expressed as:

$R = -k \cdot C_C^{\,1.84} \cdot C_B^{\,0.46}$ (C_C, concentration of the intermediate; C_B, concentration of acetyl chloride.)

$k = 37.23e^{(-2.57\times10^4/RT)}$

Chapter 6 The Deposition of Polyamide Dendron on a Solid Surface

Dendrimer-modified glass surfaces have been explored in the fields of protein adsorption and DNA microarray analysis due to their compact structure and fixed number of functionalities on the periphery for enhancing the surface immobilization density of proteins. However, the immobilization method was limited to the immersion of glass slides into dendrimer solutions, which usually takes hours or days. Our approach to the deposition of dendron on a glass surface was accomplished by a continuous flow microreactor which reduced the deposition time tremendously and simplified the reaction process.

6.1 The Procedure of Depositing Polyamide Dendron on a Glass Surface

The preparation and deposition procedure of G1 dendron on a glass surface using a continuous flow microreactor (IMM mixer) is illustrated in figure 6-1. It includes three major steps as follows:

Step 1: glass cleaning. Ultrasmooth microscope glass slides were cleaned by immersing them into a mixture of NH_4OH and H_2O_2 with a volume ratio of 2:1 for 30 minutes at room temperature. The slides were then rinsed thoroughly by MiliQ-DI water and dried under a stream of nitrogen. Next, the glass slides were fatherly cleaned by immersing them into a mixture of HCl (37%), H_2O_2 and H_2O with a volume ratio of 1:1:6 for 30 minutes at room temperature, rinsed thoroughly by MiliQ-DI water and finally dried under a stream of nitrogen.

Step 2: amino-silanisation of the glass slides. Cleaned microscope slides were immersed into a solution containing 3-aminopropyl-triethoxysilane and ethanol with a volume ratio of 1:9 overnight at 30 ^{o}C. The slides were rinsed by ethanol and water sequentially, dried under a stream of nitrogen and finally baked for 30 minutes at 110 ^{o}C.

Step 3: deposition of dendrons on the amino-silanised surface. In order to accelerate the formation of the amide bond between the dendron and the amine group on the amino-silanised surface, thionyl chloride was used to activate the carboxylic acid at the focal point of dendron. Two different approaches were used to form dendron thin film on the amino-silanised glass surfaces. The first approach was done by immersing the silanised glass slides into the solution of G1 dendron and NMP with a concentration of 0.019 mol/L. Before immersion, 1.04 equivalent of thionyl chloride (0.039 ml) wasere added to a solution containing 0.12 mmol dendron G1 in 6.4 ml NMP at 0 ^{o}C under nitrogen and stirred for 15 minutes at that temperature and then for 20 minutes at 30 ^{o}C. Two silanised glass slides were then immersed into the solution for 10 minutes and 30 minutes at 40 ^{o}C, respectively. The other approach used the microreactor to deposit G1 dendrons directly onto the silanised glass slides. A solution containing 0.12mmol dendron G1 in 3.2 ml NMP and another solution containing 0.039 ml thionyl chloride in 3.2 ml NMP were mixed through the microreactor at a flowrate of 0.026 ml/s at 30 ^{o}C. The activated G1 dendron from the microreactor was impinged onto a spinning silanised glass slide which was mounted on a heated rotating disk substrate holder

at 40 ^{o}C. The entire deposition process using the microreactor took about 2 minutes, and the residence time in the outlet tubing was 17 seconds. The glass slides were rinsed thoroughly by NMP, methanol and water sequentially, dried under a stream of nitrogen and finally baked for 30 minutes at 110 ^{o}C after the deposition.

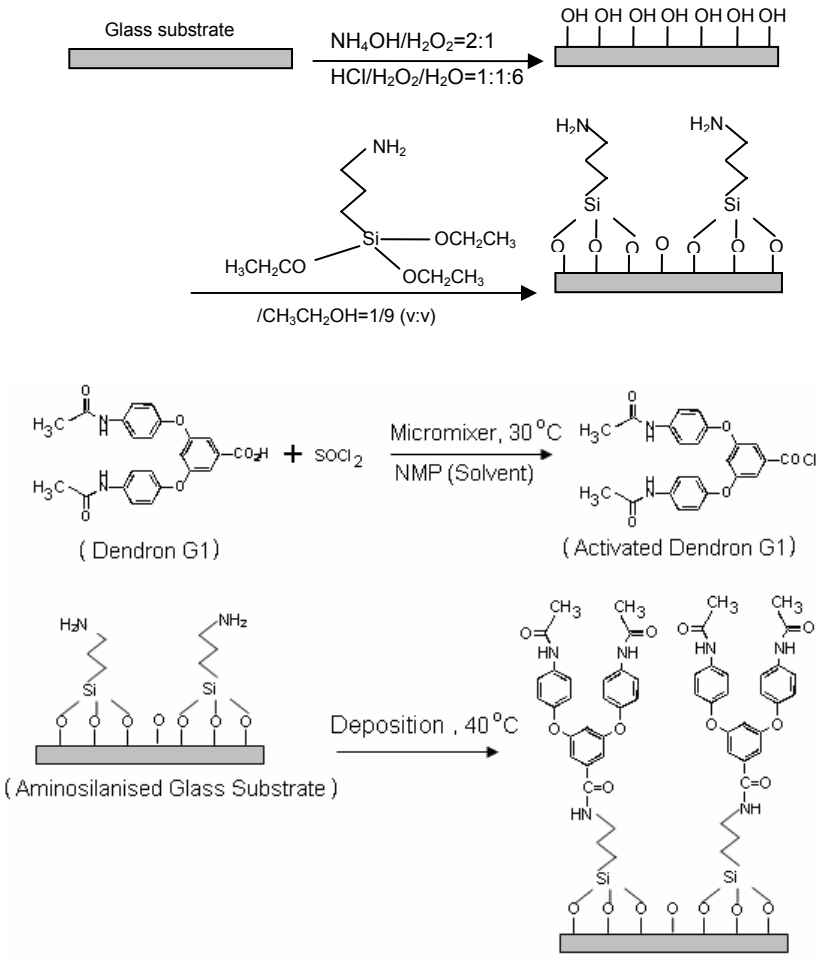

Figure 6-1. Schematic diagrams of the dendron deposition process via a microreactor.

6.2 The Characterization of Polyamide Dendron Modified Surfaces

The glass surfaces including the cleaned surface, aminosilanised surface and dendron modified surface were characterized by techniques including the water contact angle measurement, SEM, fluorescence microscope, TOF-SIMS and XPS.

6.2.1 The Water Contact Angle Measurement

The water contact angle measurements were conducted at room temperature using a FTA 135 Dynamic Contact Angle Analyzer equipped with a B/W (Monochrome) CCD camera.

The water contact angle measurement is an effective way to evaluate the effects of surface modifications. This measurement was conducted at three or four spots on the surfaces of each glass slide. The average water contact angles of glass slides with different treatments are shown in figure 6.2. The increment of the water contact angle from 24 degree (cleaned surface bearing OH groups) to 68 degree (aminosilanised surface bearing NH_2 groups) and to 84 degree (dendronized surface bearing CH_3 groups) indicated the successful deposition of 3-aminopropyl triethoxysilane on the plain surface and the deposition of G1 dendron on the aminosilanised surface, as well. These water contact angle values are in favorable agreement with the published data of glass surfaces with the same functional groups [28]. The water contact angles of the glass surfaces treated by dendron G1 through immersion and the microreactor showed very similar results, both are close to 84. This implies that the result of this microreactor approach is comparable to the immersion method, but with a much simpler handling process.

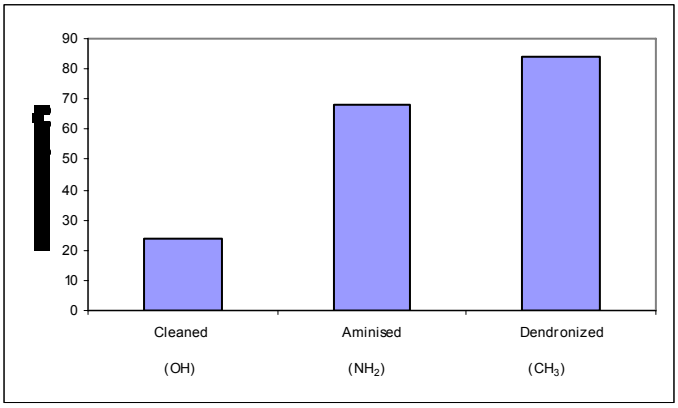

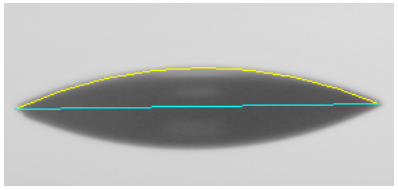

Cleaned surface, 24°

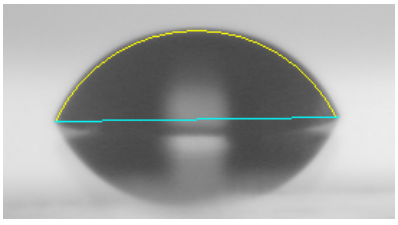

Aminosilanised surface, 68°

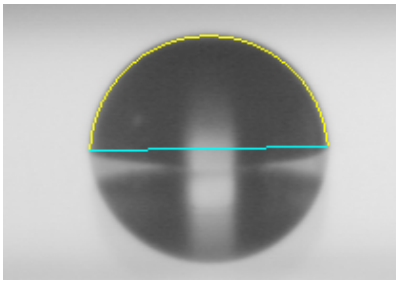

Dendronized surface, 84°

Figure 6-2. Water contact angles of glass surfaces modified by different treatments.

6.2.2 The Scanning Electron Microscopy Images of Glass Surfaces with Different Treatments

SEM (Hitachi, S-4100) was used to investigate the surface morphology of glass surfaces modified by different treatments. Figure 6-3 (A) shows a SEM image of the glass surface after cleaning by NH_4OH/H_2O_2 solution and HCl/H_2O_2 solution. Figure 6-3 (B) is the SEM image of aminosilanized glass surface. Figure 6-3 (C) and (D) show the SEM images of dendronized glass surfaces which were immersed into the G1 dendron solution in a batch reactor for 10 minutes and 30 minutes, respectively. Figure 6-3 (E) shows the SEM image of the dendronized glass surface which was exposed to the activated G1 dendron solution from the microreactor for 2 minutes. It is observed from these SEM images that nanoparticles were formed on the substrates. We believe these nanoparticles are related to the aggregation of 3-aminopropyl triethoxysilane (aminosilanized glass surface) or the G1 dendrons (dendronized surface). Comparing image B of the aminosilanized glass surface with images C, D, and E of the dendronized glass surfaces, it is obvious that the density of the nanoparticles of the aminosilanized glass surface is much less than that on the dendronized glass surfaces. Meanwhile, the distribution of the nanoparticles in image D is much denser than in image C, which means longer immersion time leads to a better dendron deposition. In addition, a similar surface morphology (image E) was obtained from a direct deposition using the microreactor in comparison with a 30 minute immersion (image D) in a batch reactor. Herein, it has to be emphasized that the deposition

time for the microreactor approach was only 2 minutes and no extra time is needed to activate the dendron G1. However, the immersion approach took an extra 35 minutes to activate the dendron G1 before the immersion of the substrates into the G1 dendron solution. It is believed that the direct deposition approach could provide a better deposition process control in terms of providing a higher temporal resolution, a constant reactant concentration flux, and an independent control over the solution and substrate temperature.

It is also found that temperature plays a very important role in the deposition of the G1 dendron to the aminosilanised glass surface, especially the temperature of the glass substrate. When both the activation reaction temperature (the temperature of the solution for the reaction between G1 dendron and thionyl chloride) and the deposition reaction temperature (the temperature of the substrate for the deposition reaction) were room temperature (from 25 to 30 ^{o}C), no deposition was observed by either approach, even after the glass substrate was immersed in the G1 dendron solution for 20 hours. Once the substrate temperature was increased to 40 ^{o}C, the dendron G1 thin film was formed by both approaches. Extended from this process, it can be imagined that some deposition needs a different activation temperature and deposition temperature. For example, the deposition needs a high temperature at which the activation reaction could have a side reaction. Therefore, the microreactor would be an appropriate tool to fulfill the deposition under this circumstance because it can provide separate control over both the solution and the substrate temperature.

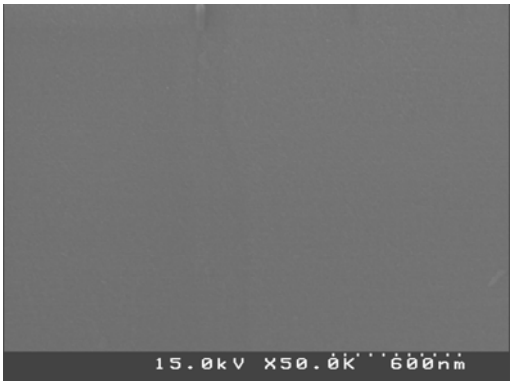

(A)

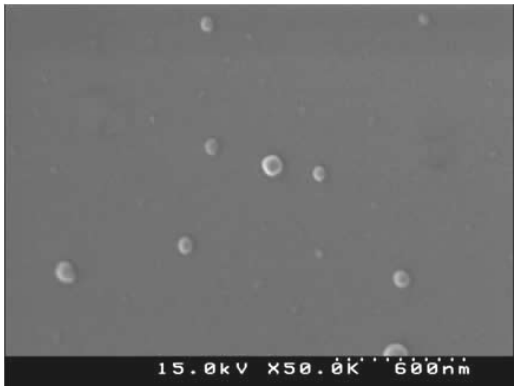

(B)

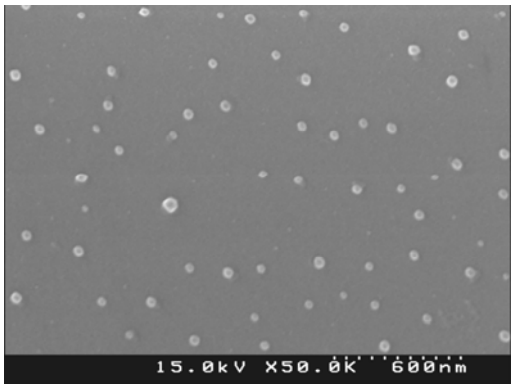

(C)

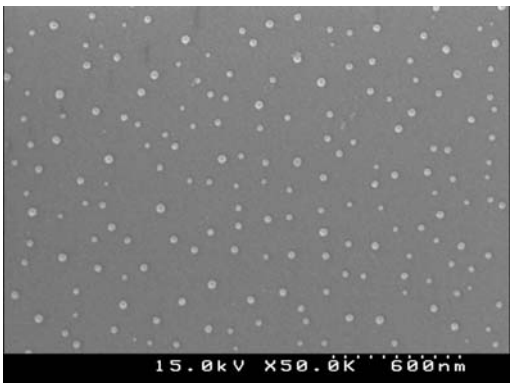

(D)

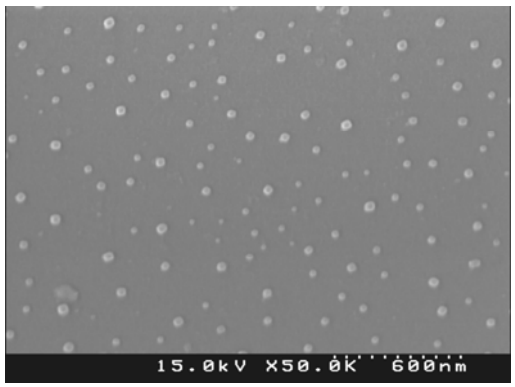

(E)

Figure 6-3.

Figure 6-3. SEM images of glass surfaces after different treatments; (A) after cleaning by NH_4OH/H_2O_2 (v/v=2:1) solution and HCl/H_2O_2 solution; (B) after immersion into 3-aminopropyl triethoxysilane solution; (C) after immersion into the G1 dendron solution for 10 minutes; (D) after immersion into the G1 dendron solution for 30 minutes; (E) after exposing to the activated G1 dendron solution from a microreactor for 2 minutes.

6.2.3 The Fluorescence Microscopy Study of Modified Glass Surfaces

From SEM images shown in the previous section, only the aggregations of nanoparticles were observed on modified glass surfaces. However the detailed morphology and structure about the depositions remained uncertain. For example, it is unclear what structure exists on the dark areas apart from the aggregation spots in those SEM images. In order to investigate the uniformity and detailed feature of the modified glass surfaces, a molecular probe, fluorescamine (purchased from Sigma-Aldrich) was used to treat the glass surfaces that were modified by 3-aminopropyl triethoxysilane and polyamide dendron. Fluorescamine itself is a non-fluorescent reagent, but it reacts readily under mild conditions with primary amines to form stable, highly fluorescent compounds. The reaction mechanism is shown in figure 6-4. The glass surface modified by 3-aminopropyl triethoxysilane is covered by primary amines. Once the primary amine covered glass surface is treated by fluorescamine, the fluorescence resulting from the reaction product can be investigated under an optical microscope by shedding light with a certain wavelength on the glass surface. The uniformity of the fluorescence reflects the uniformity of the amine coverage on the glass surface. On the other hand, if the glass surface is completely covered by polyamide dendron, rather than primary amine, there will be no appearance of fluorescence when the glass surface is treated with fluorescamine. Therefore, the fluorescence microscopy images show the uniformity of polyamide dendron coverage.

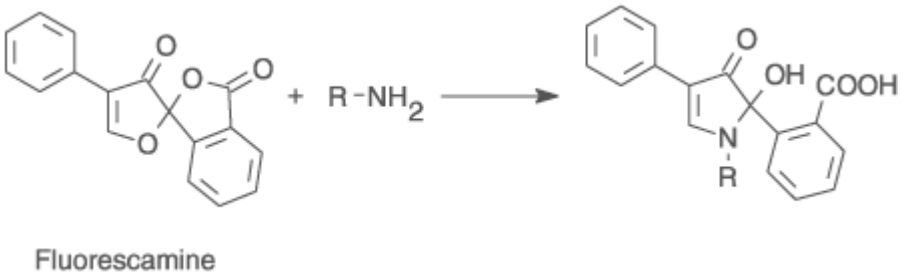

Fluorescamine

Figure 6-4. The reaction mechanism of fluorescamine with primary amine; the product has a strong fluorescence, but fluorescamine itself has no fluorescence.

Sample preparation for fluorescence measurement is described as follows.

1. Prepare a 3 ml solution of 1 mg fluorescamine (Sigma/Aldrich) in acetone in a black microcentrifuge tube, protecting this reagent from light.
2. Sonicate the solution for 30 seconds to ensure the fluorescamine has dissolved in the acetone.
3. Protecting it from light, transfer the 3ml solution into a glass beaker.
4. Put the glass which was previously modified either by the 3-aminopropyl triethoxysilane or the polyamide dendron G1 into the solution, and allow the reaction to take 8 minutes at room temperature.
5. Pick up the glass slide and dry it 10 seconds in the air; mount the glass slide on the observation stage of the optical microscope.
6. Use a 325 nm light to excite the glass surface and take an image.

6.2.3.1 The Fluorescence Microscopy Study of an Aminosilanised Glass Surface

Figures from 6-5 to 6-11 are optical microscope images of aminosilanised glass surfaces treated with or without the molecular probe. Some images including figures 6-5, 6-6, 6-8, 6-10 were taken under incidence of white light. The rests of the images were taken under incidence light with a wavelength of 325 nm. Obviously, the image (figure 6-5) of the glass slide without treatment of the molecular probe does not show the manifest feature of the deposition on the surface. However, once the aminosilanised glass surface was treated by the molecular probe, the feature of the deposition was revealed manifestly by utilizing an optical microscope under the incidence of white light (see figures 6-6, 6-8 and 6-10). Here it has to be noted that the aminosilanised glass surfaces in figure 6-5 to 6-10 were only washed by NH_4OH/H_2O_2 and no further wash by a mixture of HCl/H_2O_2 before aminosilanisation treatment. From these figures, it can be seen that the deposition of 3-aminopropyl triethoxysilane on the glass surface is not uniform. The un-uniform distribution of the deposited material results in a contrast between different parts of the surface, which helps distinguish and observe the structure of the surfaces. Films and small and big aggregation particles can be observed. Both the film and particle can be florescent, but the intensity of the fluorescence depends on the thickness of the film, and the size of the particle. The thicker the film and the bigger the particle, the more intense the fluorescence is. From figure 6-6, it can be observed that some small aggregation of particles exist

above the film. This is consistent with what is observed in the SEM image shown in figure 6-3 (B), where a few particles are observed.

It has been mentioned above that the glass substrate of the images from figure 6-5 to 6-10 was only washed by a mixture of ammonium and hydrogen peroxide. It is speculated that the un-uniformity of the deposition resulted from the previous un-even clearness of the glass substrate. After the glass substrate was subsequently washed by a mixture of hydrochloric acid and hydrogen peroxide, the optical image of the aminosilanised glass surface with a more complete cleaning reveals a more uniform deposition (figure 6-11). The fluorescence measurement is a complementary method to the SEM to investigate the deposition feature, and it helped to elucidate that if the substrate is thoroughly cleaned, the major form of the deposition of 3-aminopropyl triethoxysilane on the glass surface is film, and some aggregations of the particles also exist on the surface of the film.

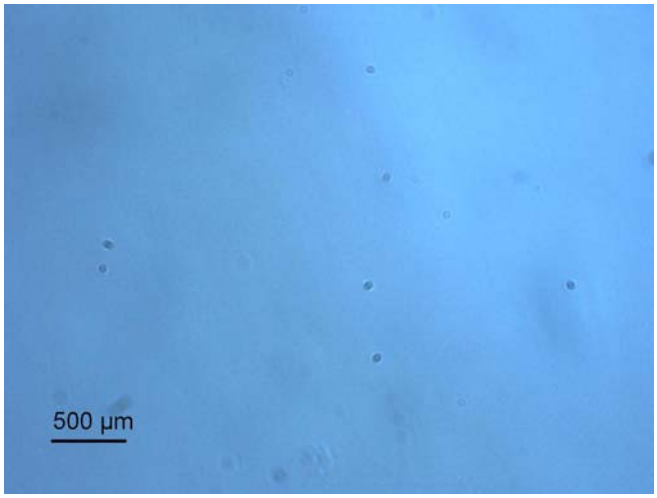

Figure 6-5. The optical microscope image (white light as incident light) of an aminosilanised glass surface before using the molecular probe; no detail feature of the deposition can be observed.

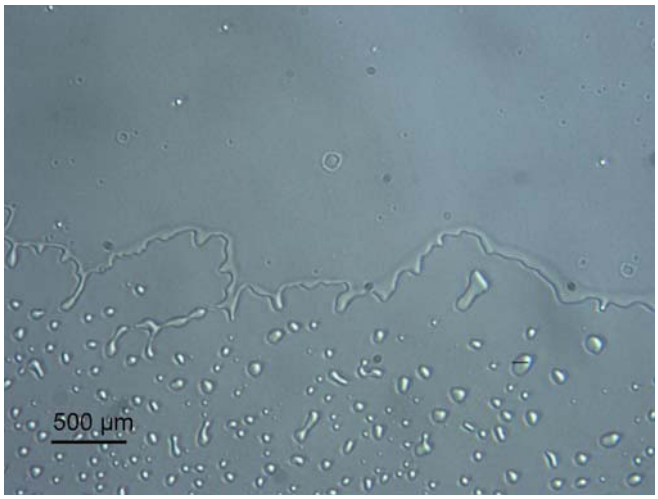

Figure 6-6. The optical microscope image (white light used as incident light) of an aminosilanised glass surface after using the molecular probe; film and aggregation particles were observed on the glass surface

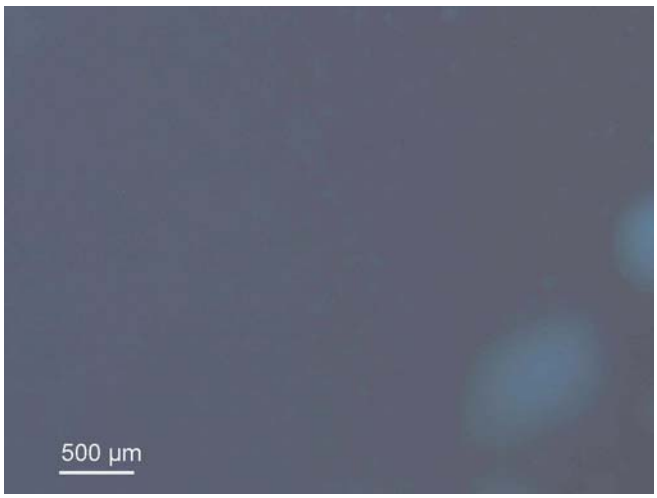

Figure 6-7. The fluorescence image (325 nm light as incident light) of one spot on the aminosilanised glass surface after using the molecular probe.

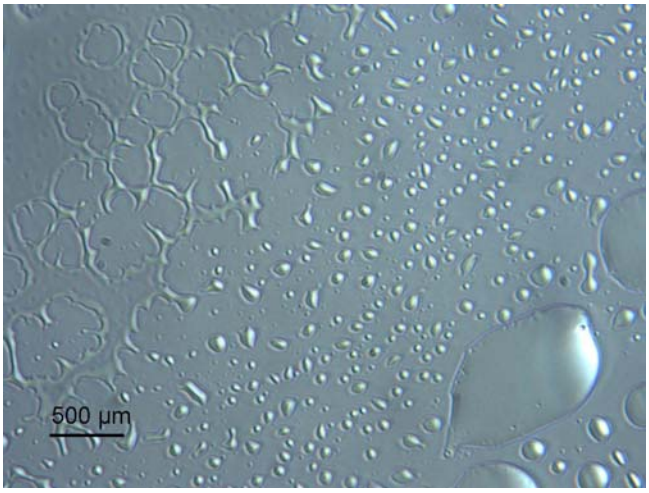

Figure 6-8. The optical microscope image (white light as incident light) of the same investigation area of the aminosilanised glass surface as figure 6-7; film and small and big aggregation particles are observed.

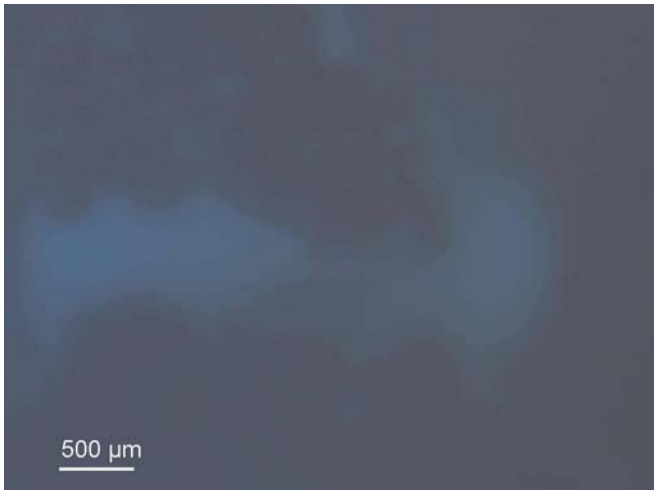

Figure 6-9. The fluorescence image (325 nm light as incident light) of another spot on the aminosilanised glass surface after using the molecular probe.

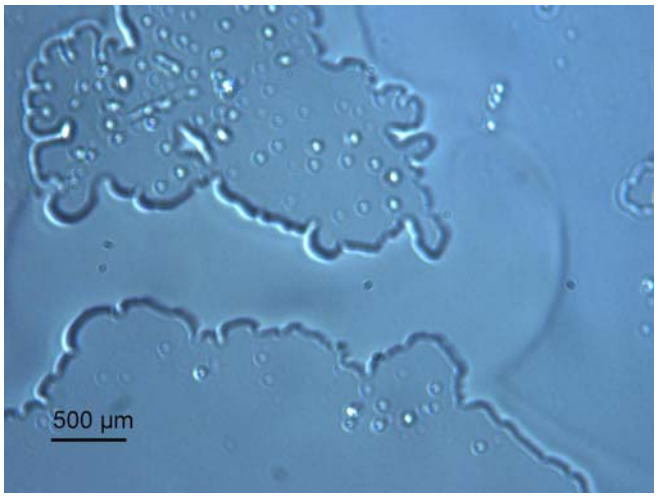

Figure 6-10. The optical microscope image (white light as incident light) of the same investigation area of the aminosilanised glass surface as figure 6-9.

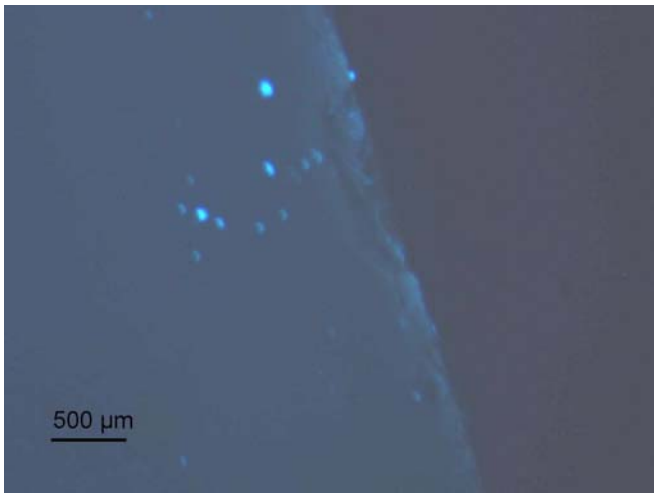

Figure 6-11. The fluorescence image (325 nm light as incident light) of the aminosilanised glass surface after using the molecular probe: the light green area is the glass slide after being treated with the molecular probe, and the dark area is another glass slide with the same aminosilanisation treatment as the left glass slide, but without being treated by the molecular probe. The uniform distribution of the green color indicates the uniform distribution of the amine groups on the glass surface. The glass slides were thoroughly washed by a mixture of ammonium and hydrogen peroxide and, subsequently, by a mixture of hydrochloric acid and hydrogen peroxide.

6.2.3.2 The Fluorescence Microscopy Study of a Glass Surface Modified by Polyamide Dendron

Figure 6-12 and 6-13 show the images of the same region of a glass surface treated by polyamide dendron G1. Figure 6-12 is the image showing the fluorescence of the glass surface which was shed by light with a wavelength of 325 nm. Figure 6-13 shows the image of the same region of the same glass surface which was shed by white light. When compared, these two images, some conclusions about the deposition can be obtained as follows.

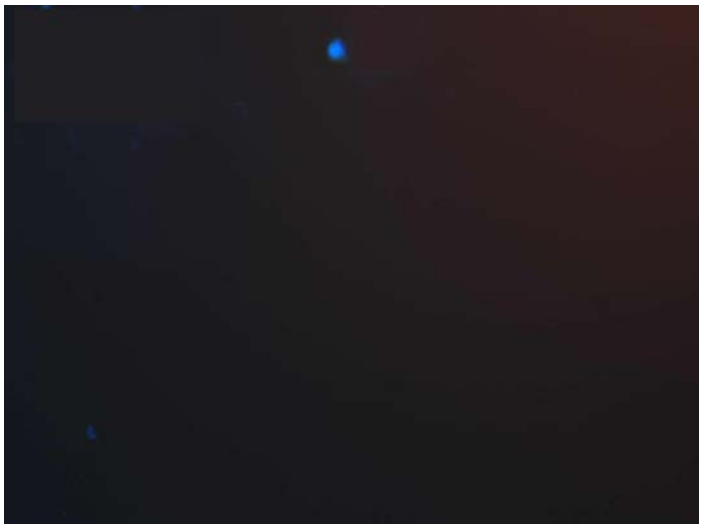

Figure 6-12. The fluorescence image (325 nm light as incident light) of the dendronized glass surface after using the molecular probe;

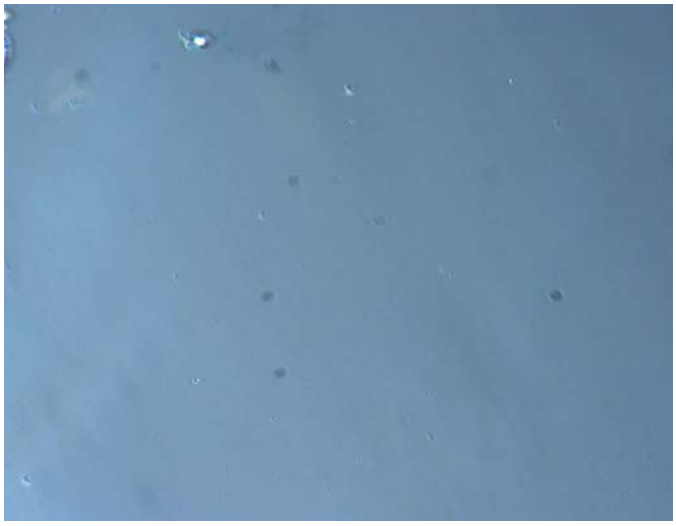

Figure 6-13. The optical microscope image (white light used as incident light) of the same investigation area of the dendronized glass surface as figure 6-12.

The coverage of the polyamide dendron G1 is comparatively uniform and most areas are deposited by the polyamide dendron G1. It can be seen from figure 6-13 that the area and size of the bright spots (amine spots where amines were not reacted with polyamide dendron G1) are much smaller than that in the 3-aminopropyl triethoxysilane deposited glass surface (i. e. in figures 6-6 and 6-8). This can be explained because the deposition of polyamide dendron G1 on the amine group sites reduced the reaction sites of amine to the fluorescamine.

From the fluorescence images of the dendronized glass surfaces (figure 6-13), the aggregation of dendron particles cannot be observed. However, this is not contrary to what was observed in the SEM images (figure 6-3 C. D. and E). The SEM images were taken under a magnification of 50,000, so even small particles with a size of 60 nm can be detected. On the other hand, these small particles of

polyamide dendron aggregation cannot be resolved under an optical microscope with a magnification of 40. As we know, the aggregation of particles made of 3-aminopropyl triethoxysilane can be observed under optical microscope with magnification of 40. This is because after the amine groups reacted with the fluorescamine, they had a different optical property which generates a strong contrast with the background. Unlike the aggregation of particles made of 3-aminopropyl triethoxysilane, the nanoparticles made of polyamide dendron do not react with fluorescamine, and they do not have a different optical property from that of the background. Therefore, these polyamide dendron nanoparticles cannot be observed under an optical microscope with a magnification of 40. However, it is reasonable that the polyamide dendron exists in two forms: film and aggregation of nanoparticles on the glass surface because it is determined that the major form of the precursor, 3-aminopropyl triethoxysilane, is film. Some polyamide dendron molecules must react with the amine groups on the film region to form the polyamide dendron film.

The combination of SEM and fluorescence measurement effectively elucidated the feature of depositions of the 3-aminopropyl triethoxysilane and the polyamide dendron on the glass surface. It is evident that the major deposition form of the 3-aminopropyl triethoxysilane is film, and scattered nanoparticles are distributed on the film. Polyamide dendrons tend to aggregate to form nanoparticles which have a much denser distribution on the glass surface compared to the distribution of the 3-aminopropyl triethoxysilane nanoparticles. It is also speculated that besides the

existence of the nanoparticles of the polyamide dendron which was observed, the polyamide dendron film exists, as well.

6.2.4 The TOF-SIMS Characterization of Aminosilanised and Dendronized Glass Surfaces

The TOF-SIMS was utilized to study the chemical component of the modified glass surfaces and to investigate whether the substances were covalently bonded or physically absorbed on the glass surfaces. Figure 6-14 shows the TOF-SIMS spectrum of the aminosilanised glass surface, the chemical structure of the 3-aminopropyl triethoxysilane and the proposed chemical structures of the deposition. Peaks at 139 and 165 mass/u in figure 6-14(E) match the molecular weights of the speculated chemical structures of the covalently bounded 3-aminopropyl triethoxysilane shown in figure 6-14 (C) and (D). Moreover, there is no peak at 221.37 mass/u (molecular weight of 3-aminopropyl triethoxysilane molecule) observed in the spectrum, which implies the 3-aminopropyl triethoxysilane molecules were covalently bonded on the glass surface, rather than physically absorbed on the surface.

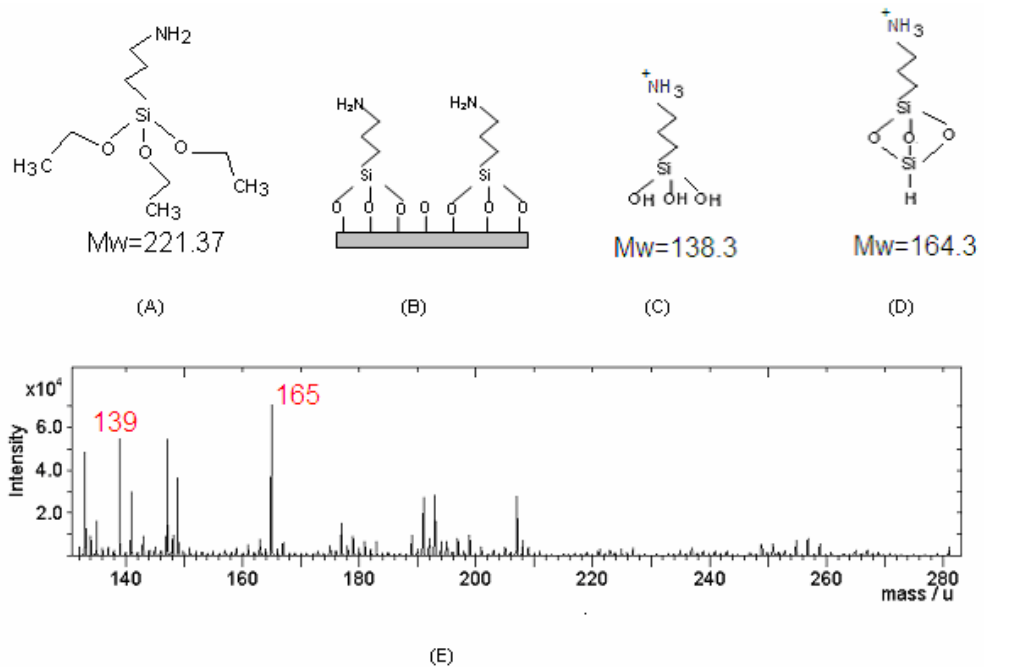

Figure 6-14. (A) The chemical structure of a 3-aminopropyl triethoxysilane molecule with a molecular weight of 221.37; (B) The desired deposition of the 3-aminopropyl triethoxysilane on a glass surface; (C) One speculated chemical structure of the deposition of the 3-aminopropyl triethoxysilane on a glass surface with a molecular weight of 138.3; (D) Another speculated chemical structure of the deposition of the 3-aminopropyl triethoxysilane on a glass surface with a molecular weight of 164.3; (E) The TOF-SIMS spectrum of the aminosilanised glass slide shows peaks at 139 and 165 mass/ u, which match the speculated chemical structures shown in (C) and (D).

Figure 6-15 shows the TOF-SIMS spectrum of the polyamide dendron modified glass surface. Figure 6-16 shows the chemical structure of the polyamide dendron molecule and the various proposed chemical structures of the polyamide dendron desposition. The peaks at 523 and 551 in figure 6-15 match the molecular weights of the speculated chemical structures shown in figure 6-16 (D) and (E) respectively. These two structures are two different possible forms of the covalently bonded polyamide dendron to the amine group. The polyamide dendron G1, itself, has a molecular weight of 420 (figure 6-16 (A)), and the product of the reaction between the dendron G1 and the 3aminopropyl triethoxysilane (chemical structure shown in figure 6-16 (B)) has a molecular weight of 623.37. Previously, it is known that the molecular weight of 3-aminopropyl triethoxysilane is 221.37. From the spectrum 6-15, none of the three peaks: 221.37, 420 and 623.37 are observed, which means that the 3aminopropyl triethoxysilane was covalently bonded on the glass surface; furthermore, the polyamide dendron G1 was covalently bonded to the amine group, but not physically absorbed on the glass surface.

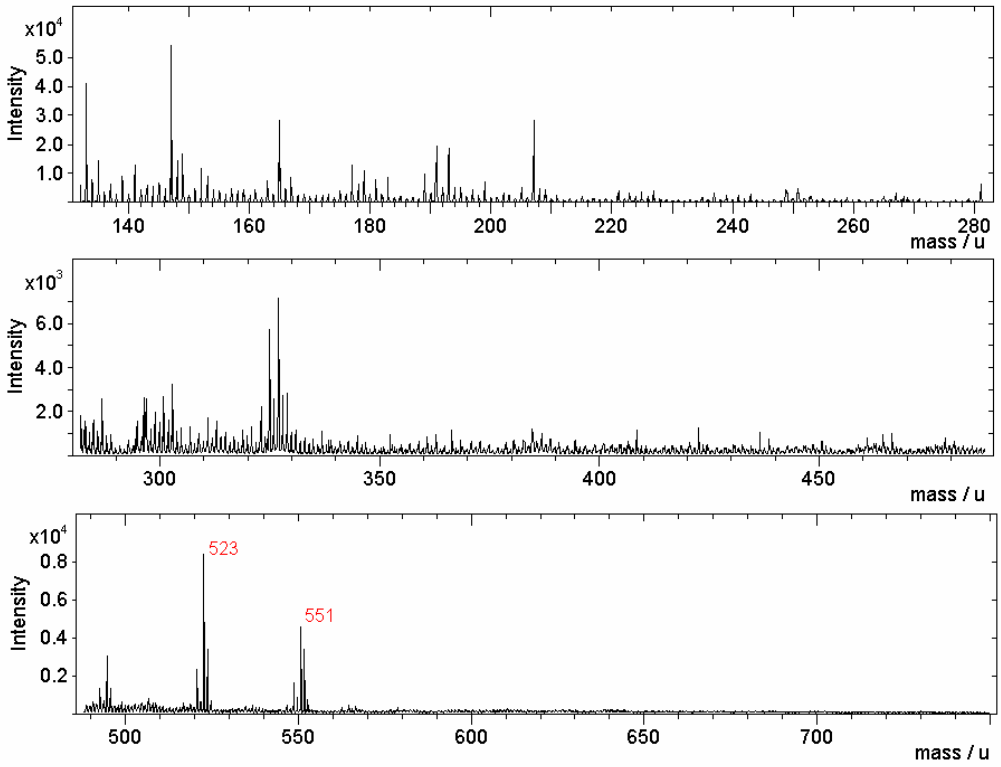

Figure 6-15. The TOF-SIMS spectra of the dendronized glass slide show peaks at 523 and 551 mass/ u, which match the speculated chemical structures shown in figure 6-16 (D) and (E).

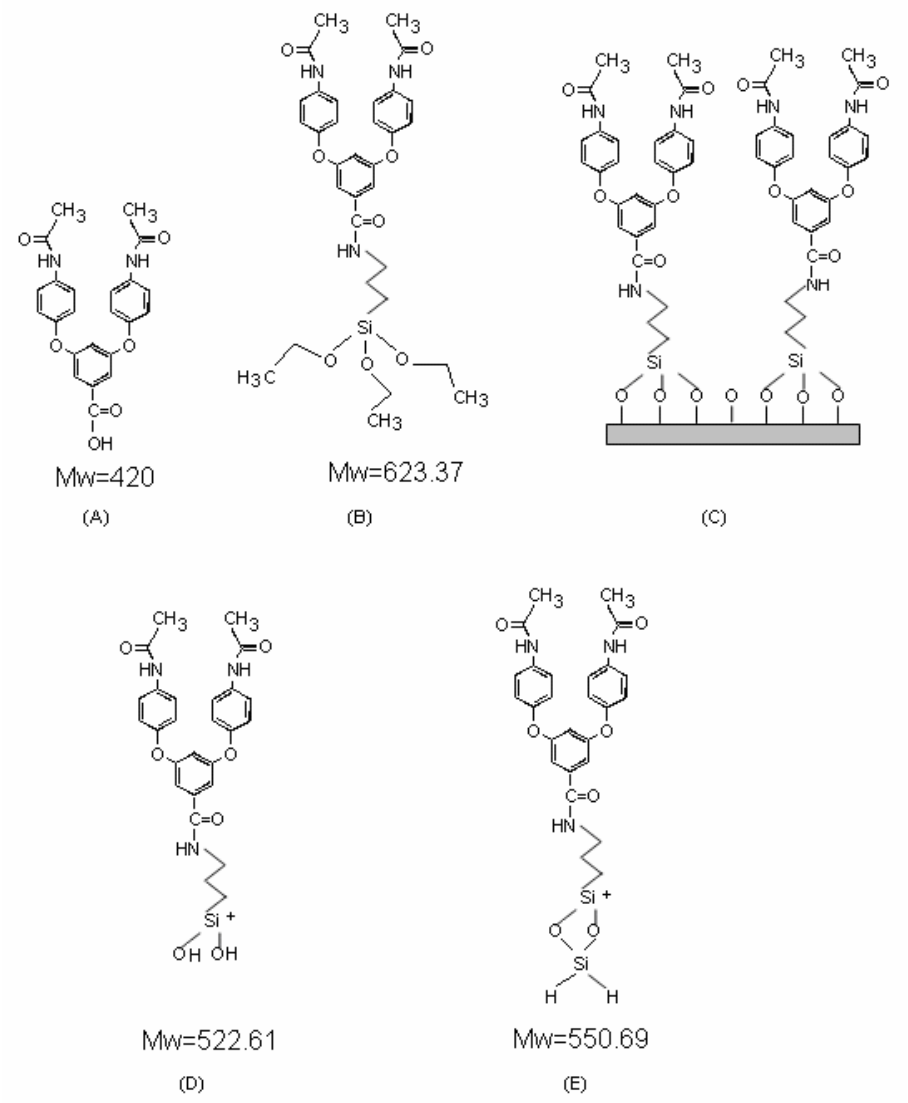

Figure 6-16. (A) The chemical structure of the polyamide dendron G1 with a molecular weight of 420; (B) The chemical structure of the product of the reaction between the polyamide dendron G1 and the 3-aminopropyl triethoxysilane, with a molecular of 623.37; (C) The desired deposition of the polyamide dendron on a glass surface; (D) One speculated chemical structure of the deposition of the polyamide dendron G1 on a glass surface with a molecular weight of 522.61; (E) Another speculated chemical structure of the deposition of the polyamide dendron G1 on a glass surface with a molecular weight of 550.69;

6.2.5 XPS Characterization of the Modified Glass Surfaces

XPS was performed to determine the chemical composition of the clean, 3-aminopropyl triethoxysilane modified and the polyamide dendron G1 modified glass surfaces. It is a complementary tool to confirm the covalent bonding of the substances on the glass surfaces. The Si2p, C1s and N1s XPS spectra of the glass surfaces with different treatments are shown in figure 6-17, 6-18, and 6-19, respectively. From figure 6-17, it is obviously seen that the silicon percentage decreased after the surface modification of the aminsilanisation and dendronization, as expected since XPS is a depth sensitive technique. XPS characterizes only the uppermost (7-10nm) surface chemistries, so the bulk silicon photoelectron generated from the glass substrate is masked as more layers are deposited. The position of the binding energy of the silicon is shifted after modifying the glass surface, indicating the chemical state of the silicon has been changed after the modification. This is strong support that the 3-aminopropyl triethoxysilane is covalently bonded to the glass surface, which therefore changed the bonding state of the silicon. The C1s XPS spectra (figure 6-18) show that the surface carbon increased after modification with the aminosilane and the subsequent immobilization of the polyamide dendron, and the carbon intensity of the dendronized surface was higher than the aminosilanised surface. These increases are expected since aminosilane and dendron are composed predominantly of carbon, and the dendronized surface has more carbons. The N1s XPS (figure 6-19) spectra show the appearance of nitrogen after modification of

the glass surface. From the above analysis, it is clear that the aminosilane and the dendron were covalently bonded on the glass surface by comparing the XPS spectra of the different surfaces.

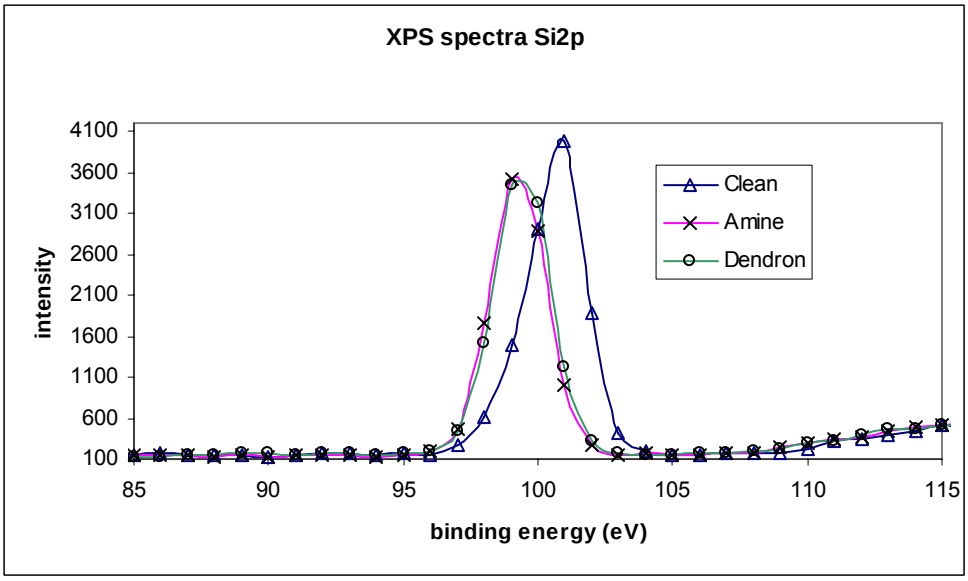

Figure 6-17. Si2p XPS spectra of the clean, the 3-aminopropyl triethoxysilane -modified and the polyamide dendron G1-modified glass surfaces.

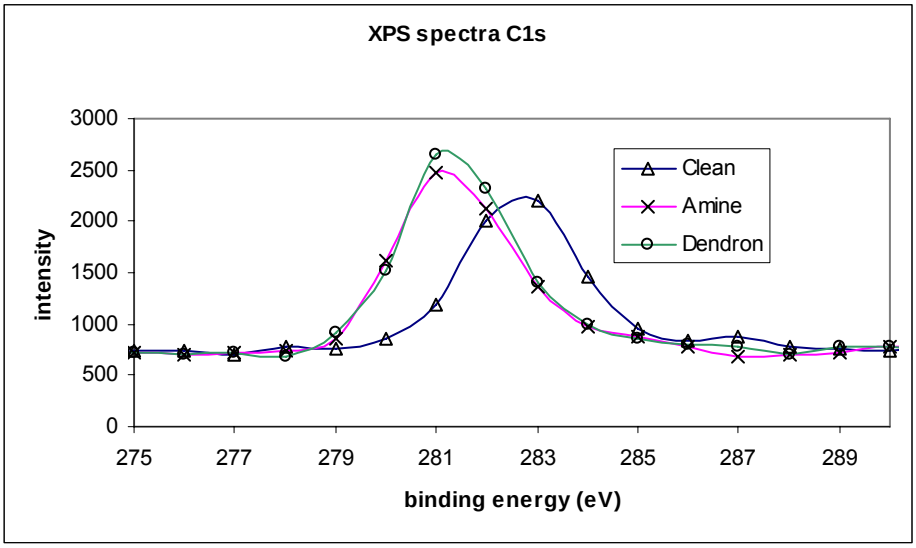

Figure 6-18. C1s XPS spectra of the clean, the 3-aminopropyl triethoxysilane-modified and the polyamide dendron G1-modified glass surfaces.

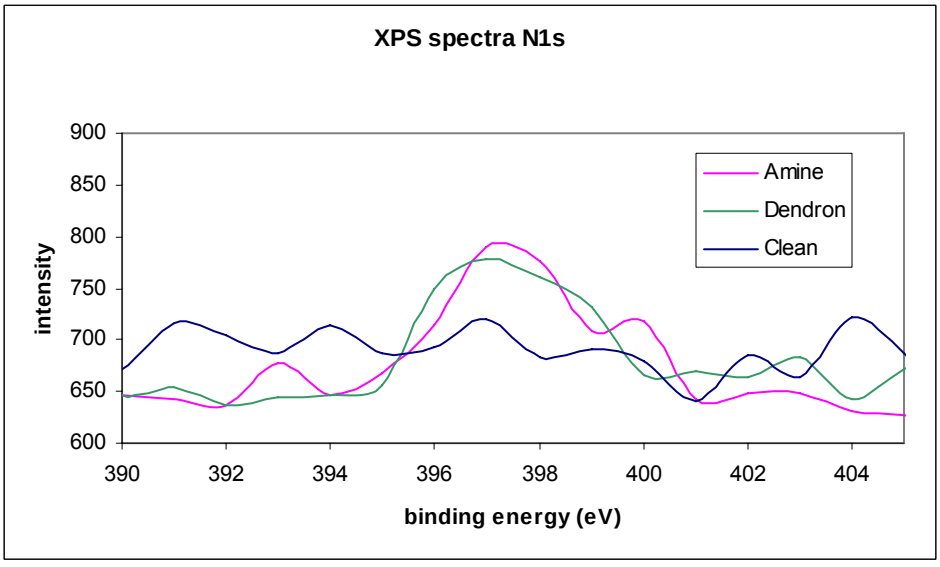

Figure 6-19. N1s XPS spectra of the clean, the 3-aminopropyl triethoxysilane-modified and the polyamide dendron G1-modified glass surfaces.

6.3 Conclusions of Plolamide Dendron Deposition

The deposition of the polyamide dendron G1 on the aminosilanised glass surfaces were realized by using a continuous-flow microreactor. The utilization of techniques, such as the water-contact angle measurement, SEM, fluorescence image, TOF-SIMS, and XPS provided sufficient evidence that the 3-aminopropyl triethoxysilane and the polyamide dendron G1 were covalently bonded on the glass surfaces and featured with a uniform distribution of film and nanoparticles.

The water contact angle is the most convenient technique to initially test the existence of deposition, based on the fact that a different modification of the surface will result in functional groups with a different hydrophilicity on the glass surface. The combination of SEM and fluorescence microscopy provided visualized images indicating the feature of the deposition: the precursor, the 3-aminopropyl triethoxysilane forms a uniform film and the scattered aggregation of nanoparticles on the glass surface; the polyamide dendron G1 tends to form aggregation of nanoparticles with a much denser distribution than that of the 3-aminopropyl triethoxysilane. It is speculated that besides the nanoparticles, the film of the polyamide dendron also exists due to the existence of the precursor film, the 3-aminopropyl triethoxysilane. The combination of the techniques of TOF-SIMS and XPS confirmed that the 3-aminopropyl triethoxysilane and the polyamide dendron G1 were covalently bonded to the glass surface, rather than physically absorbed on the glass surface.

Compared with the traditional method used to modify the glass surface by immersing it into a solution, the approach by utilizing a micromixer provided a comparable result with an easy deposition process control within a much shorter reaction time.

Chapter 7 The Divergent Synthesis of PAMAM dendrimer

7.1 The Reactions of PAMAM Dendrimer Synthesis

Figure 7-1 illustrates the reactions of the divergent dendrimer synthesis, the synthesis of PAMAM dendrimer. The synthesis of a high generation PAMAM dendrimer is realized by iterative reactions of a Michael addition of primary amine to methylacrylate and the subsequent amindation reaction of ester and ethylenediamine (EDA). The core of the dendrimer is chosen as EDA. Based on the nomenclature tradition of this kind of dendrimer, dendrimers with the terminal functional groups of methyl are named as half generations starting from generation G-0.5. Meanwhile, the dendrimers with the terminal functional groups of amine are named as full generations such as G0, G1, and so on.

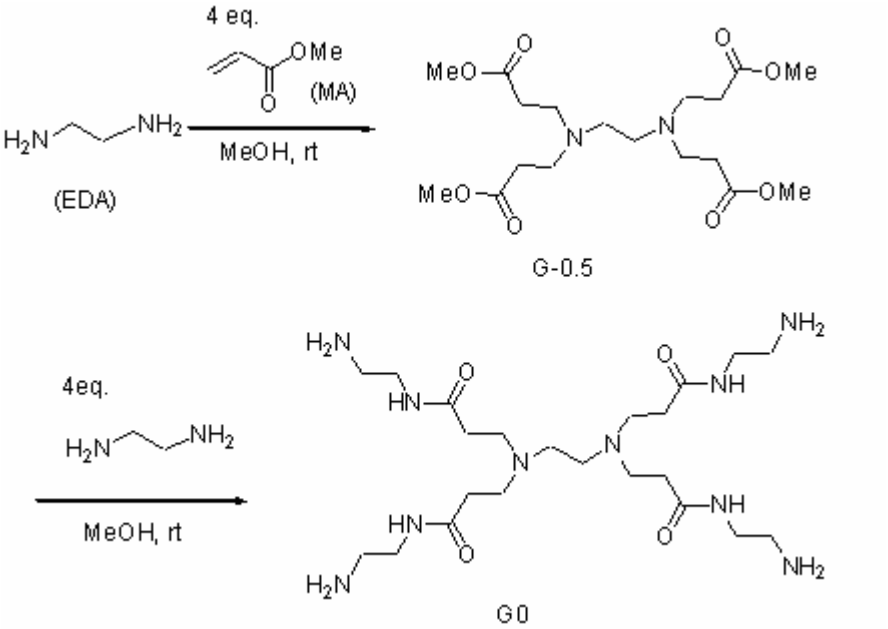

Figure 7-1. The synthesis of PAMAM dendrimers of G–0.5 and G0.0

The reaction mechanism of the Michael addition reaction is illustrated in figure 7-2. For the sake of convenience to illustrate the mechanism, full generation dendrimers (including EDA) are expressed as $R1NH_2$, where R1 represents the remaining parts of the molecule other than the primary amine group. There are a number of reaction cites for each dendrimer molecule, both for half and full generation dendrimers. The reactions taking place at all sites in the same molecule follow the same mechanism. For example, there are four reaction cites (NH locations) in an EDA molecule to complete the Michael addition reaction, further to produce the desired product, dendrimer generation G-0.5. To simplify the

drawing of the chemical structure, in order to elucidate the mechanism, only the reaction taking place at one reaction cite is illustrated in figure 7-2.

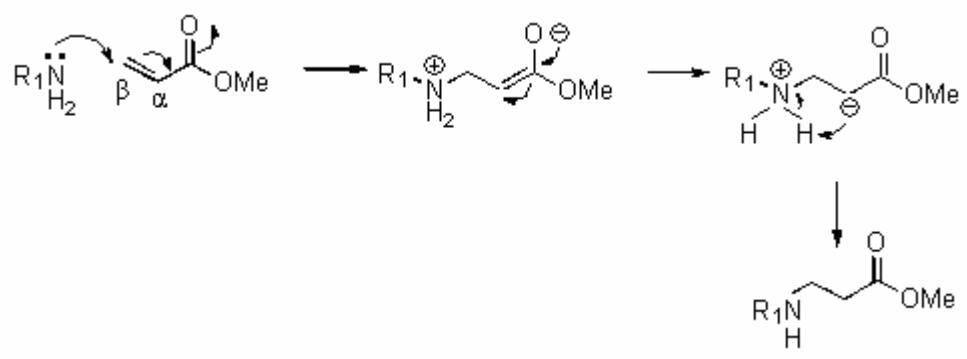

Figure 7-2. The schematic reaction mechanism of the Michael addition of the amine to the methylacrylate.

The nitrogen in the nucleophile, primary amine, attacks the β carbon of methyl acrylate. The transfer of electrons leads to the bonding between the nitrogen and the β carbon, causing the positive and negative parts in the molecule. Finally, the negative part catches the hydrogen, so the molecule is neutralized and a new branch of the half generation dendrimer molecule is generated.

The mechanism of the amidation reaction following the Michael addition reaction is illustrated in figure 7-3. Similarly, in order to simplify the drawing of the structure, half generation dendrimers and methyl acrylate are expressed as $R2COOCH_3$, where R2 represents the rest parts of the molecule apart from the group, $COOCH_3$.

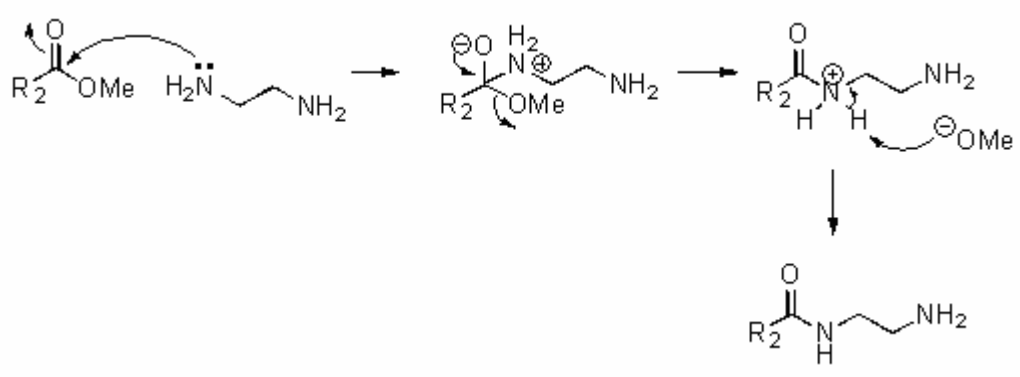

Figure 7-3. The schematic reaction mechanism of the amidation reaction to form full generation dendrimers.

The reactions above are exothermic, so cooling and stirring are critical in the conventional synthesis of the PAMAM to avoid hot spots, which promotes side reactions and reduce the selectivity of the desired product. Additionally, the amidation reaction (synthesis of full generations) could easily involve the formation of cyclic compounds derived from intra-dendritic cyclization (figure 7-4). These problems will inevitably increase the difficulty of the synthesis and post-separation processes, especially for large-scale synthetic processes. Within conventional batch reactors, the intra-molecular amidation that gives rise to the

cyclic product will be much more likely to occur due to poor mass transfer. To remedy this, a large excess of EDA (50 equivalents) and a prolonged reaction time (96 hr) are normally required for the conventional synthesis of full generation PAMAM.

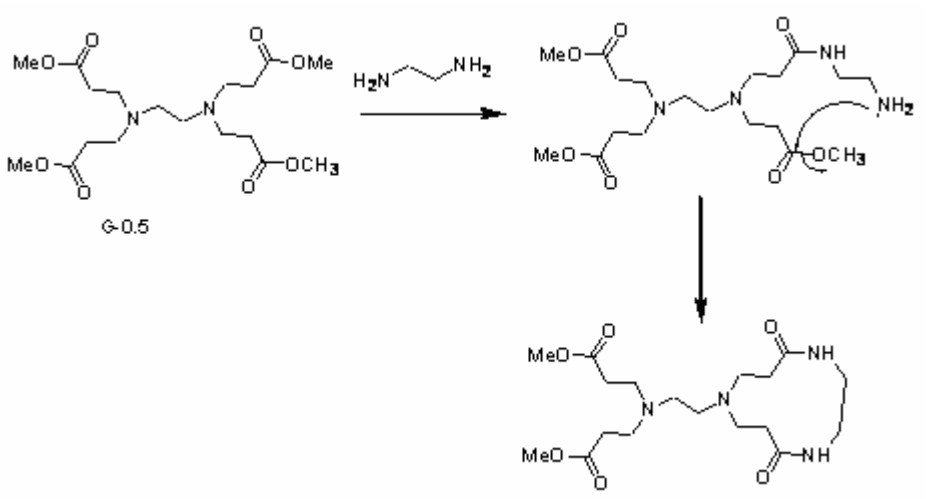

Figure 7-4. Non-ideal amidation (cyclization) of EDA-core PAMAM

7.2 The Synthesis of PAMAM Dendrimer via the Interdigital Micromixer

7.2.1 Experimental Method of Utilizing the Interdigital Micromixer

Synthesis of G-0.5:

A 5 ml solution of 1 mol/l of EDA (5 mmol) dissolved in methanol and a 5 ml solution of 5 mol/l methyl acrylate (25 mmol) dissolved in methanol were introduced into microchannels by syringe pumps at a flowrate of 0.026 ml/s,

respectively. The residence time in the outlet tubing was 17 seconds, and the product was collected at the outlet, and aliquots of the product were taken to remove the solvent by vacuum quickly for NMR analysis. The solvent in the remaining bulk product was removed by a rotary evaporator under reduced pressure at 40 ^{o}C resulting in a colorless oil as the final product.

Synthesis of G0.0:

A 3 ml solution of 0.25 M of G-0.5 dissolved in methanol and a 3 ml solution of EDA (30 mmol) dissolved in methanol were introduced into microchannels by syringe pumps at a flowrate of 0.026 ml/s, respectively. The product was collected at the outlet, and aliquots of the product were taken to remove the solvent by vacuum for NMR analysis. The solvent in the remaining bulk product was removed by a rotary evaporator under reduced pressure at 40 ^{o}C resulting in a colorless oil as the final product.

7.2.2 The PAMAM Synthesis Results via the Interdigital Micromixer

Generation G-0.5 Dendrimer:

The synthesis of G-0.5 was conducted at different times using an interdigital micromixer. Originally, the synthesis came up with a high selectivity and a high space-time yield. Figure 7-5 (a) and (b) show the NMR spectra of the generation G-0.5 synthesized in a conventional flask reactor and in a microreactor, respectively. It shows no detectable side products were produced with the microreactor approach. On the other hand, the NMR spectrum from the batch reactor shows some side products (shoulders appeared at peak 3.67ppm in figure

7-5. a) even after 3 days of vigorous mixing. The detailed NMR spectral characterization is described as follows:

The molecular formula of G-0.5 is ($^{a}CH_2$ $^{a}CH_2$)[N($^{b}CH_2$ $^{c}CH_2$ $^{d}CO_2$ $^{e}CH_3$)$_2$]$_2$. In the NMR spectra of the G-0.5 displayed in figure 7-5 (a) and (b), the single peak at 3.67ppm is assigned to proton ‘e’; the triplet peak centered at 2.76 to proton ‘b’; the singlet peak at 2.49ppm to proton ‘a’; and the triplet peak centered at 2.44 to proton ‘c’.

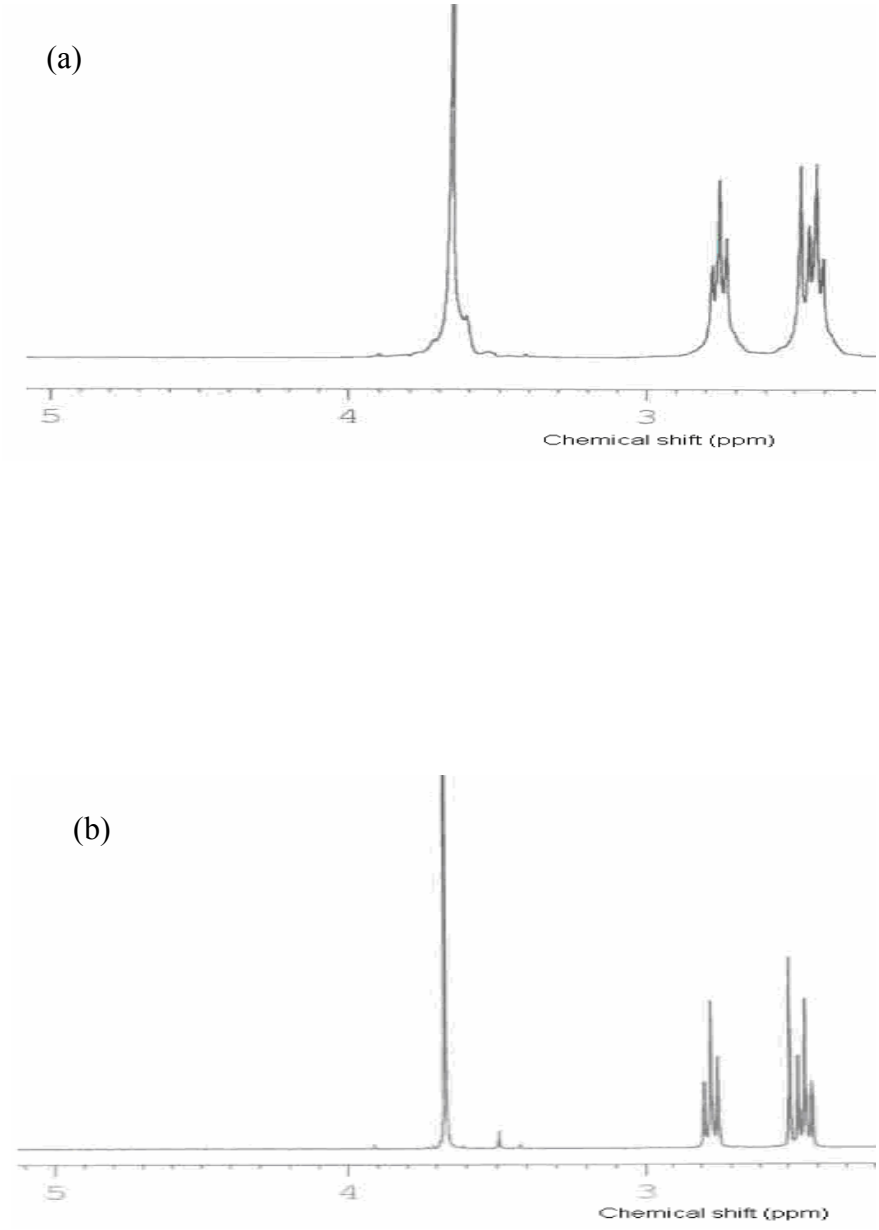

Figure 7-5. The NMR spectra of PAMAM G-0.5. (a). synthesized in a flask for 3 days, (b) synthesized in a microreactor.

The mass spectrum of the G-0.5 (molecular weight of 404) synthesized via the microreactor is shown in figure 7-6. The appearance of the peak at m/z 405 (M+H) indicates the successful synthesis of the product of the G-0.5 via the microreactor.

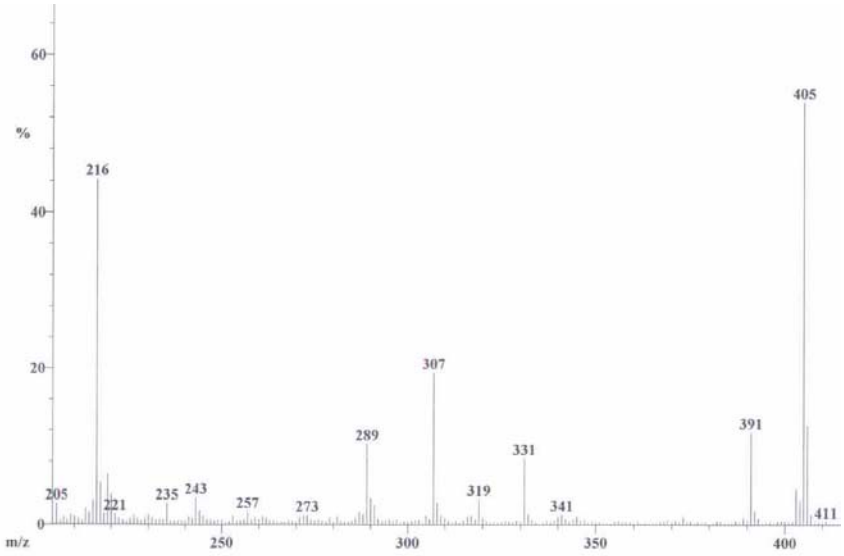

Figure 7-6. The MS spectrum of the PAMAM G-0.5 synthesized via the microreactor.

The synthesis of the G-0.5 by using the IMM microreactor was repeated lots of times at a curtain period of time with excellent repeatability. It generated G-0.5 product with high purity within 17 seconds. However, it was found that the same result could not be realized under the same reaction conditions afterward when new chemicals were purchased. Figure 7-7 and 7-8 show the NMR spectra of the synthesized product at different times. The experiment to produce the product in figure 7-7 was conducted in the year, 2005. It shows a 90% conversion to the desired product when the residence time is 17 seconds. At that time, it was not

monitored that how long time was needed to realize a 100% conversion, and it was speculated that the lower conversion was due to the change of the dimension of the microchannels since the interdigital micromixer had been used for more than one 1 year. However, the result was not improved when a new identical micromixer was utilized to conduct the reaction under the same conditions. Therefore, the possibility that the declined mixing quality of the old micromixer could cause the reduced conversion is ruled out.

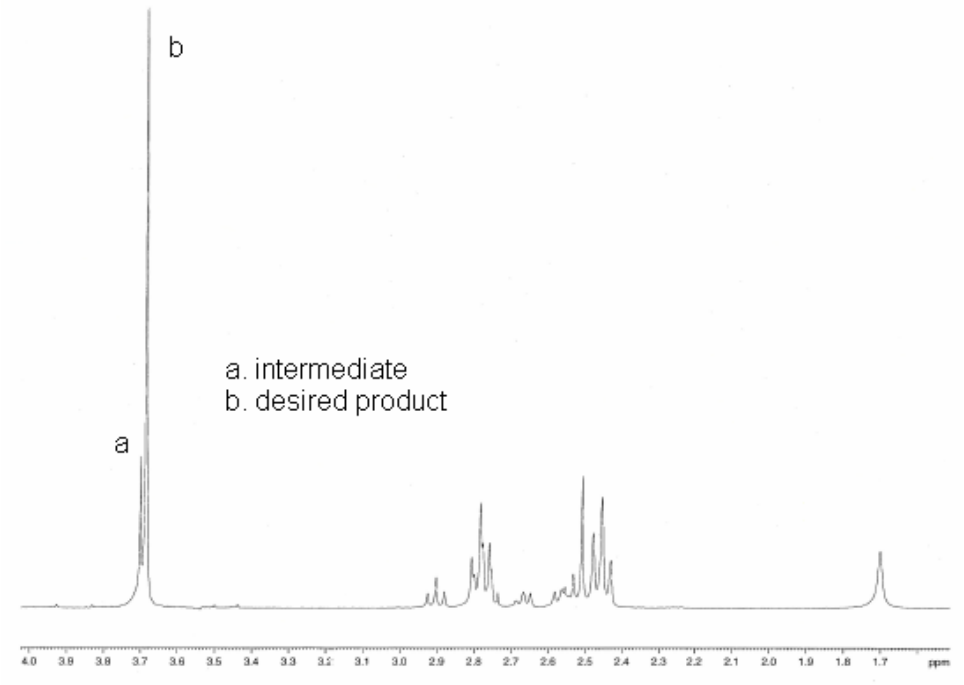

Figure 7-7. The NMR spectrum of the G-0.5 synthesized via the micromixer shows a lower yield when the new chemical was used. The experiment was conducted in the year of 2005. This is a representative spectrum among the experimental results at that period of time.

Figure 7-8 shows NMR spectra of G-0.5 dendrimers synthesized via the interdigital micromixer in the year, 2007. New chemicals were used for these reactions. It is investigated that the conversion to the desired product is only about 25% with a residence time of 17 seconds. It was monitored that the conversion was almost completed in 30 minutes.

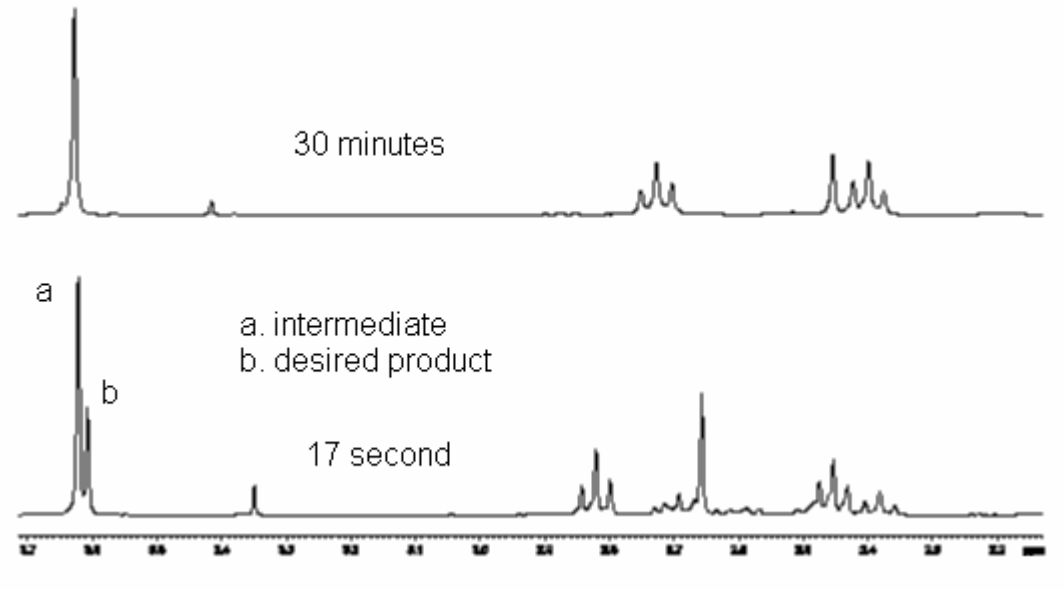

Figure 7-8. The NMR spectra of the G-0.5 synthesized via the micromixer shows a lower yield when the new chemical was used. The experiment was conducted in the year, 2007.

It has to be noticed that all of the reactions were conducted under the same conditions, except the starting materials were purchased at a different period of time. Ruling out the possibility that the micromixer itself could cause the reduced conversion, the most possible reason for causing this non-repeatability is

speculated to be due to the change of chemical properties. The chemical property of the starting materials was tested by H-NMR and compared with the original corresponding materials. The NMR spectra showed no difference between the starting materials used at different times. It is hard to verify how the physical property changes. However, if the physical property of the material changes, for example, the degree of molecule aggregation is increased, the reaction rate must be reduced. This can be explained with figure 7-9 which illustrates two fluid streams mixing with each other. Assume that stream A consists of molecules A and the aggregation of molecule A packets, and stream B is individual molecules. Apparently, the individual molecules A and B are free to move around and collide with each other. However, the molecules inside of the aggregation do not have chance to collide with each other; therefore, the reaction rate could be dramatically reduced.

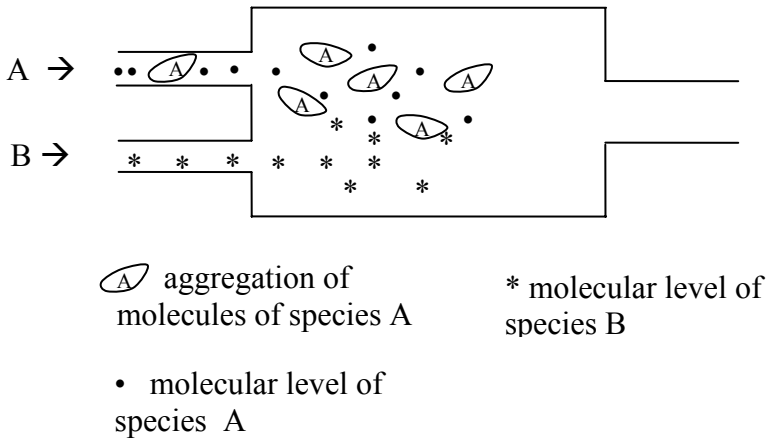

Figure 7-9. The schematic illustration of the mixing of two fluid streams.

Generation G0 Dendrimer:

The molecular formula of G0.0 is ($^{a}CH_2$ $^{a}CH_2$)[N($^{b}CH_2$ $^{c}CH_2$ ^{d}CO ^{e}NH $^{f}CH_2$ $^{g}CH_2$ $^{h}NH_2)_2]_2$. In the NMR spectra of G0.0 displayed in figure 7-10, the detailed assignments of hydrogen are as follows: δ 7.48 (4H, t, e), 3.26 (8H, q, f), 2.81 (8H, t, b), 2.66 (8H, t, c), 2.41 (4H, s, a), 2.34 (8H, t, h).

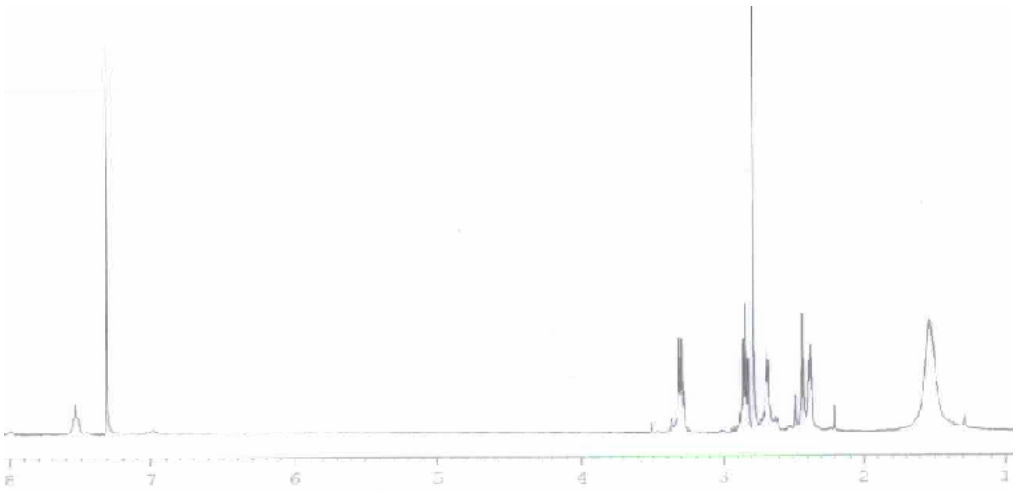

Figure 7-10. H-NMR spectrum of the PAMAM G0 synthesized in the microreactor.

The mass spectrum of the G0.0 synthesized via the microreactor is displayed in figure 7-11. The molecular weight of the G0.0 is 516, and the peak at m/z = 517 (M+H) indicates the successful synthesis of the products of the G0.0 via the microreactor.

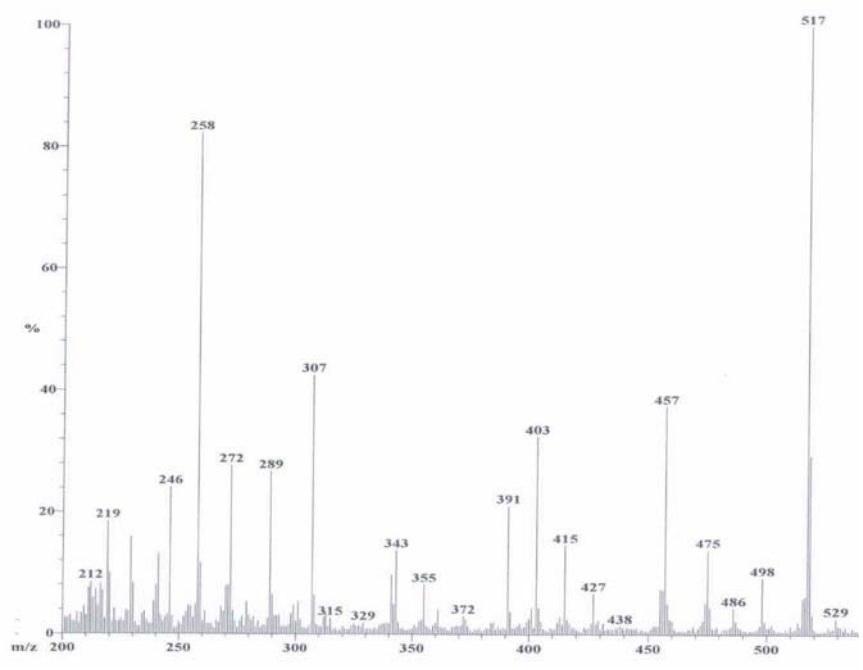

Figure 7-11. The MS spectrum of the PAMAM G0.0 synthesized via the microreactor.

7.3 The Summary of the Synthesis of the PAMAM Dendrimer via the Interdigital Micromixer

The microreactor demonstrates the feasibility to synthesize PAMAM dendrimers with a high purity and yield. It shows several advantages over the conventional batch process. The conventional reaction required cooling and stirring, inert gas protection and the dropwise addition of reagents at the beginning to minimize heat generation. All of the reactions using the microreactor were performed continuously at an ambient temperature without the need for an inert atmosphere**.** The most attractive advantage of the microreactor approach is that the

residence time is 17 seconds versus 3 days (for half generation) and 96 hours (for full generation) in a conventional batch reaction. A number of experiments were conducted using the microreactor at a certain period of time, and the results demonstrated good reproducibility. However, when new chemicals were purchased and used for the reaction, the same result could not be realized. It is speculated that the physical property of the chemicals, especially the aggregation of the molecules, lead to segregation causing the reduced reaction rate. This hypothesis needs to be verified in future work.

Chapter 8 Conclusion

The mixing quality, the most significant property of micromixers, was measured experimentally and studied computationally. The experimental method is an easy access way, and it used a pair of competitive parallel reactions to characterize the relative mixing quality of different micromixers. The computational method, COMSOL software, is a convenient tool to simulate processes taking place in micromixers. It provided a comprehensive understanding of how hydrodynamics, reaction kinetic, and other parameters influence the outcome. The combination of these two methods is an effective tool for testing the mixing quality of micromixers and for the designing of efficient micromixers. These two methods showed a clear agreement with each other on the result: from the perspective of the synthesis yield, the interdigital micromixer has much better performance than the Tee mixer under all conditions. Therefore, the interdigital micromixer was chosen as the major tool to synthesize dendrimers.

The interdigital micromixer was used to fulfill the syntheses of two different kinds of dendrimers: PAMAM dendrimer and polyamide dendrimer, via divergent and convergent synthesis strategies. The synthesis results via the micromixer were compared with that via the Tee mixer and the conventional flask reactor. It was proven that the interdigital micromixer was an efficient tool to synthesize both dendrimers. The microreactor demonstrated several advantages over a

conventional batch reactor. One of the most attractive advantages is that dendrons and dendrimers with a high purity could be synthesized within tens seconds of residence time in contrast to hours of stirring in a flask. In addition, the required reaction conditions are much easier to implement. Besides, the microreactor is an efficient tool to conduct a parameterization study and kinetics study. The reaction kinetics of the polyamide dendron G1 was studied in detail via the interdigital micromixer. The reasons that the microreactor was advantageous over batch reactor was that it was analyzed based on experimental results. For most exothermic fast reactions such as the synthesis of the G1 dendron, the prolonged reaction time in the batch reactor was not only due to its bad mixing quality, but also due to the long dosing time to avoid hot spots and, therefore, side reactions. The latter is the predominant factor for reactions with a small volume scale.

In addition, the interdigital micromixer was utilized to deposit the polyamide dendron onto a functionalized glass surface through the formation of an amide bond using a facile coupling procedure. A variety of techniques were applied to characterize the deposition on glass surfaces, and provided sufficient evidence that the 3-aminopropyl triethoxysilane and the polyamide dendron G1 were covalently bonded on the glass surfaces and featured with a uniform distribution of film. Compared with the traditional method to modify the glass surface by immersing it into solution, the approach utilizing micromixer provided a comparable result with an easy deposition process control in a much shorter time.

Future Work

(1) The PAMAM G-0.5 dendrimer synthesis via a micromixer needs further study to figure out the exact reasons causing the non-repeatability. The hypothesis that the change of the physical property, especially the aggregation, resulted in the lower yield needs to be verified.

(2) The deposition of the higher generation dendrons and dedrimers on a solid surface via a microreactor is worth further study because the higher generation dendrimers own denser distribution of the surface functional groups which benefits the conjugation of small molecules on the surface. The proposed depositions of PAMAM dendrimers on solid surfaces are illustrated in figure 9-1. There are two methods to deposit high full generation PAMAM dendrimer on a solid surface. For both methods, the first step is to modify a clean gold layer on a silicon wafer by $HS(CH_2)_{10}COOH$ to bear COOH groups.

The first method is to deposit the previously synthesized dendrimers onto a solid surface. A certain full generation PAMAM dendrimer (already synthesized) will be activated by thionyl chloride via a micromixer and then introduced onto a spinning modified surface. The second method is to alternatively deposit ethylenediamine and methylacrylate on to a modified solid surface via spin coating.

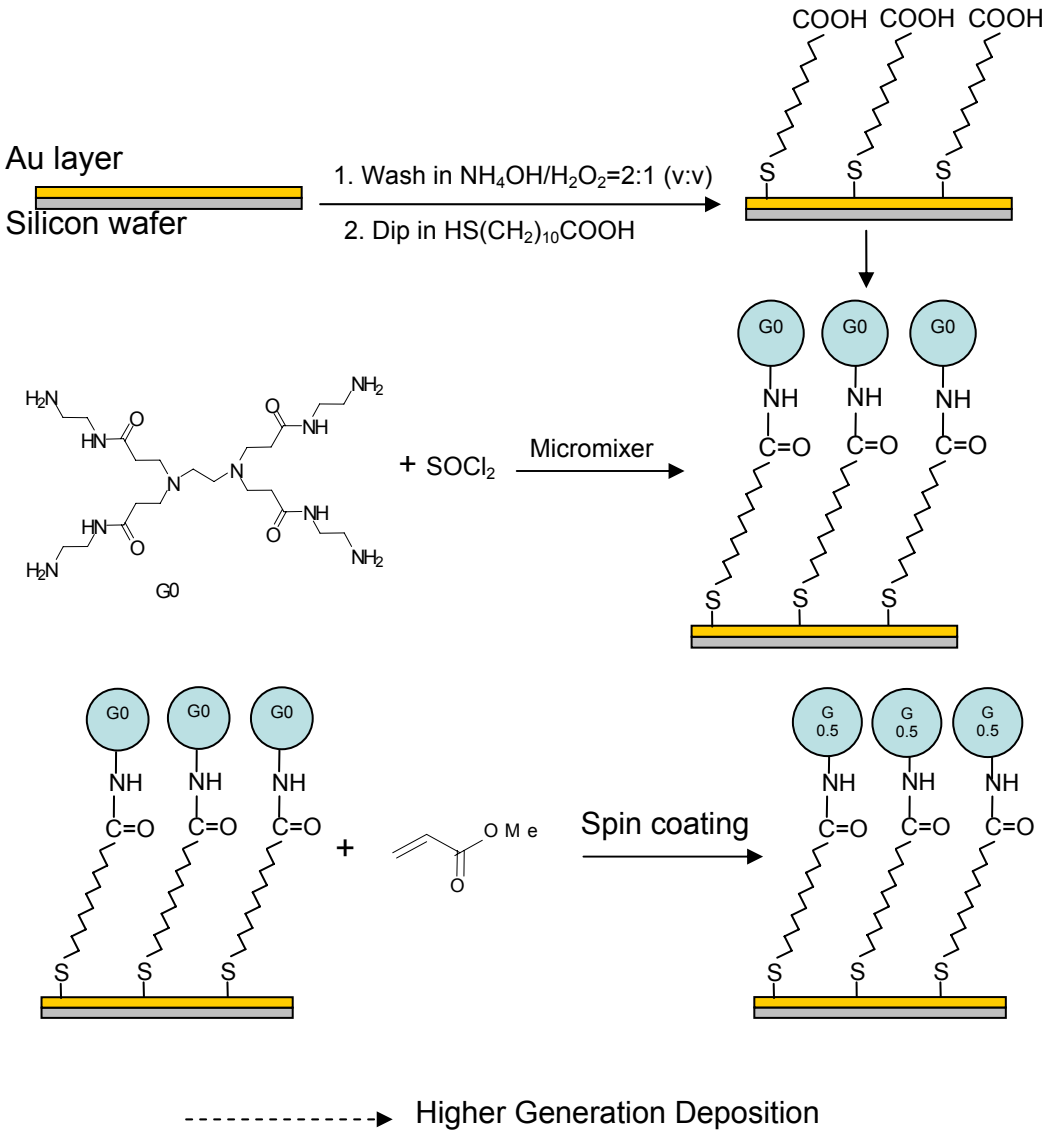

Figure 9-1. The schematic illustration of the deposition of PAMAM dendrimer on a solid surface.

The deposition of the combination of PAMAM dendrimer and a polyamide dendron by utilizing a micromixer is illustrated in figure 9-2.

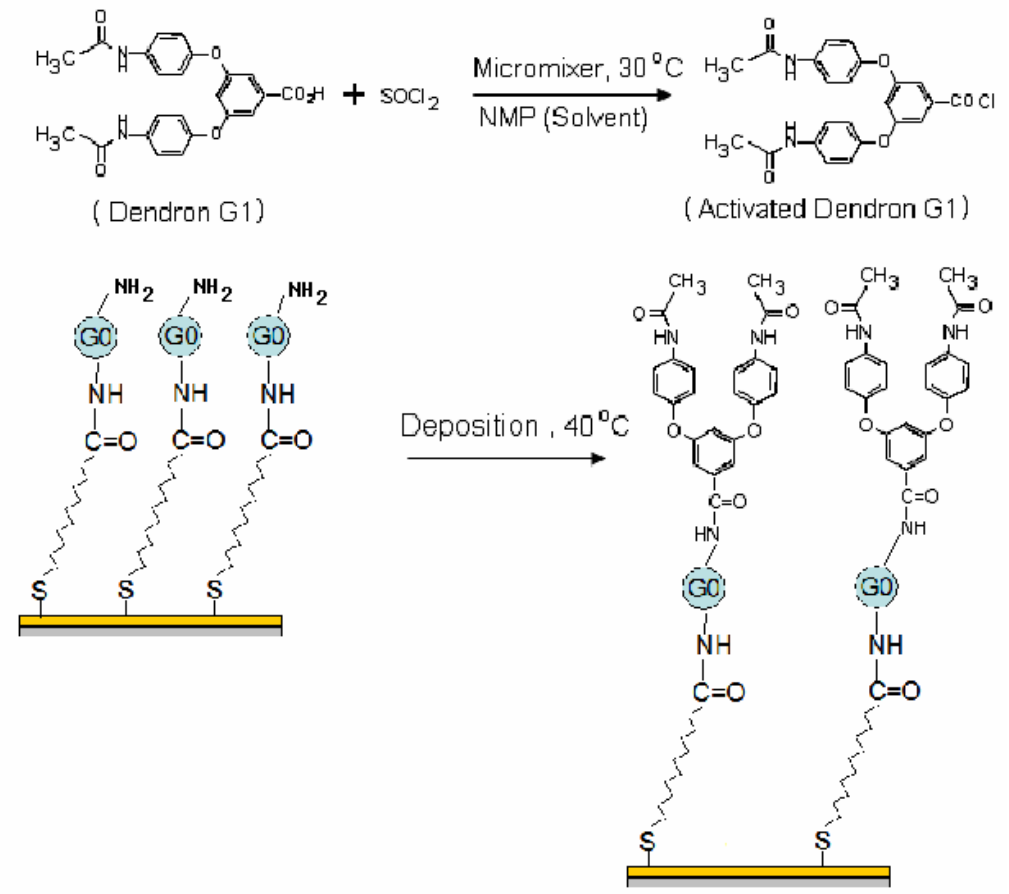

Figure 9-2. The schematic illustration of the deposition of the combination of PAMAM dendrimer and the polyamide dendron onto a solid surface.

(3) The deposited dendrimer and dendron solid surfaces can be applied in protein absorption and microbial study.

REFERENCES

[1] (a) Flory, P. J. *J. Am. Chem. Soc*. **1952**, *74*, 2718-2723. (b) Flory, P. J. *Principles of Polymer Chemistry*, Cornell University Press: Ithica, NY, **1953**.

[2] Buhleier, E.; Wehner, W.; Vögtle, F. *Synthesis*, **1978**, 155.

[3] (a) Tomalia, D. A.; Baker, H.; Dewald, J. R.; Hall, M.; Kallos, G.; Martin, S.; Roech, J.; Ryder, J.; Smith, P. *Polym. J. (Tokyo)*, **1985**, *17*, 117-132. (b) Tomalia, D. A.; Baker, H.; Dewald, J. R.; Hall, M.; Kallos, G.; Martin, S.; Roech, J.; Ryder, J.; Smith, P. *Macromolecules* **1986**, *19*, 2466-2468.

[4] Wörner, C.; Mülhaupt, R. *Angew. Chem., Int. Ed. Engl*. **1993**, *32*, 1306-1308.

[5] (a) Frechét, J. M. J.; Jiang, Y.; Hawker, C. J.; Philippides, A. E. *Proc. IUPAC Int. Symp., Macromol. (Seoul)* **1989**, 19-20. (b) Hawker, C. J.; Frechét, J. M. J. *J. Am. Chem. Soc.* **1990**, *112*, 7638-7647.

[6] Newkome, G. R.; Yao, Z. Q.; Baker, G. R.; Gupta, V. K. *J. Org. Chem*. **1985**, *50*, 2003-2005.

[7] Dykes, G. M. *J. Chem. Tech & Biotech*. **2001**, *76*, 903-918.

[8] Brunner, H. *J. Organomet. Chem*. **1995**, *500*, 39-46.

[9] Collman, J. P.; Fu, L.; Zingg, A.; Diederich, F. *Chem Commun*. **1997**, 193-194.

[10] Smith, D. K.; Diederich F. *Chem Commun*. **1998**, 2501-2502.

[11] Newkome, G. R.; Moorefield, C. N.; Baker, G. R.; Saunders, M. J.; Grossman, S. H. A. *Angew. Chem., Int. Ed. Engl*. **1991**, *30*, 1178-1180.

[12] Piorri, M. E.; Rivera, F.; Bond, R.; Hawker, C. J.; Frechét, J. M. J. *J. Am. Chem. Soc.* **1999**, *121*, 9471-9472.

[13] Kovvali, A. S.; Chen, H.; Sirkar, K. K. *J. Am. Chem. Soc.* **2000**, *122*, 7594-7595.

[14] (a) Balzabu, N.; Ceroni, P.; Gestermann, S.; Kauffmann C.; Gorka, M.; Vogtle F. *Chem. Commun*., **2000**, 853-854. (b) James, T. D.; Shinmori, H.; Takeuchi, M.; Shinakai, S. *Chem. Commun*, **1996**, 705-706.

[15] Toth, E.; Pubanz, D.; Vauthey, S.; Helm, L.; Merbach, A. E. *Chem. Eur. J.* **1996**, *2*, 1607-1615.

[16] Baussanne, I.; Benito, J. M.; Mellet, C. O.; Fernandez, J. M. G.; Law, H.; Defaye, J. *Chem. Commun*. **2000**, 1489-1490.

[17] Kukowsha-Lattallo,, J. F.; Bielinska, A. U.; Johnson, J.; Spindler, R.; Tomalia, D. A.; Baker, J. R. *Proc. Natl. Acad. Sci. USA* **1996**, *93*, 4897-4902.

[18] Barbara, K.; Bryszewska, M. *Acta Biochimica Polonic* **2001**, *48*, 199-208.

[19] DECHEMA-Monographs, ed. W. Ehrfeld, DECHEMA, Frankfurt, 1995, p. 132.

[20] Hessel,V.; Hardt, S; Lőwe, H. in *Chemical micro process engineering*, (Wiley-Vech, 2004), pp. 74.

[21] Schwalbe, T.; Autze, V.; Hohmann, M.; Stirner, W. *Org. proc. Res. Dev.* **2004,** 440-454.

[22] Boswell, C. *Chemical MarketRreporter*, **2004,** October 4.

[23] Hessel, V.; Löwe, H.; Schönfeld, F. *Chemical Engineering Science*, **2005,** *60*, 2479-2501.

[24] Wensink, H.; Benito-Lopez, F.; Hermes, D. C.; Verboom, W. Lab on a Chip, **2005,** *5,* 280-284.

[25] Connors, K. A. in *Chemical Kinetics: The Study of Reaction Rates in Solution,* (Wiley-VCH 1990), pp. 27.

[26] Washio, I.; Shibasaki, Y.; Ueda, M. *Macromolecules,* **2005,** *38*, 2237-2246.

[27] Levenspiel, O.; Weinstein, N. J.; Li, J. C. R. Ind. Eng. Chem., **1956,** *48*, 324-326.

[28] Faucheux, N.; Schweiss, R.; Lutzow, K.; Werner, C.; Groth, T. *Biomaterials,* **2004,** *25,* 2721-2730.

APPENDICES

Appendix A The Inlet flowrate of each stream and corresponding velocity in the Tee mixer and the IMM mixer used in the COMSOL simulation

Table 1. Inlet flowrate and corresponding velocity

inlet flowrate of each stream V (ml/min)	0.94	1.56	2.18	2.58	2.8
inlet velocity of Tee mixer u (m/s)	0.08	0.13	0.19	0.22	0.24
inlet velocity of IMM mixer u (m/s)	0.35	0.58	0.81	0.96	1.04

Appendix B The COMSOL simulation result of the Tee mixer

Table 2. D=1e-9, V=1.56 ml/min, change k (Tee)

	k=0.001	k=0.01	k=0.1	k=1
Eta1	0.0013			
Eta2	0.001			
Eta3	0.001			
Roa1	1100			
Roa2	1000			
Roa3	1000			
D1	1e-9			
D2	1e-9			
D3	1e-9			
u01	0.13			
u02	0.13			
C10	400			
C20	1200			
k	0.001	0.01	0.1	1
c3	0.015	0.135	0.996	2.85
X (%)	0.0076	0.067	0.498	1.425

Table 3. D=1e-9 , k=0.001, change u(Tee)

	u0=0.08	u0=0.13	u0=0.19	u0=0.24
Eta1	0.0013			
Eta2	0.001			
Eta3	0.001			
Roa1	1100			
Roa2	1000			
Roa3	1000			
D1	1e-9			
D2	1e-9			
D3	1e-9			
u01	0.08	0.13	0.19	0.24
u02	0.08	0.13	0.19	0.24
C10	400			
C20	1200			
k	0.001			
c3	0.031	0.015	0.0099	0.0077
X(%)	0.0156	0.0077	0.0050	0.00385

Table 4. D=1e-9 , k=1, change u(Tee)

	u0=0.08 (m/s)	u0=0.13	u0=0.19	u0=0.22
Eta1	0.0013			
Eta2	0.001			
Eta3	0.001			
Roa1	1100			
Roa2	1000			
Roa3	1000			
D1	1e-9			
D2	1e-9			
D3	1e-9			
u01	0.08	0.13	0.19	0.22
u02	0.08	0.13	0.19	0.22
C10	400			
C20	1200			
k	0.001			
c3	4.48	2.85	2.36	2.20
X(%)	2.24	1.43	1.18	1.10

Table 5. V=1.56, k=0.001, change D(Tee)

	D=1e-9	D=1e-8	D=1e-7	D=1e-6
Eta1	0.0013			
Eta2	0.001			
Eta3	0.001			
Roa1	1100			
Roa2	1000			
Roa3	1000			
D1	1e-9	1e-8	1e-7	1e-6
D2	1e-9	1e-8	1e-7	1e-6
D3	1e-9	1e-8	1e-7	1e-6
u01	0.13			
u02	0.13			
C10	400			
C20	1200			
k	0.001			
c3	0.015	0.044	0.14	0.890
X(%)	0.0077	0.022	0.071	0.444

Table 6.V=1.56, k=1, change D(Tee)

	D=1e-9	D=1e-8	D=1e-7	D=1e-6
Eta1	0.0013			
Eta2	0.001			
Eta3	0.001			
Roa1	1100			
Roa2	1000			
Roa3	1000			
D1	1e-9	1e-8	1e-7	1e-6
D2	1e-9	1e-8	1e-7	1e-6
D3	1e-9	1e-8	1e-7	1e-6
u01	0.13			
u02	0.13			
C10	400			
C20	1200			
k	0.001			
c3	2.85	10.91	35.37	154.5
X(%)	1.43	5.46	17.69	77.25

Appendix C The COMSOL simulation result of the IMM mixer

Table 7. D=1e-9, V=1.56 ml/min, change k(IMM)

	K=1e-3	K=0.01	0.1	K=1
Eta1	0.0013			
Eta2	0.001			
Eta3	0.001			
Roa1	1100			
Roa2	1000			
Roa3	1000			
D1	1e-9			
D2	1e-9			
D3	1e-9			
u01	0.58			
u02	0.58			
C10	400			
C20	1200			
k	0.001	0.01	0.1	1
c3	1.24	11.29	75.73	193.44
X(%)	0.62	5.65	37.87	96.72

Table 8. D=1e-9 , k=0.001, change u(IMM)

	u0=0.35	u0=0.58	u0=0.81	u0=1.04
Eta1	0.0013			
Eta2	0.001			
Eta3	0.001			
Roa1	1100			
Roa2	1000			
Roa3	1000			
D1	1e-9			
D2	1e-9			
D3	1e-9			
u01	0.35	0.58	0.81	1.04
u02	0.35	0.58	0.81	1.04
C10	400			
C20	1200			
k	0.001			
c3	2.03	1.23	0.89	0.69
X	1.02	0.62	0.45	0.35

Table 9. D=1e-9 , k=1, change u(IMM)

	u0=0.35	u0=0.58	u0=0.81	u0=0.96
Eta1	0.0013			
Eta2	0.001			
Eta3	0.001			
Roa1	1100			
Roa2	1000			
Roa3	1000			
D1	1e-9			
D2	1e-9			
D3	1e-9			
u01	0.35	0.58	0.81	0.96
u02	0.35	0.58	0.81	0.96
C10	400			
C20	1200			
k	0.001			
c3	198.93	193.43	184.52	178.03
X	99.47	96.72	92.26	89.02

Table 10. u=0.58, k=0.001, change D (IMM)

	D=1e-9	D=1e-8	D=1e-7	D=1e-6
Eta1	0.0013			
Eta2	0.001			
Eta3	0.001			
Roa1	1100			
Roa2	1000			
Roa3	1000			
D1	1e-9	1e-8	1e-7	1e-6
D2	1e-9	1e-8	1e-7	1e-6
D3	1e-9	1e-8	1e-7	1e-6
u01	0.58			
u02	0.58			
C10	400			
C20	1200			
k	0.001			
c3	1.24	1.25	1.25	1.26
X(%)	0.62	0.625	0.625	0.63

Table 11. u=0.58, k=1, change D (IMM)

	D=1e-9	D=1e-8	D=1e-7	D=1e-6
Eta1	0.0013			
Eta2	0.001			
Eta3	0.001			
Roa1	1100			
Roa2	1000			
Roa3	1000			
D1	1e-9	1e-8	1e-7	1e-6
D2	1e-9	1e-8	1e-7	1e-6
D3	1e-9	1e-8	1e-7	1e-6
u01	0.58			
u02	0.58			
C10	400			
C20	1200			
k	0.001			
c3	193.44	193.44	193.48	193.48
X(%)	96.72	96.72	96.74	96.74

Appendix D The computation of the reaction constant and the reaction order of the second step of producing the dendron G1 under temperatures of 18 ^{o}C and 30 ^{o}C

Table 12. The data required for the calculation of the reaction constant and the reaction order when the temperature is 18 ^{o}C (291 K).

run			y		x1		x2
	Time (s)	-dc/dt	log(-dc/dt)	Cc	logC_C	C_B	logC_B
1	0.63	40	1.60206	80	1.90309	280	2.447158
2	1	26	1.414973	65.3	1.814913	265.3	2.423737
3	2	15	1.176091	53	1.724276	253	2.403121
4	2.5	14	1.146128	48	1.681241	248	2.394452
5	3	10	1	43.8	1.641474	243.8	2.387034
6	4	8	0.90309	38.6	1.586587	238.6	2.37767
7	5	8	0.90309	34	1.531479	234	2.369216
		Sum	8.144433		11.88306		16.80239
		Notation	Σy		Σx1		Σx2

Table 13. Details of computation based on table12.

run	x1·y	x2·y	$x1^2$	$x2^2$	x1·x2
1	3.048864	3.920494	3.621751	5.988582	4.657162
2	2.568054	3.429524	3.29391	5.874502	4.398873
3	2.027906	2.826289	2.973127	5.774988	4.143643
4	1.926918	2.744348	2.826572	5.733399	4.025651
5	1.641474	2.387034	2.694437	5.69793	3.918254
6	1.432831	2.14725	2.517259	5.653317	3.772382
7	1.383063	2.139615	2.345428	5.613184	3.628404
Sum	14.02911	19.59745	20.27248	40.3359	28.54437
Notation	Σ(x1·y)	Σ(x2·y)	$\Sigma\ x1^2$	$\Sigma\ x2^2$	Σ(x1·x2)

solve({7*x C 11.88 * y C 16.8 *z = 8.14 , 11.88 *x C 20.27*y C 28.54*z = 14.03, 16.8$x C 28.54$ y C 40.34$ z = 19.597}, [x, y, z]);

[[x = K 3.015960100, y = 1.889027431, z = 0.4053615960]]

Table 14. The data required for the calculation of the reaction constant and the reaction order when the temperature is 30 ^{o}C (303 K).

run			y		x1		x2
	Time (s)	-dc/dt	log(-dc/dt)	Cc	$\log C_C$	C_B	$\log C_B$
1	0.63	90	1.954243	56	1.748188	256	2.40824
2	1	23.5	1.371068	40.5	1.607455	240.5	2.381115
3	2	7	0.845098	31.6	1.499687	231.6	2.364739
4	2.5	10	1	28	1.447158	228	2.357935
5	3	7	0.845098	23.5	1.371068	223.5	2.349278
6	4	7	0.845098	16.6	1.220108	216.6	2.335658
		Sum	6.860604		8.893664		14.19696
		Notation	Σy		Σx1		Σx2

Table 15. Details of computation based on table14.

run	x1·y	x2·y	$x1^2$	$x2^2$	x1·x2
1	3.416383	4.706285	3.056161	5.79962	4.210056
2	2.20393	3.26467	2.583912	5.669709	3.827535
3	1.267383	1.998436	2.249061	5.591988	3.546368
4	1.447158	2.357935	2.094266	5.559857	3.412304
5	1.158687	1.98537	1.879827	5.519105	3.221019
6	1.031111	1.97386	1.488664	5.4553	2.849756
Sum	10.52465	16.28656	13.35189	33.59558	21.06704
Notation	Σ(x1·y)	Σ(x2·y)	$\Sigma\ x1^2$	$\Sigma\ x2^2$	Σ(x1·x2)

```
solve( {6*x C 8.89* y C 14.2 *z = 6.86 , 8.89 *x
    C 13.35*y C 21.07*z = 10.52, 14.2$x C 21.07$ y
    C 33.6$ z = 16.29}, [x, y, z]);

  [ [x = K 2.883939873, y = 1.912974684, z = 0.5040348101 ] ]
```

Nomenclature of Appendices

Eta1: absolute viscosity of stream 1, Pa.s;

Eta2: absolute viscosity of stream 2, Pa.s;

Eta3: absolute viscosity of mixed stream, Pa.s;

Roa1: density of stream 1, kg/m^3;

Roa2: density of stream 2, kg/m^3;

Roa3: density of mixed stream, kg/m^3;

D1: diffusivity of stream 1, m^2/s;

D2: diffusivity of stream 2, m^2/s;

D3: diffusivity of mixed stream, m^2/s;

u01: inlet velocity of stream 1, m/s;

u02: inlet velocity of stream 2, m/s;

C10: inlet concentration of stream1, mol/m^3;

C20: inlet concentration of stream2, mol/m^3;

k: reaction constant, $m^3/(mol.s)$;

C3: outlet concentration of product, mol/m^3;

X: outlet conversion of product, %;

V: flowrate, ml/min.